

Diagnosis of Rolling Mill Cycloconverters Using Time-Frequency Signature Analysis

Timothy Mitchell Thompkins

The Graduate School

Yonsei University

School of Engineering

Diagnosis of Rolling Mill Cycloconverters Using Time-Frequency Signature Analysis

A Master's Thesis

Submitted to the Department of Electrical and Electronic Engineering

and the Graduate School of Yonsei University

in partial fulfilment of the

requirements for the degree of Master of Science

Timothy Mitchell Thompkins

December 2015

This certifies that the master's thesis of
Timothy Mitchell Thompkins is approved.

Thesis Supervisor: Prof. Yong-June Shin

Prof. Youngcheol Chae

Prof. Kyeon Hur

The Graduate School

Yonsei University

December 2015

ACKNOWLEDGEMENTS

I owe many thanks to the numerous people that have supported me not just with the development of this thesis, but also in my personal development as an engineer, a student, and as a person. I am indebted to Dr. Yong-June Shin for his extreme kindness and guidance for both leading me to the point where I am today and lifting me to the places I will go. Though bound by no obligation, he has devoted significant time and energy into my academic and personal growth. I'm particularly grateful for the unique opportunity to study at Yonsei University that has allowed me to cultivate an appreciation and love for the beautiful Korean culture and its people. Having met Dr. Yong-June Shin as an undergraduate at the University of South Carolina, Columbia, I never would have expected that several years later I would find myself completing a degree at Yonsei University with him as my advisor. Truly I offer my many thanks from the warmest part of my heart.

I must also acknowledge all of the professors at the University of South Carolina and Yonsei University which have played no small part in helping mold me. Dr. Enrico Santi, whose advice to develop an intuition and deep understanding about concepts rather than a superficial knowledge is a continual inspiration and reminder of how to approach problems and find solutions. Dr. Tangali S. Sudarshan, whose notion of the pursuit of life-long learning and its importance is something that I find myself mulling over frequently. David Metts, a man with a disposition that I believe can be aptly described as "mutedly optimistic" and for whom I have deep respect. My gratitude is also extended to Drs. Dougal and Ginn. Their advisement has been of great importance to me as I've made decisions about my academic career and future. I would also like to thank Drs. Hur and Yoon for their graduate course instruction, and Drs. Hur and Chae for taking time to review these thesis materials.

In a similar vein, I would like to recognize all my classmates and colleagues; I have a profound admiration and gratitude for all of them. Jordan Rogers, Jonathan Siegers, Gabriel Brown, and Cale Workman, along with other members of the University of South Carolina Graduate School have helped me foster an understanding of many topics; without them I would not be writing this document today. Do-In Kim, Yee Jin Han, Hyeong Min Lee, Seon Hyeog Kim, Geon Seok Lee, Sung Hwa Yoon, Gyul Lee, Gu Young Kwon, Yong Gu Lee, Su Sik Bang, Young Hwan Kim, Jon Min Kim, Joo Young Jung, Young Ho Lee, Chun Kwon Lee, Jin-Sil Kim, and all the other members of the Yonsei University EE department whose names are too numerous to list in complete here have helped turn Korea into a home away from home; I'm forever grateful to all of them.

I also must thank all of my friends both home and abroad, especially Kyle Berry and Chris Sim, who have stayed my closest friends despite being a world apart. I of course owe my entire family, but especially my parents and sister Mary, Mike, and MariAmber Thompkins for their perpetual support and love.

Finally, I must say a special thanks to Nucor Steel Berkeley, notably Marcus Parrish and Harry Weatherford, for both providing the data used in this analysis and offering technical discussion and guidance. It is my hope that they find use in the results compiled here.

CONTENTS

Acknowledgements	i
List of Figures	iv
List of Tables	vii
Abstract	viii
1. Introduction	1
1.1 Proposed Cycloconverter Diagnostic Technique Traits	2
2. Theory	3
2.1 Cycloconverter Operation	3
2.1.1 The Cycloconverter's Place in Rolling Mills	3
2.1.2 Cycloconverter General Principles	4
2.1.3 Cycloconverter Harmonics	7
2.1.4 Frequency Modulation in the Time-Frequency Domain	9
2.2 Time-Frequency Analysis	9
2.2.1 The Spectrogram	9
2.2.2 Frequency Average	12
2.3 Spectrogram and Data Analysis	12
2.3.1 Input Current Data and Spectrogram Modifications	12
2.3.2 Output Frequency	15
2.3.3 Frequency Centers	17
2.3.4 Harmonic Slopes	24
2.4 Modeling	32
2.4.1 Modeling Equation	32
2.4.2 Filtering Undesired Harmonic Components and Normalizing Data	39
2.4.3 Model Definition	39
3. Operating Status Decision Boundary	42
3.1 Analysis in the Time-Frequency	42
3.2 Error Analysis Technique	43
3.2.1 Error Analysis for Damaged Cycloconverters Driving Loaded Motors	43
3.2.2 Error Analysis for Undamaged Cycloconverters Driving Loaded Motors	46
3.2.3 Error Analysis for Undamaged Cycloconverters Driving Unloaded Motors	48
3.3 Loaded Motors Error Analysis	49
3.3.1 Local Minima Values for Loaded Motors	50
3.3.2 Local Minima Differences for Loaded Motors	55
3.4 Unloaded Motors Error Analysis	58
3.4.1 Local Minima Values for Unloaded Motors	58
3.5 Decision Boundary Thresholds	62
4. Summary	64

4.1	Method Shortcomings and Potential Improvements	64
4.2	Future Work	65
5.	Conclusion	66
6.	References.....	67

LIST OF FIGURES

Figure 2-1. Four-high rolling mill-stand diagram [25].	3
Figure 2-2. 6-Pulse (36 thyristor) cycloconverter diagram.....	4
Figure 2-3. a.) 3- ϕ Input voltages (high frequency) and reference output (low frequency). b.) Output voltage (solid line) and reference output (dotted line) [26].	5
Figure 2-4. Example reference signal, cosine timing waves, and corresponding firing instants for an individual thyristor.	6
Figure 2-5. The expected harmonic centers (red solid lines) and associated side band frequencies (dotted blue lines) as a function of the ratio of output to input frequency for a 6 pulse cycloconverter with a balanced 3- ϕ output.	8
Figure 2-6. Sample spectrogram taken over one second.	10
Figure 2-7. 3-D view of sample spectrogram from Figure 2-6.....	11
Figure 2-8. Spectrogram of F6 input current data with a threshold of 0.....	13
Figure 2-9. Spectrogram of F6 input current data with linear, not logarithmic, scaling.....	14
Figure 2-10. Spectrogram of one second of data for a loaded F6.	14
Figure 2-11. Spectrogram of one second of data for a loaded F1.....	15
Figure 2-12. Spectrogram of one second of data for a loaded F6.	15
Figure 2-13. Sample signal envelope and signal of output frequency.	16
Figure 2-14. Maximum values taken along the x-axis of the thresholded and logarithmically scaled spectrogram for Figure 2-12.	17
Figure 2-15. Fourier transform of the maximum values taken along the x-axis of the thresholded and logarithmically scaled spectrogram of Figure 2-12.....	17
Figure 2-16. 10 th order elliptic filters with a stopband attenuation of 150 dB and passband ripple of 3 dB.	18
Figure 2-17. Frequency centers (white dotted lines) associated with each harmonic chirp for a loaded motor on F6 with ratio of approximately 0.0846.	19
Figure 2-18. Frequency centers (white dotted lines) associated with each harmonic chirp for a loaded motor on F2 with ratio of approximately 0.1693.	20
Figure 2-19. Frequency centers (white dotted lines) associated with each harmonic chirp for an unloaded motor on F1 with ratio of approximately 0.0456.	22
Figure 2-20. Frequency centers (white dotted lines) associated with each harmonic chirp for an unloaded motor on F6 with ratio of approximately 0.1302.	22

Figure 2-21. Transitional loading case.....	23
Figure 2-22. Frequency centers of input current harmonics for unloaded datasets.	24
Figure 2-23. Spectrogram for a loaded motor on F6 with a ratio of approximately .0846....	26
Figure 2-24. Bode for filtering maximum values in windows of interest. Here it corresponds to Figure 2-23 and is centered about a frequency of 5.0781 Hz with a lower cut-off frequency of 1.0781 Hz and an upper cut-off frequency of 9.0781 Hz.	26
Figure 2-25. All images correspond to the spectrogram in Figure 2-23.....	28
Figure 2-26. All images correspond to the spectrogram in Figure 2-23.....	29
Figure 2-27. All images correspond to the spectrogram in Figure 2-23 ..	30
Figure 2-28. Harmonic slopes for the 5 th , 11 th , and 17 th harmonics for loaded datasets.....	31
Figure 2-29. ϕt , the frequency modulation function.	34
Figure 2-30. $\phi' t$, the derivative of frequency modulation function.....	34
Figure 2-31. $\phi'' t$, the 2 nd derivative of frequency modulation function.	35
Figure 2-32. Spectrogram of real filtered input current for a loaded cycloconverter with ratio of approximately .084635.	36
Figure 2-33. Spectrogram of modeled and filtered input current for a loaded cycloconverter with ratio of approximately .084635.....	37
Figure 2-34. Spectrogram of real filtered input current for a loaded cycloconverter with ratio of approximately 0.16276.	37
Figure 2-35. Spectrogram of modeled and filtered input current for a loaded cycloconverter with ratio of approximately 0.16276.....	38
Figure 2-36. Reference window for the loaded motor of Figure 2-33 at a ratio of 0.084635.	39
Figure 2-37. Proposed Cycloconverter Status Diagnosis Model.	41
Figure 3-1. Input current for a damaged F1.....	42
Figure 3-2. Spectrogram of input current for a damaged and loaded F1.....	43
Figure 3-3. Spectrogram of filtered input current for a damaged and loaded F1.	44
Figure 3-4. Reference window for a loaded motor at a ratio of 0.078125.....	44
Figure 3-5. Error window between reference and real filtered data for a damaged and loaded cycloconverter F1.....	45
Figure 3-6. MSE and error differences for an undamaged and loaded F1.....	46
Figure 3-7. Spectrogram of filtered input current for an undamaged and loaded F1.	47
Figure 3-8. MSE and error differences for an undamaged and loaded F1.....	47

Figure 3-9. Spectrogram of filtered input current for an undamaged and unloaded F2.	48
Figure 3-10. Reference window for a loaded motor at a ratio of 0.13021.....	49
Figure 3-11. MSE and error differences for an undamaged and unloaded F2.....	49
Figure 3-12. MSE data and associated linear regression from Table 3-1.....	51
Figure 3-13. Standard deviation of MSE data and associated linear regression from Table 3-1.....	51
Figure 3-14. Probability distribution functions created by (3-4) with data from Figure 3-12.....	53
Figure 3-15. Probability distribution functions created by (3-4) with data from Figure 3-12.....	54
Figure 3-16. Probability distribution functions created by (3-4) with data from Figure 3-12.....	54
Figure 3-17. PDF of MSE data and threshold from Table 3-1 and Figure 3-12.....	55
Figure 3-18. MSE differences, mean, and standard deviation from Table 3-3.....	56
Figure 3-19. Probability distribution function created by (3-4) with data from Figure 3-18.	57
Figure 3-20. PDF of MSE differences and threshold.....	57
Figure 3-21. MSE data and associated linear regression from Table 3-5.....	59
Figure 3-22. Standard deviation of MSE data and associated linear regression from Table 3-5.....	59
Figure 3-23. Probability distribution functions created by (3-4) with data from Figure 3-21.....	60
Figure 3-24. Probability distribution functions created by (3-4) with data from Figure 3-21.....	61
Figure 3-25. Probability distribution functions created by (3-4) with data from Figure 3-21.....	61
Figure 3-26. PDF of MSE data and threshold from Table 3-5 and Figure 3-21.....	62
Figure 3-27. Cycloconverter Status Decision Tree.....	63

LIST OF TABLES

Table 2-1. Differences in frequency centers of input current harmonics from the expected frequency centers for loaded datasets	21
Table 2-2. Frequency centers of input current harmonics for unloaded datasets.....	23
Table 2-3. Coefficients for equation (2-16). h = 1 corresponds to the fundamental.....	24
Table 2-4. Harmonic slopes of input current harmonics for loaded datasets.....	31
Table 2-5. Coefficients for equation (2-17). h = 1 corresponds to the fundamental.....	32
Table 3-1. Loaded Motor Local Minima MSE.	50
Table 3-2. Coefficients for equation (3-3) corresponding to Figure 3-12 and Figure 3-13....	52
Table 3-3. Loaded Motor Local Minima MSE Differences.....	56
Table 3-4. Coefficients for equation (3-3) corresponding to Figure 3-21 and Figure 3-22....	58
Table 3-5. Unloaded Motor Local Minima MSE.....	58
Table 3-6. Decision Boundary Status Diagnosis.....	63

ABSTRACT

Diagnosis of Rolling Mill Cycloconverters Using Time-Frequency Signature Analysis

Timothy Mitchell Thompkins

Department of Electrical and Electronic Engineering

The Graduate School

Yonsei University

High power industrial rolling mills rely heavily on the sustained operation of cycloconverters, a type of variable frequency drive. This research proposes a means to diagnose the operation of the cycloconverter as either normal or abnormal by use of time-frequency signature analysis. Various features of the cycloconverter's input current in the time-frequency domain are identified and used to derive parameters that describe each of these states. A reference model using the parameters is then developed and comparisons in the time-frequency domain to real data are made. Based on these comparisons a statistical decision boundary is delineated that is used to classify the cycloconverter.

Keywords: Rolling Mill, Cycloconverter, Drive, Time-Frequency, Status Diagnosis

1. INTRODUCTION

Historically DC machines were preferred in industrial applications due to the relative ease with which their speed can be controlled [1]. However, as asynchronous and synchronous motors became more economically viable new methods were required to control their speeds. Variable-frequency-drives (VFD), also known as AC drives, solve this issue. There are two topologies of VFDs, AC-AC and DC-AC, the former of which is the concern of this research. Under the AC-AC umbrella, two main types exist, those that include DC links and those that do not. Those that contain a DC link must first rectify the input AC signal then invert it to an output signal of the desired frequency; hence, there are two stages. Those that lack a DC link accomplish much the same goal but are instead one stage, converting an AC signal of some frequency directly to an AC signal of some different frequency. Though there are several types of drives which accomplish this, one of the most common and also the concern of this research is the cycloconverter. These types of drives consist of an array of switches, made of semi-conductor devices called thyristors¹, the controlled opening and closing (gating) of which allows for the fabrication of an output waveform of a desired lower frequency.

Cycloconverters are inherently capable of bidirectional power flow, have continuous independent control of both the output frequency and voltage, and are able to operate with loads of any power factor [1]. For these reasons, chief among them the last one, cycloconverters are frequently paired with synchronous machines [2]. As they are line commutated, their electrical size is limited only by the rating of the thyristors which they employ [3]. In addition, they can output nearly sinusoidal waveforms, and have a typical maximum output frequency of up to $\frac{2}{3}$ the input frequency [1]. These characteristics make the cycloconverter particularly suited to metal rolling applications where high power and low speed² are often requirements [4].

Their sustained and dependable performance is essential to the safe and effective production of a variety of metal products. Cycloconverters however, like any other drive, experience failures which are often expensive both in repairs and time lost. It would be advantageous then to be able to recognize abnormalities in cycloconverter operation which may be precursors to failure. With this in mind, if we can identify defining characteristics which we can consider natural, then it would be possible to distinguish between normal and abnormal cycloconverter operation. The distinction between these two states would allow us to develop intelligent compensation techniques that take action to prevent either failure or further harm of the system. This research deals with the identification of those characteristics and the development of metrics and a method to dichotomize these two states. Dichotomization is achieved by comparison of a reference model generated from the observed characteristics to real-world data. In this research the reference model architecture and required decision boundaries to determine the operating status of the cycloconverter are developed. A fully functioning state diagnosis machine is not implemented as this is left to further research. However, the information presented here is a very strong foundation from which to evolve.

¹ Thyristors are also commonly referred to as Silicon-Controlled Rectifiers (SCRs) and are used synonymously in this research.

² Low speed is a relative term, and here denotes a speed significantly lower than the frequency of the input signal to the cycloconverter.

1.1 Proposed Cycloconverter Diagnostic Technique Traits

Not all drives provide readily available data for all input and output currents and voltages; older large drive systems in particular lack this ability. Moreover, it is neither cost-effective to change out often multi-million dollar systems nor practical to monitor every data point due to hardware costs [5]. Therefore in this research, only the input current is analyzed and used to determine the defining characteristics and develop the aforementioned dichotomization method.

The majority of techniques for cycloconverter failure analysis either monitor a combination of input and output signals or attempt to identify abnormalities exclusively in the time domain [6] [7] [8]. The analysis tool utilized in this research however is time-frequency analysis. The cycloconverter input current is rich in harmonics and, for reasons that will be justified, not necessarily stationary in the traditional sense. That is to say that for a given portion of the input current, the frequency content may change in time, even though those changes may be consistent and periodic over longer instances of time. The uniqueness of this waveform makes it a prime candidate for analysis in the joint time-frequency domain. Indeed, as is discussed at length in following sections, it is scrutiny of these attributes in this domain which will allow us to delineate normal cycloconverter operation. Furthermore, there exist conditions where a slight shift in the load balance, i.e., from a balanced load to an unbalanced load may produce changes in the harmonic content, but not necessarily significant changes in the monitored current [9]. If analyzed solely in the time domain, these features may be missed. Analysis in the time-frequency domain has the benefit of detecting abnormalities in both the time and frequency domains simultaneously that may not be clear if analyzed in either only a single domain or asynchronously. Lastly, because only one input is considered, the more points of comparison that can be considered the more accurate of a prognosis can be provided. As was mentioned before, analysis in the join time-frequency domain provides well defined attributes which can be utilized as these points of comparison; this makes the use of such a tool particularly valuable.

Cycloconverters in general are well studied and many of their problems, including some defining features of abnormal operation, are well documented, particularly for their use in the mining industry and rolling mill industries [10] [11]. Cycloconverter harmonics tend to be of interest because of their role as a generator of sometimes atypical harmonic content [12] [13] [14]. Though there has been research into several time-frequency analysis methods on motors, it tends to be very specific, such as trying to detect mechanical failure through either vibration analysis or by utilization of the stator current [15] [16] [17] [18]. There has been some investigation into the use of time-frequency analysis as a motor fault detection technique and to model drives which helps establish a precedent for the validity of the method [19] [20] [21] [22] [23] [24]. The research presented here provides a solid basis on which drive fault detection and failure prognosis methods can be expanded. In total it covers the theory of cycloconverter operation, the underlying theory behind time-frequency analysis and the selection of the chosen distribution, the methods utilized for feature extraction from the time-frequency transformation, and proposes a method to properly distinguish between the normal and abnormal cycloconverter operation states.

2. THEORY

2.1 Cycloconverter Operation

To expand on the proposed method, it is necessary to first discuss some specific terminology and the role of cycloconverters in the mill, the general operating theory behind cycloconverters, and their part as a source of harmonics.

2.1.1 The Cycloconverter's Place in Rolling Mills

The general layout for a mill-stand is shown below in Figure 2-1. This configuration is called four-high, and is the configuration considered here, although there are other possible topologies [25]. The cycloconverter turns a large synchronous motor which in-turn rotates the rolls illustrated below. Through a gearing system, the top roll rotates counter-clockwise and the bottom roll rotates clockwise such that both spin in the direction of movement the product. The product itself is represented by the dark horizontal line that moves constantly through the mill-stand from west to east. In this case the product is a slab of steel whose gauge will be reduced from H to h by an immense forces placed on it by the rolls while they turn.

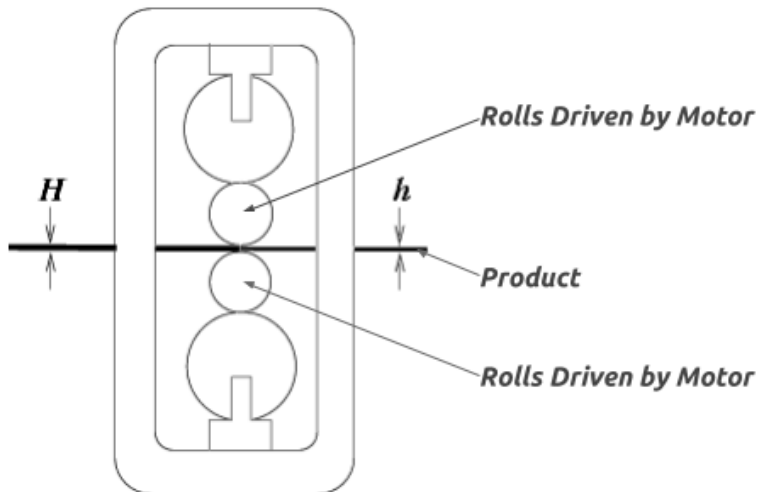


Figure 2-1. Four-high rolling mill-stand diagram [26].

There are two cycloconverter conditions that are considered, that of the unloaded motor and that of the loaded motor. An unloaded motor is a condition in which there is no product between the rolls, i.e. the horizontal black line shown in Figure 2-1 is absent, however the rolls are still spinning at the anticipated speed because product is about to be introduced into the mill-stand. This is because the forward velocity of the product and the rolls must be turning at the same or very nearly the same speed when the product is introduced³. The motor torque, and therefore input current draw, during this unloaded motor condition are lower than that of the loaded motor condition. Conversely, when the motor is loaded, the product is

³ As was discussed in the introduction but iterated here, the low fine speed control of the cycloconverter is one of its advantages.

present as is depicted in Figure 2-1. The torque and input current draw in this case is much higher. The unique effect on the spectrogram is discussed in subsequent sections.

2.1.2 Cycloconverter General Principles

There are several different types of cycloconverters, though they all operate on the same principles. The number of thyristors and number of output and input phases dictates the topology of the drive. In this case the cycloconverter considered is a 3φ-to-3φ 6-pulse (36 thyristor) cycloconverter. The diagram of such a cycloconverter is shown in Figure 2-2. Let it also be noted that this cycloconverter operates in circulating current-free mode, one of the two modes available for cycloconverters. The type does have an impact on the distortion of the input current signal and consequential presence of certain harmonic content.

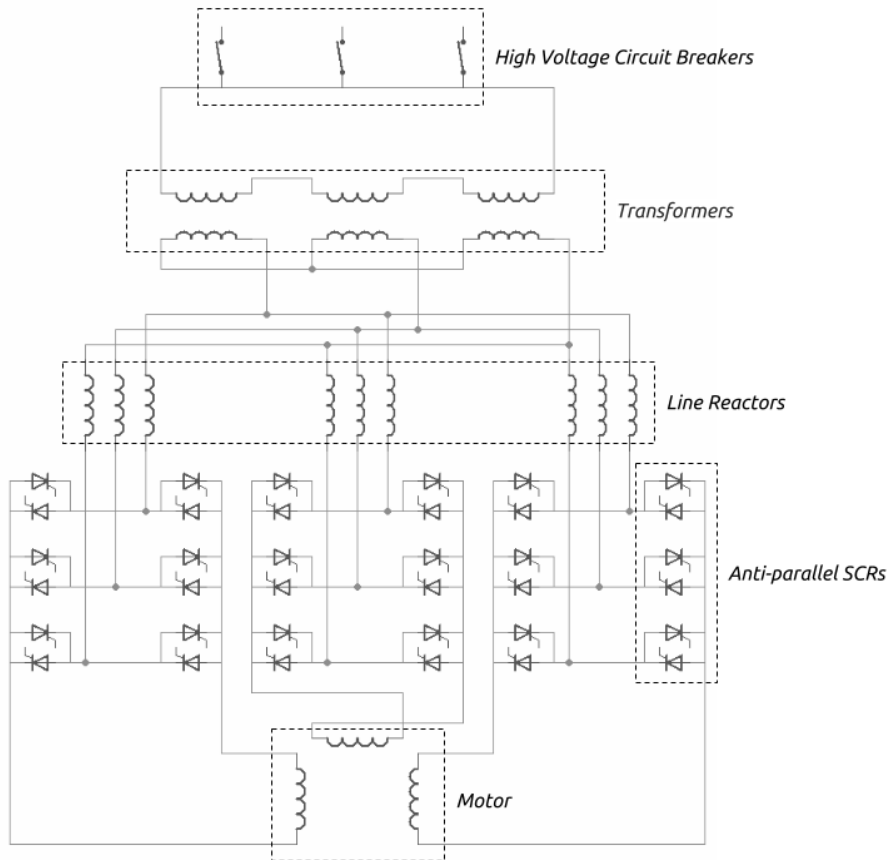


Figure 2-2. 6-Pulse (36 thyristor) cycloconverter diagram.

As was briefly mentioned in the introduction, like any drive a cycloconverter is used to output a signal at a desired frequency which is different than that of its input. In the case of the cycloconverter that frequency is lower than the input frequency. Consider the waveforms shown in Figure 2-3. The top waveform in Figure 2-3 a. shows the high frequency input voltage waveforms and output reference for a cycloconverter while Figure 2-3 b. shows in the solid line the theoretical unfiltered output voltage waveform and the desired output, illustrated by the dashed line. The output is constructed by enabling and disabling thyristors,

a type of bistable switch, in a very specific sequence such that the output waveform is pieced together by extracting portions of the inputs.

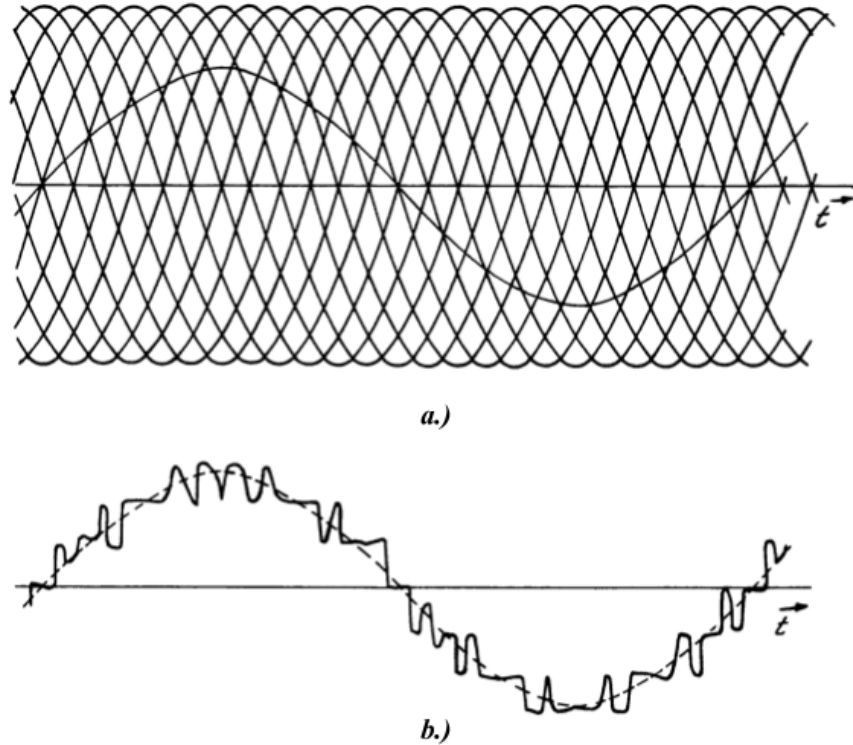


Figure 2-3. a.) 3- φ Input voltages (high frequency) and reference output (low frequency). **b.)** Output voltage (solid line) and reference output (dotted line) [27].

The thyristor is a type of solid-state semiconductor device consisting of an anode, cathode, and gate, that conducts current while the device is both forward biased and whose gate has been enabled by a sufficiently high current [1]. Once a current trigger is received the thyristor will latch and continue to conduct while forward biased. In 3 phase 6-pulse drives, thyristors are arranged in anti-parallel and into positive and negative banks. This is because traditional thyristors are unidirectional current conducting devices thus for ac waveforms, it is necessary to provide conduction for both positive and negative portions of the waveform. [1]

There are many methods to control the firing pulse sequences of the thyristors, but the method used most frequently, and also the method considered the most natural is that of the cosine wave crossing method [1] [28]. Each thyristor is turned on, or latched, at a specific time with respect to a sinusoidal desired output reference waveform. The time at which an individual thyristor fires is determined by the crossing point of an associated cosine timing wave. The cosine timing waves are derived from and synchronized to the converter input ac voltages. Their phase is such that their peaks occur at the earliest possible commutation angle $\alpha = 0^\circ$, also called the firing angle, of the associated thyristor [28]. Figure 2-4 shows a single sinusoidal reference waveform and the cosine timing wave corresponding to a single thyristor.

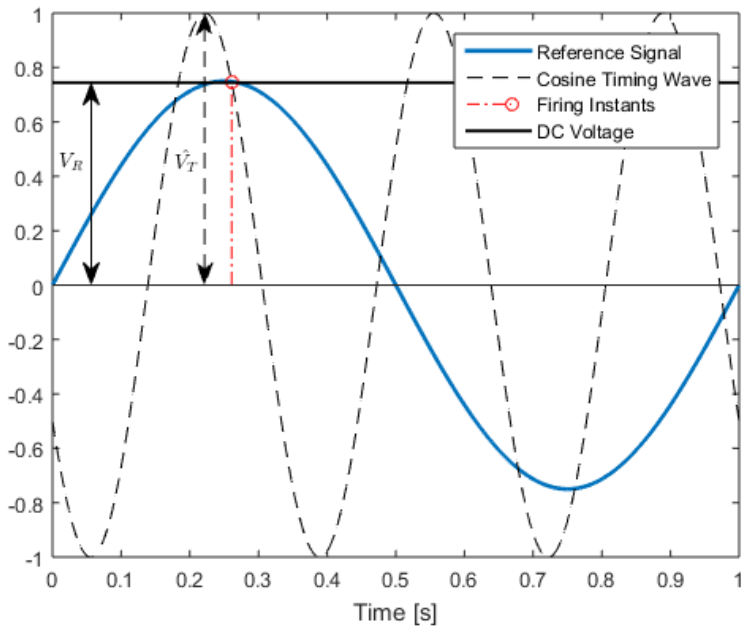


Figure 2-4. Example reference signal, cosine timing waves, and corresponding firing instants for an individual thyristor.

A firing pulse is initiated at the point at which the associated cosine timing wave becomes equal to the reference voltage. This is defined by [1]

$$V_R = \hat{V}_T \cos \theta_i \quad (2-1)$$

where \hat{V}_T is the peak value of the timing wave, V_R is the value of the analog reference voltage, and θ_i is $2\pi f_i t$ and f_i is the input frequency. At the required firing instant θ_i is equal to the firing angle α . Equation (2-1) becomes [1]

$$V_R = \hat{V}_T \cos \alpha \quad (2-2)$$

The firing angle α can be seen to directly relate to an output dc voltage. If this voltage can be modified continuously, then a sinusoidal output voltage can be obtained that is varied by the firing angle. The timing of the firing pulses of the cycloconverter are controlled such that it produces an alternating output. Thus, by controlling the frequency of the phase modulation of the firing angles of the converter, it is possible to control the frequency and amplitude of the desired component output voltage [1]. That is to say then that by continuously passing a varying reference voltage so that it looks sinusoidal, the firing angles will be modified such that they trigger the appropriate thyristor in order to construct the output waveform. With this in mind, it is possible to define the reference voltage waveform. Such a reference voltage waveform is given by [1]

$$v_r = r \hat{V}_T \sin \theta_o \quad (2-3)$$

where r is the ratio of the dc voltage of the converter at a firing angle α to the maximum possible mean dc voltage obtained at $\alpha = 0^\circ$, \hat{V}_T is the peak value of the cosine timing waves, and θ_o is $2\pi f_o t$ and f_o is the desired output frequency. Each thyristor has its own switching

function which has unity amplitude when the thyristor is activated, and zero amplitude at all other times. This function is shifted in time by the firing angle, thus is written [1]

$$F_T(\theta_i - \alpha) \quad (2-4)$$

where F_T is the thyristor of interest. Equation (2-4) is an infinite shifted harmonic series which makes up the square switching function. The position of this function in time, or the phase, is controlled by α . Pelly makes the case that by analysis of the waveforms and the times at which they become equal to the reference signal, the phase of each thyristor switching function can be defined as [1]

$$\alpha = f(\theta_o) = \sin^{-1} r \sin \theta_o \quad (2-5)$$

It is the control of these thyristor switching functions by which the output waveform can be constructed. In the next section, the implication of these facts on the harmonic content will be made apparent.

2.1.3 Cycloconverter Harmonics

Because of the fabricated nature of the output waveform, the cycloconverter input currents are inherently rich in harmonic content. These harmonics are the result of the input frequency and selected output frequency for the cycloconverter. Knowledge of these harmonics enables their prediction; this will allow for the development of a reference model to which the cycloconverter waveforms can be compared.

It is known that for a cycloconverter the input harmonics are both a function of the pulse order of the cycloconverter and the input and output frequencies chosen. The expression for this is given as [1] [29] [30]

$$f_H = |[kq \pm 1]f_i \pm 6nf_o| \quad (2-6)$$

where k is any integer from 1 to ∞ , n is any integer from 0 to ∞ , q is the drive pulse number, f_i is the input frequency, and f_o is the output frequency. This provides both the expected typical harmonic centers for any q pulse converter as well as the side band harmonics present around that harmonic as a result of the input and output frequencies. These frequencies, as a function of the ratio of the output to input frequency, for a 6 pulse cycloconverter with a balanced 3-phase output are expressed graphically in Figure 2-5.

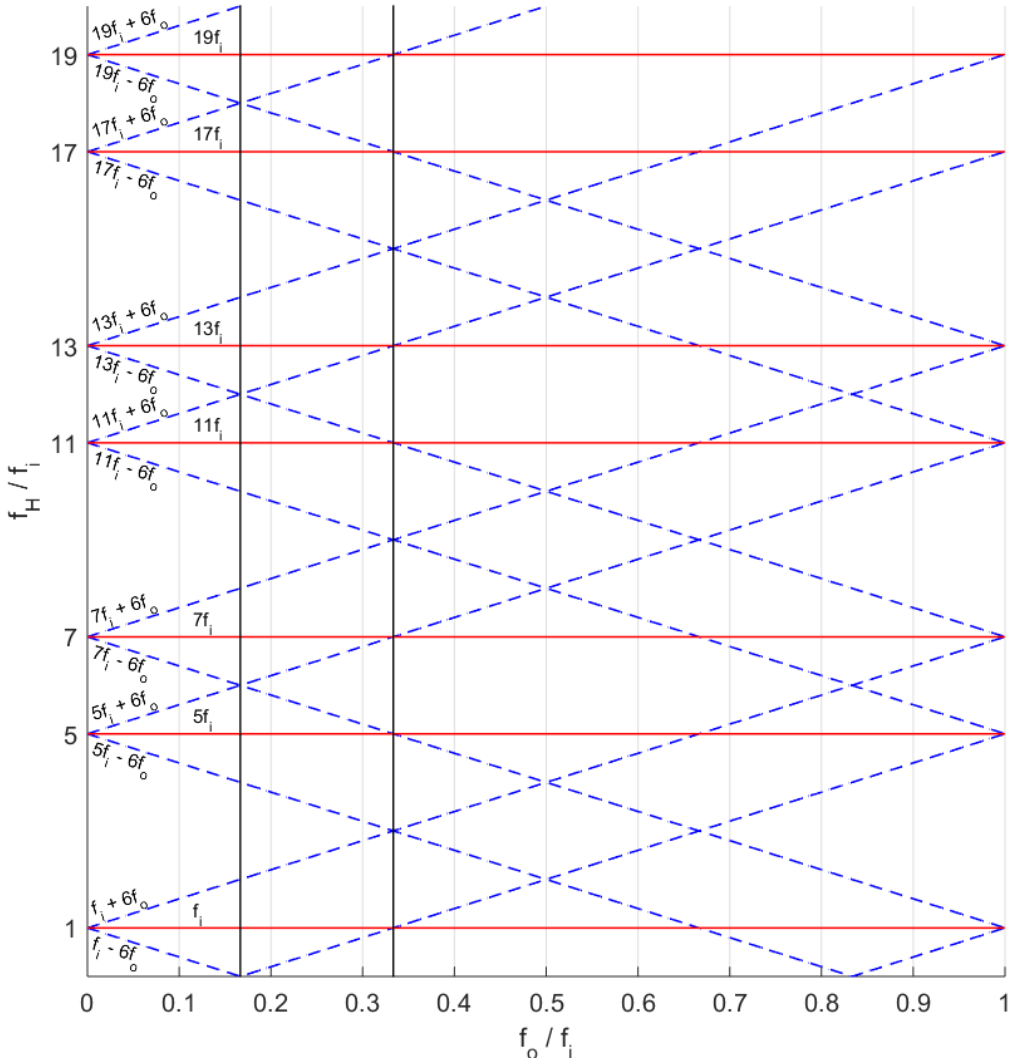


Figure 2-5. The expected harmonic centers (red solid lines) and associated side band frequencies (dotted blue lines) as a function of the ratio of output to input frequency for a 6 pulse cycloconverter with a balanced 3- φ output.

These frequencies and their importance will become evident in the joint time-frequency domain, but for now it is sufficient to make note that the frequency content found within the input current can be predicted.

An important caveat to note about the frequencies is that equation (2-6) describes only what frequencies are present, not their amplitudes. The amplitudes of the associated harmonics and their sidebands are a function of both the output voltage ratio and the load displacement angle ϕ_o [1]. Although these amplitudes are fixed and independent of the output to input frequencies, Pelly provides quantitative data that shows in general, as the harmonic order is increased the relative amplitudes of each harmonic decrease. This fact will play a role in helping define the modeling equation and error analysis to be discussed.

2.1.4 Frequency Modulation in the Time-Frequency Domain

Besides the frequencies of the harmonics, it is possible to derive an exact expression for the input current for a cycloconverter. Pelly considers the case of the 3-pulse single phase converter, but the same principles apply to the converters of any pulse number. As described by Pelly, the current waveform at the input terminals of the 3-pulse cycloconverter supplying a single phase load at its output can be expressed in terms of the output current, thyristor, and converter switching functions [1]. Mathematically this is [1]

$$i_A = \hat{I}_o \sin(\theta_o + \phi_o) \cdot F_1 \left(\theta_i - \frac{\pi}{2} + f(\theta_0) \right) \cdot F_P(\theta_o) \\ + \hat{I}_o \sin(\theta_o + \phi_o) \cdot F_1 \left(\theta_i + \frac{\pi}{2} - f(\theta_0) \right) \cdot F_N(\theta_o) \quad (2-7)$$

where \hat{I}_o is the peak value of the output current of the cycloconverter, F_1 is the thyristor switching function for thyristor 1 and takes the form of equation (2-4), and $F_P(\theta_o)$ and $F_N(\theta_o)$ are respectively the switching functions of the positive and negative converter banks. $F_P(\theta_o)$ has unity amplitude when the positive converter is enabled is zero otherwise; $F_N(\theta_o)$ is unity whenever the negative converter is in conduction and zero otherwise [1]. Because they are square waves, both of these are described by an infinite harmonic series of sinusoids. Let it be noted that the phase of the thyristor switching function is modified by the modulation function in equation (2-5). The takeaway from equation (2-7) however is not necessarily that the input current can be exactly described, although it can if given all of the terms, but instead that the thyristor switching functions are modulated sinusoidally. Because of this fact, it is proposed that the change in frequency over time which is observed in the joint time-frequency domain in subsequent sections is, at least in part, a result of this fact. Note also that equation (2-7) is dependent on the output current and the load displacement angle, which as was discussed in the introduction, are not data points that are monitored nor required by the method being proposed here. Therefore while this fact is a useful key, it is not the end-all.

2.2 Time-Frequency Analysis

2.2.1 The Spectrogram

As was previously discussed, the input current waveforms of the cycloconverter experience fluctuations in their frequencies over individual cycles. Before considering the definitions of the selected time-frequency distribution, it is beneficial to first review a sample of input current data and the corresponding time-frequency distribution. Figure 2-6 is an example of such a distribution.

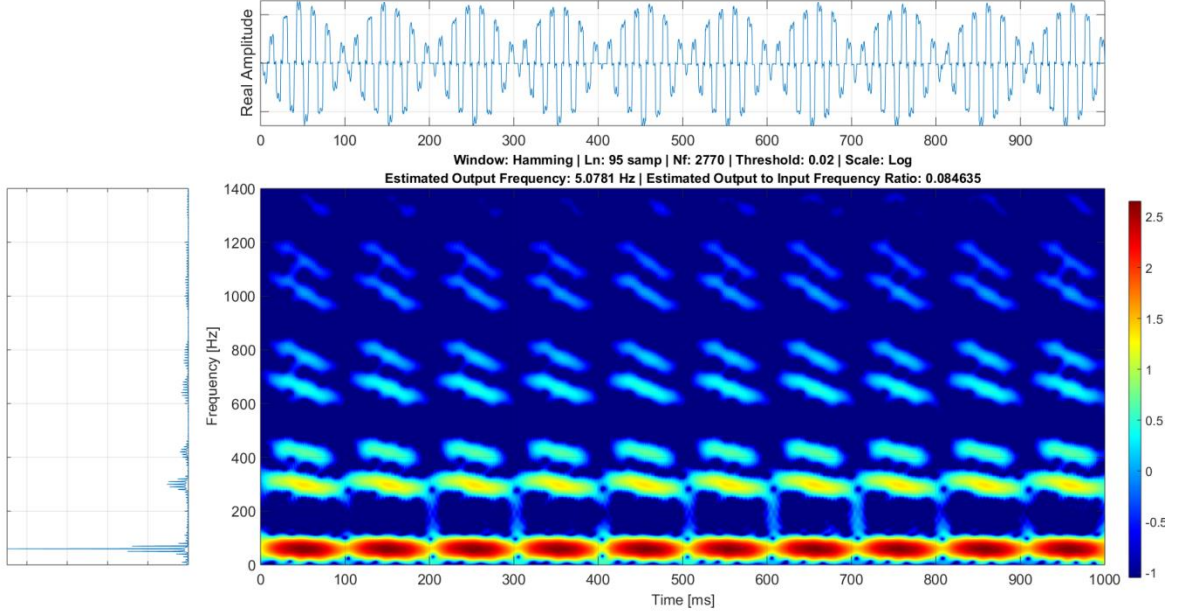


Figure 2-6. Sample spectrogram taken over one second.

Shown in the top graph is the raw current, the far left displays the frequency domain, and the center graph is the distribution itself.

This distribution is taken over a one second interval and between the frequencies of 0 and 1400 Hz. The change in frequencies over a single “island” (seen here as a high energy low frequency ellipse) exhibits why the cycloconverter input current is a prime candidate for analysis in the time-frequency domain and as was mentioned in the previous section, is believed to be the result of modulating the switching frequency sinusoidally. Though perhaps obvious, it is worth mentioning that the distribution shown in Figure 2-6 is three dimensional. An alternative view can be seen in Figure 2-7.

Before it is discussed in depth, it’s important to understand that all time-frequency representations can be obtained from [31]

$$C(t, \omega) = \frac{1}{4\pi^2} \iiint s^* \left(u - \frac{1}{2}\tau \right) s \left(u + \frac{1}{2}\tau \right) \phi(\theta, \tau) e^{-j\theta t - j\tau\omega + j\theta u} du d\tau d\theta \quad (2-8)$$

where $\phi(\theta, \tau)$ is a two dimensional function called the kernel which determines the distribution and its properties. The selection of the kernel provides a degree of control over the cross terms and other aspects of the signal in the time-frequency domain. In general, the visibility of cross terms, often seen as ripples or the presence of unexpected components in the time-frequency distribution, do not correspond to an intuitive sense of how the energy should be distributed. Moreover, time-frequency distributions are not strictly non-negative, that is, they contain negative components. The spectrogram limits the visibility of the cross terms and is always non-negative. These features provide a certain intuition about the energy content and spread found within the signal; for these reasons it is the distribution of choice in this research [32]. Its kernel function $\phi(\theta, \tau)$ is [31]

$$\phi(t, \tau) = \int h^* \left(u - \frac{1}{2}\tau \right) e^{-j\theta u} h \left(u + \frac{1}{2}\tau \right) du \quad (2-9)$$

This gives the definition of the spectrogram as [31]

$$C(t, \omega) = \left| \frac{1}{\sqrt{2\pi}} \int e^{-j\omega t} s(\tau) h(\tau - t) d\tau \right|^2 \quad (2-10)$$

where $s(\tau)$ is a windowed signal and $h(\tau - t)$ is a windowing function centered about t with running time τ . Multiplying the signal by the window function serves to emphasize portions of the signal individually and thus to take many different short-time Fourier transforms centered at time t . The magnitude squared of this calculation is the energy density spectrum at that specific time and the spectrogram is then the totality of these spectra [31]. It's worth noting however that the spectrogram does not satisfy the marginals for joint densities, expressed mathematically in equations (2-11) and (2-12). This is because the spectrogram scrambles the energy distributions of the window with those of the signal [31]. It also does not ever satisfy the uncertainty principle expressed in equation (2-13) [31].

$$C(t) \neq |s(t)|^2 \quad (2-11)$$

$$C(\omega) \neq |S(\omega)|^2 \quad (2-12)$$

$$\sigma_t \sigma_\omega \geq \frac{1}{2} \quad (2-13)$$

where σ_t is the signal duration and σ_ω is the bandwidth. If the window were narrowed, then $\sigma_\omega \rightarrow \infty$ and would be the equivalent of taking the general Fourier transform. Other time-frequency distributions were taken, but none provided the same level of clarity or intuition as the spectrogram. The window size used was 95 samples. Note that the number of samples corresponds to the frequency content found within the signal, and the signal was decimated such that it only contained frequencies up to 1380 Hz. The chosen window size provided good localization in both the time and frequency domains.

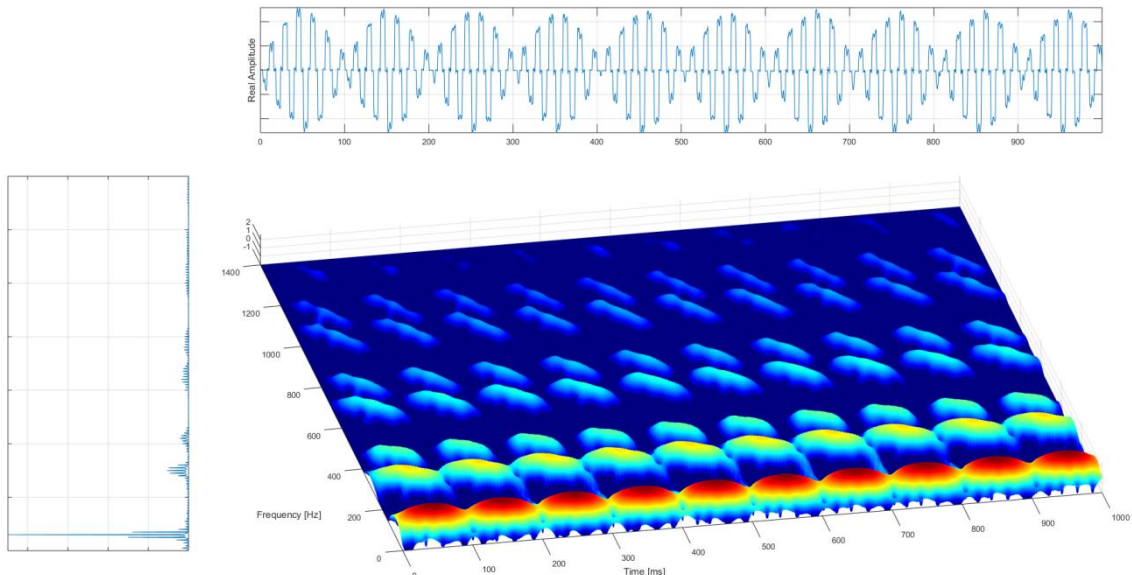


Figure 2-7. 3-D view of sample spectrogram from Figure 2-6.

2.2.2 Frequency Average

Though not strictly related to the time-frequency domain, an important method utilized for analysis of the cycloconverter input current is the average frequency of the signal. This is defined as is shown in equation (2-14) [31].

$$\langle \omega \rangle = \int \omega |S(\omega)|^2 d\omega \quad (2-14)$$

Its importance has to do with the identification of the centers of the chirps found in the spectrogram as is shown in Figure 2-6 and Figure 2-7. A chirp in this instance refers to the content in the spectrogram associated with a specific frequency. The center frequency can be seen as the peak in the frequency domain, therefore a chirp is the frequency content found about this center. The center itself is known as the harmonic and corresponds to the solid red lines of Figure 2-5. Passing equation (2-14) upper and lower bounds as dictated by the dotted blue lines of Figure 2-5 for the chirp of interest provides us with a frequency center associated with that specific chirp.

2.3 Spectrogram and Data Analysis

2.3.1 Input Current Data and Spectrogram Modifications

Input current data for the cycloconverters was provided by Nucor Steel Berkeley located in Huger, South Carolina, United States of America. Data was provided from three different cycloconverters. There are a total of seven cycloconverters currently in use at Nucor Steel Berkeley, and the cycloconverters will be referred to as F1, F2, F3, F4, F5, F6, or F7. Data was provided for F1, F2, and F6. Nine datasets for loaded motors were provided, one of which was that of a damaged cycloconverter⁴. Ten datasets were provided for unloaded motors, none of which were damaged. Some of these datasets overlap so there are not 19 datasets in total, only 19 analyses that can be made. For loaded motors, spectrograms of one second were taken. This tended to provide clarity such that the characteristics of the signal were very easily distinguishable. It's also notable that computational time increases dramatically the longer the period of analysis. Unloaded motors were analyzed over one second where data was available. For some of the datasets that combine the unloaded and loaded states the motor transitioned before one second. In these instances the data was analyzed until the point of transition (usually between .5 and .75 seconds). The point at which data is taken is the input phases to the cycloconverters, that is, after the secondary of the step-down transformers for the cycloconverters. Data was provided with a sample rate f_s of 74,767 samples/second which was decimated to 2,769 samples/second to decrease the required computation time. The hope is that the cycloconverters can be analyzed and features which characterize the normal functioning state of the cycloconverter can be identified and used to diagnosis the cycloconverter status. For all cases at least one phase was provided and in all of the research presented here, the phase current for a single phase is analyzed. All data analysis was

⁴ Shortly before the completion of this document, Nucor provided an extra dataset for loaded motors. This dataset was not included in the harmonic slope analysis, but is for the statistical analysis in following sections.

performed using MATLAB in conjunction with a third party time-frequency toolbox plugin developed by Rice University (USA) and CNRS (France).

Two important modifications that have been made to the spectrogram are a threshold level implementation and the utilization of logarithmic scaling. The threshold value is chosen as a percentage of the maximum value found within the spectrogram and is given by equation (2-15). Here, a threshold level of .02% was chosen.

$$C[n, m] = \max \left(C_{min}, C_{max} \frac{L}{100} \right) \quad (2-15)$$

where C corresponds to spectrogram, n and m are the corresponding coordinates in the two dimensional matrix that composes the discrete spectrogram, C_{min} is the minimum value found within the spectrogram, C_{max} is the maximum value found within the spectrogram, L is the desired threshold level as a percent, and max is a function which selects the maximum value between the arguments given. Logarithmic scaling serves to emphasize high frequency content. Spectrograms that do not enable thresholding or log scaling are shown in Figure 2-8 and Figure 2-9. It is evident from these images that both thresholding and log scaling are required.

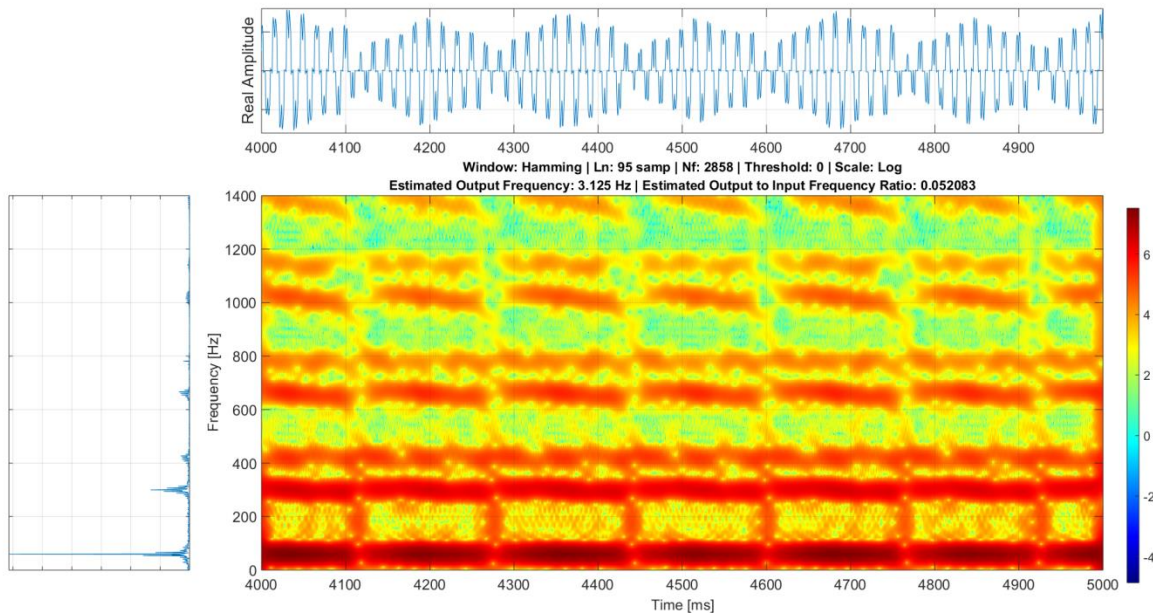


Figure 2-8. Spectrogram of F6 input current data with a threshold of 0.

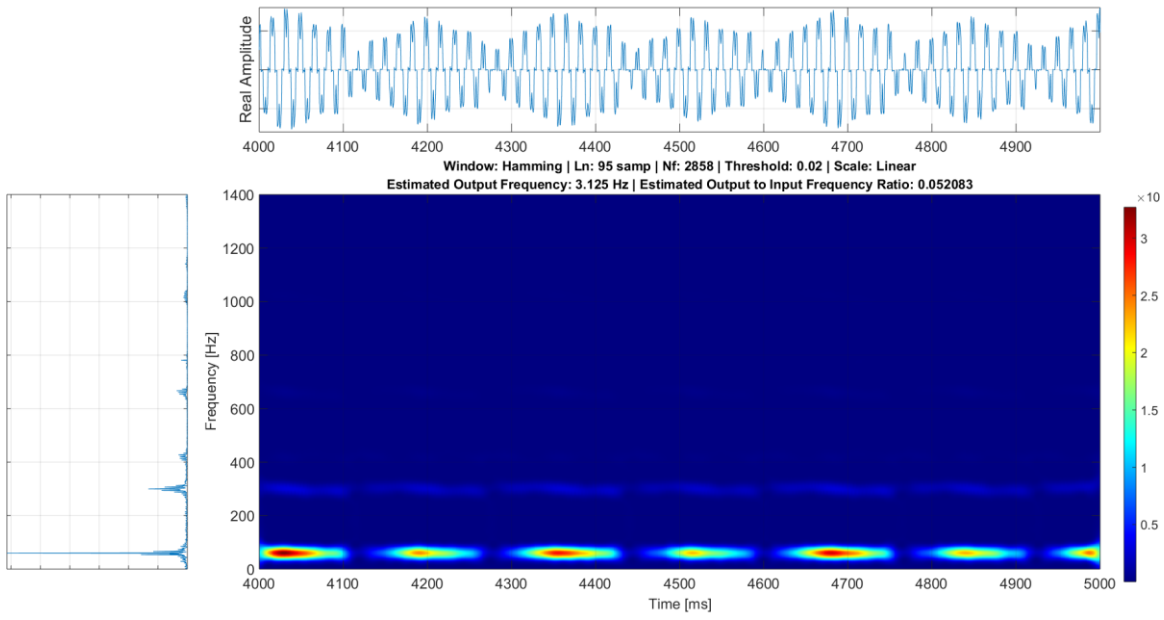


Figure 2-9. Spectrogram of F6 input current data with linear, not logarithmic, scaling.

Below are several spectrograms that show appropriate thresholding and scaling. Looking at these spectrograms it is clear that the highest energy content is found at 60 Hz. This follows from the 60 Hz frequency utilized in North America for electric power transmission and is expected.

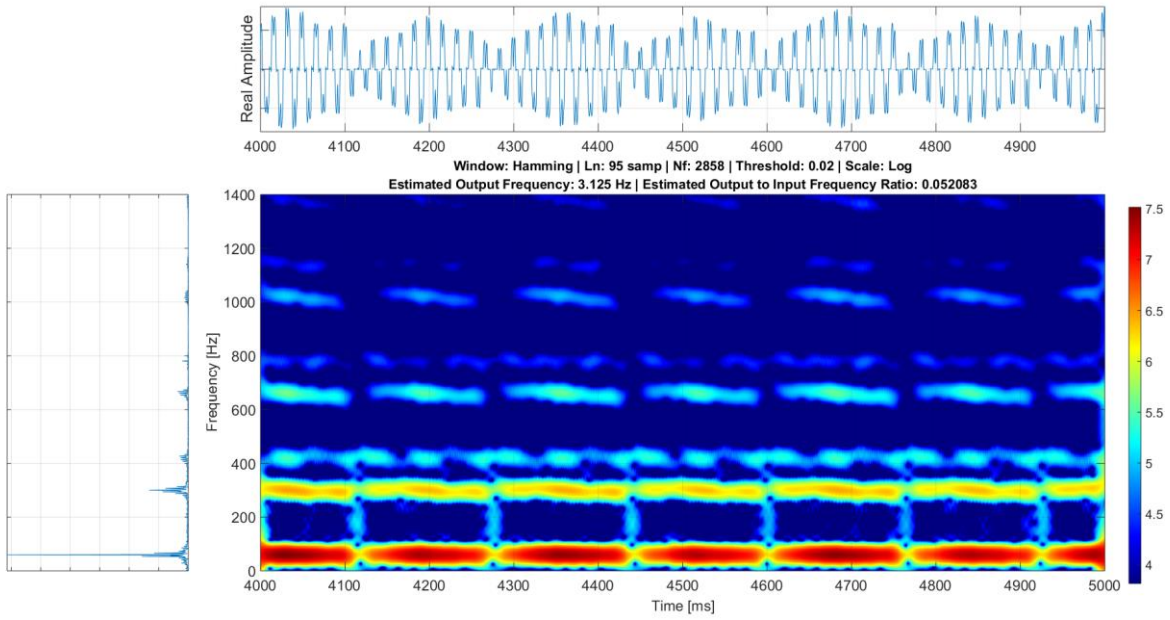


Figure 2-10. Spectrogram of one second of data for a loaded F6.

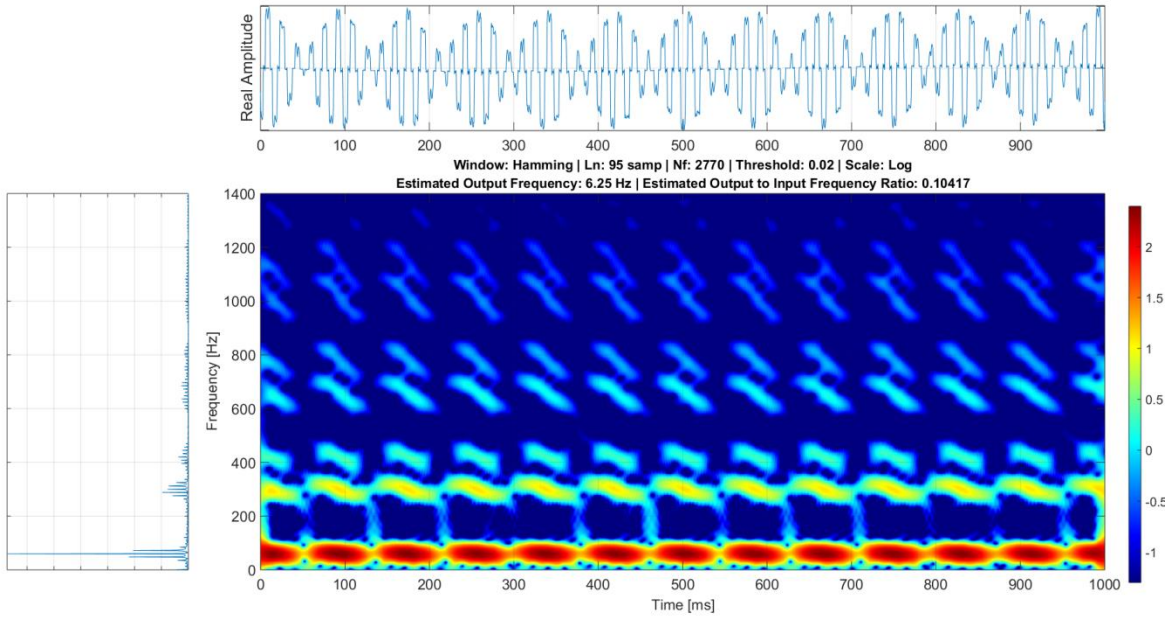


Figure 2-11. Spectrogram of one second of data for a loaded F1.

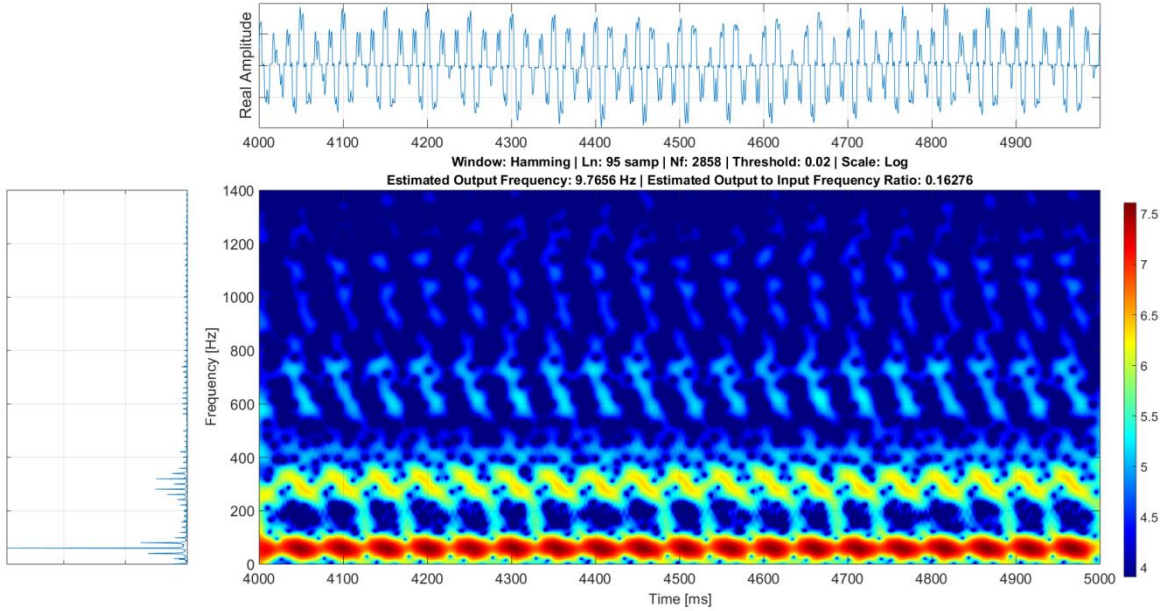


Figure 2-12. Spectrogram of one second of data for a loaded F6.

2.3.2 Output Frequency

For each cycloconverter, only the input current data was provided, not the corresponding output frequency reference. It was required then to estimate the output frequency from this data. The frequency estimation technique is rudimentary, but appears to be effective. The maximum value of each column along the x-axis is taken to produce a 1 dimensional matrix, and then their average is taken and subtracted in order to remove the dc component. These values invariably correspond to the values which fall along the 60 Hz fundamental frequency

as these contain the highest energy content. A sample of this for Figure 2-12 is visualized in Figure 2-14. One could imagine that Figure 2-14 is a single slice of the 3 dimensional spectrogram along the x-axis where that slice is centered at 60 Hz. The fact that the slice corresponds to an approximately straight line centered at 60 Hz is a result of the fact that the maximum values lie along this frequency. If there were a fault this would not be the case. The Fourier transform of this data is then taken where the frequency corresponding to maximum peak is the frequency of interest. Note that the dc component was removed such that the maximum peak corresponds to the frequency content of interest and not the zero frequency component. The Fourier transform of this data is shown in Figure 2-15.

The frequency location of the maximum peak is twice the output frequency. This is because the spectrogram is the magnitude and corresponds to the upper envelope of the time domain signal; therefore the frequency of the maximum values in Figure 2-14 corresponds to the frequency of the upper envelope which is twice the output frequency. The output frequency is then half of the location of the peak. An example of this concept is demonstrated in Figure 2-13. The signal in bottom graph represents the output frequency of the cycloconverter, whereas the top one is an envelope with twice that frequency.

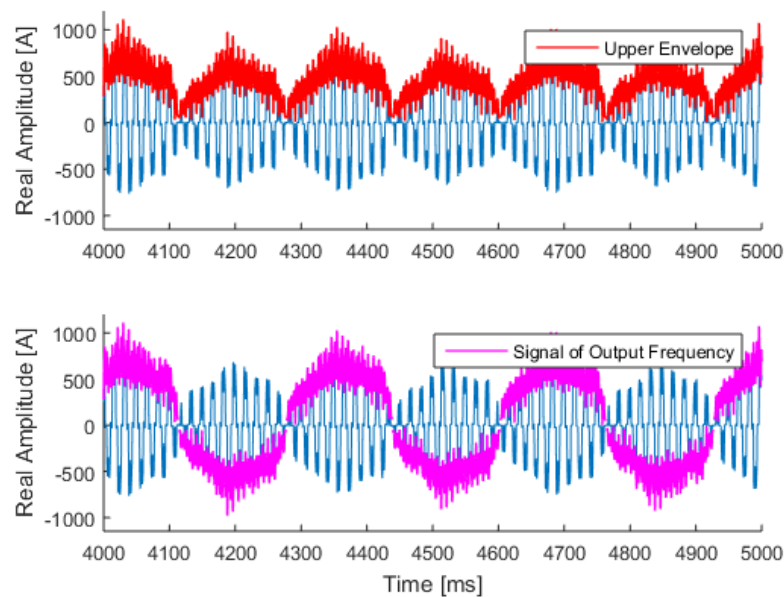


Figure 2-13. Sample signal envelope and signal of output frequency.

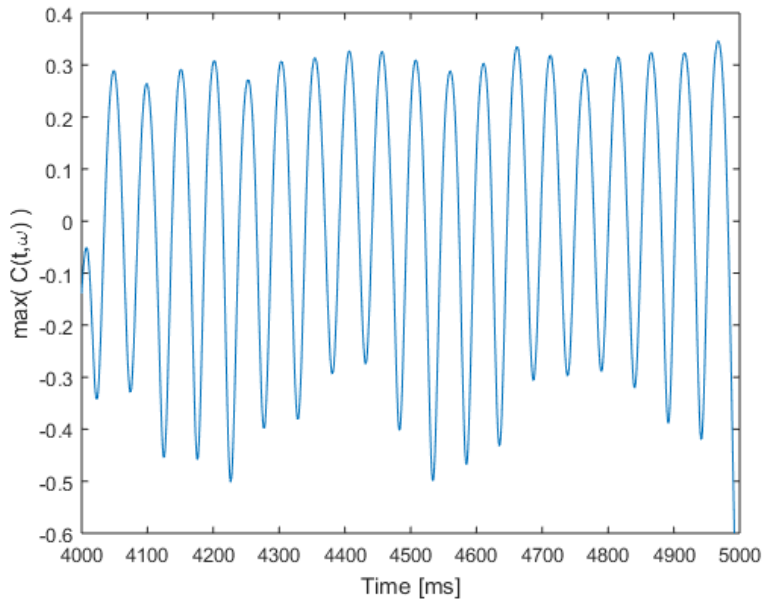


Figure 2-14. Maximum values taken along the x-axis of the thresholded and logarithmically scaled spectrogram for Figure 2-12.

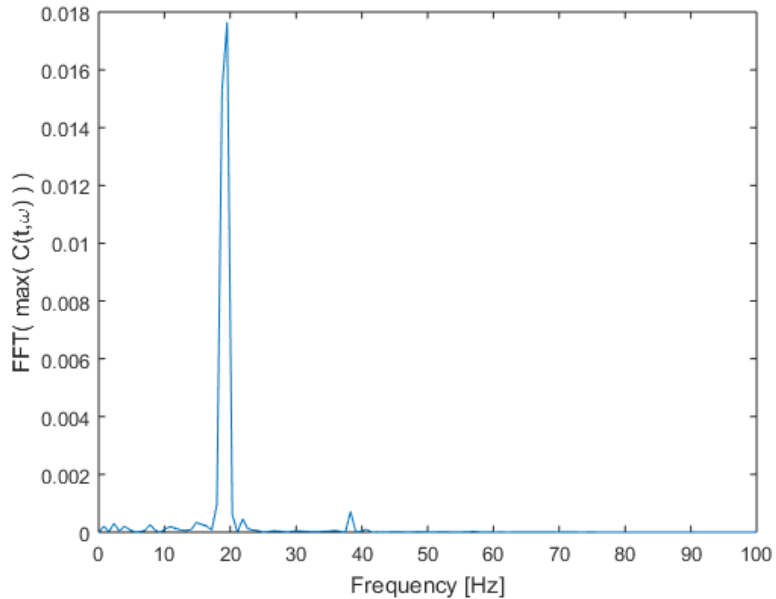


Figure 2-15. Fourier transform of the maximum values taken along the x-axis of the thresholded and logarithmically scaled spectrogram of Figure 2-12.

2.3.3 Frequency Centers

The frequency harmonics found within the spectrogram correspond to the frequency centers of each chirp. As expected by equation (2-6), the harmonics expected for a 6 pulse drive are the 5th, 7th, 11th, 13th, 17th, and 19th. With a fundamental frequency of 60 Hz, these harmonics correspond to frequencies of 300 Hz, 420 Hz, 660 Hz, 780 Hz, 1020 Hz, and 1140

Hz. Obviously this pattern for the harmonic order will continue until infinity, but this research only analyzes up to the 19th harmonic. Energy content in the spectrogram after this is so diminished that even in a log scale it becomes insignificant. Equation (2-14) allows us to find the average frequency which will correspond to a frequency center, but because the computational tools utilized compute the average frequency of the entire signal, it is necessary to first filter the time domain data to localize the chirp of interest. A 10th order bandpass elliptic filter with a stopband attenuation of 150 dB and a peak-to-peak passband ripple of 3 dB centered about the expected harmonic was used for the 5th, 7th, 11th, 13th, and 17th harmonics. A lowpass filter was used for the fundamental and a highpass for the 19th harmonic. This was chosen after various filter trials and provided sufficient attenuation of the chirps which are not of interest and localization of the chirp of interest. The upper and lower cut-off frequencies for filters (or upper or lower cut-off frequencies respectively for the fundamental and 19th harmonic) are provided by the frequency spread predicted by equation (2-6). Samples of several of these bode plots are given in Figure 2-16.

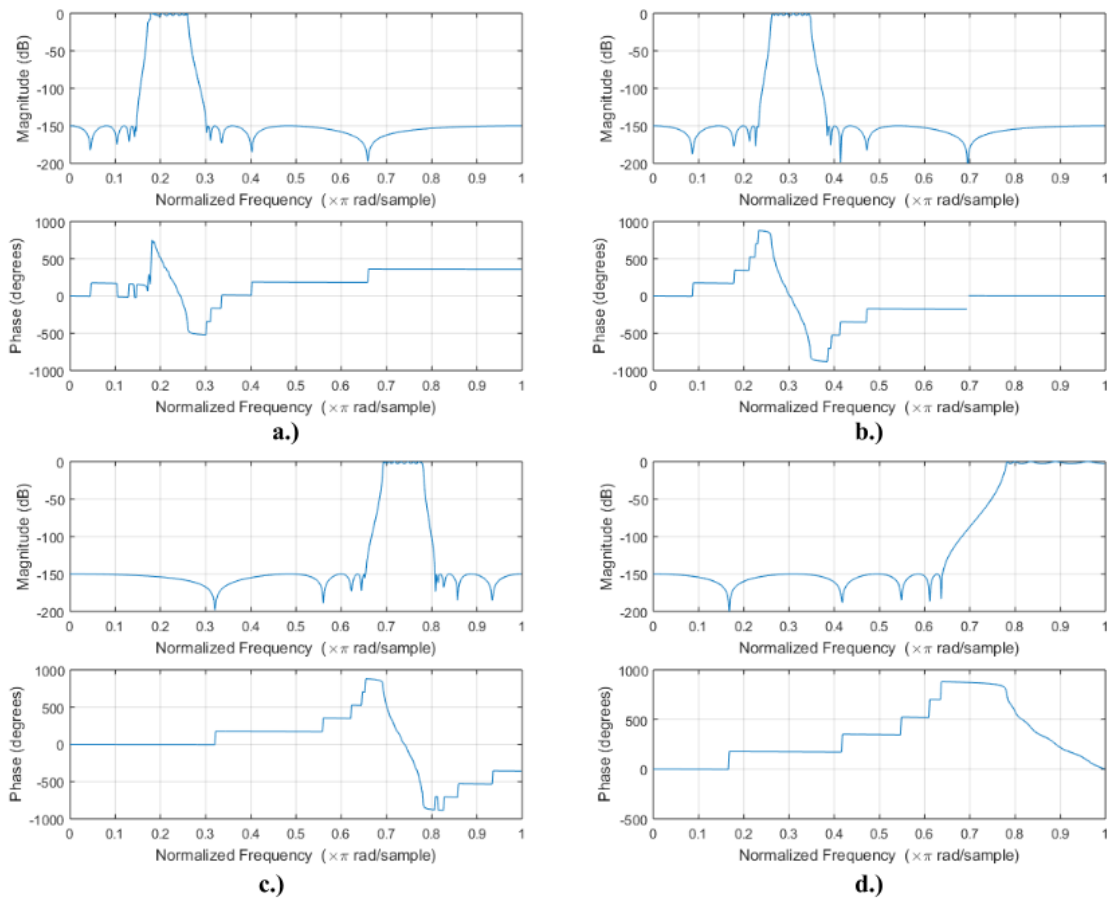


Figure 2-16. 10th order elliptic filters with a stopband attenuation of 150 dB and passband ripple of 3 dB.
a.) 5th Harmonic. b.) 7th Harmonic. c.) 17th Harmonic. d.) 19th Harmonic.

It is expected that the frequency centers of each harmonic always lie about the harmonic center. For loaded motors this is generally true, except in the case where the frequency spread of an individual harmonic becomes great enough that it begins to interfere with harmonics which are close together (for example the 5th and 7th harmonics). This can be seen graphically

as the left-most solid vertical black line in Figure 2-5 as the point where the dotted blue lines from any two harmonics intersect; this corresponds to an output to input frequency ratio of $\frac{1}{6}$. When interference is present, the frequency averages are no longer accurate because we are then including frequency content from other chirps in the frequency average calculation. This is one of two reasons, the other of which is discussed in the following section, why certain harmonics are ignored in the modeling technique proposed by this study.

Table 2-1 shows the frequency averages as calculated by this method for the various harmonics. Note that the fundamental chirp is consistently centered at 60 Hz and is therefore not listed. It's known that for three phase cycloconverters and motors in general having a balanced load, the energy content of lower order harmonics is typically greater [1]; this was mentioned in section 2.1.3. For this reason, when the output to input frequency ratio spread becomes greater and interfere, the lower order harmonic energy content will dominate the nearby high order harmonic. Although most of these ratios are below the required $\frac{1}{6}$ crossover point shown in Figure 2-5, interference can be seen even at lower ratios. The presence of this increased harmonic spreading is likely due to non-idealities in the system. Consider first that the motor's load is not necessarily perfectly balanced. This will cause equation (2-6) to not hold perfectly, and unexpected frequency content can be introduced into the harmonic series which defines the input current and causing the THD to rise even at lower ratios [1] [33]. Other non-idealities include torque fluctuations which can result in speed deviations and a consequential shift in the output to input speed ratio [34].

Figure 2-17 shows the spectrogram for a loaded motor with an input to output ratio of approximately 0.0846. This ratio is below the point of interference, yet still it can be seen that the upper frequency of some of the higher order chirps start to interfere with some of the lower order chirps. The dotted white lines represent the frequency center of that chirp.

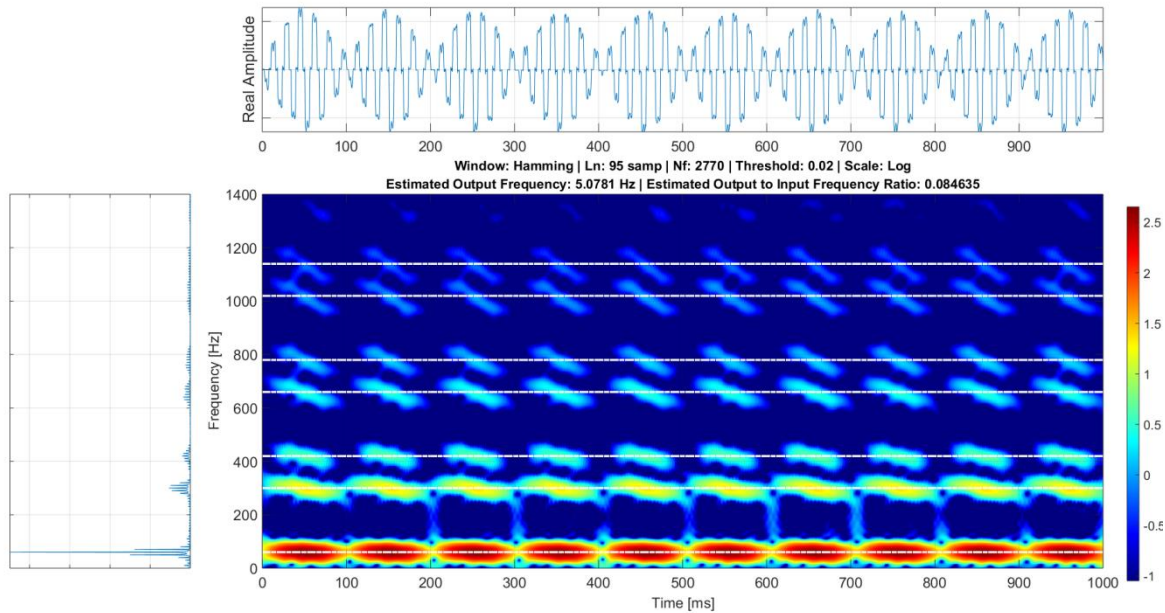


Figure 2-17. Frequency centers (white dotted lines) associated with each harmonic chirp for a loaded motor on F1 with ratio of approximately 0.0846.

Consider now Figure 2-18. The energy content at this output frequency is much more spread, and some chirps, especially the higher order harmonic corresponding to a nearby lower order harmonic neighbor⁵ (so the 7th, 13th, and 19th) are not particularly well defined.

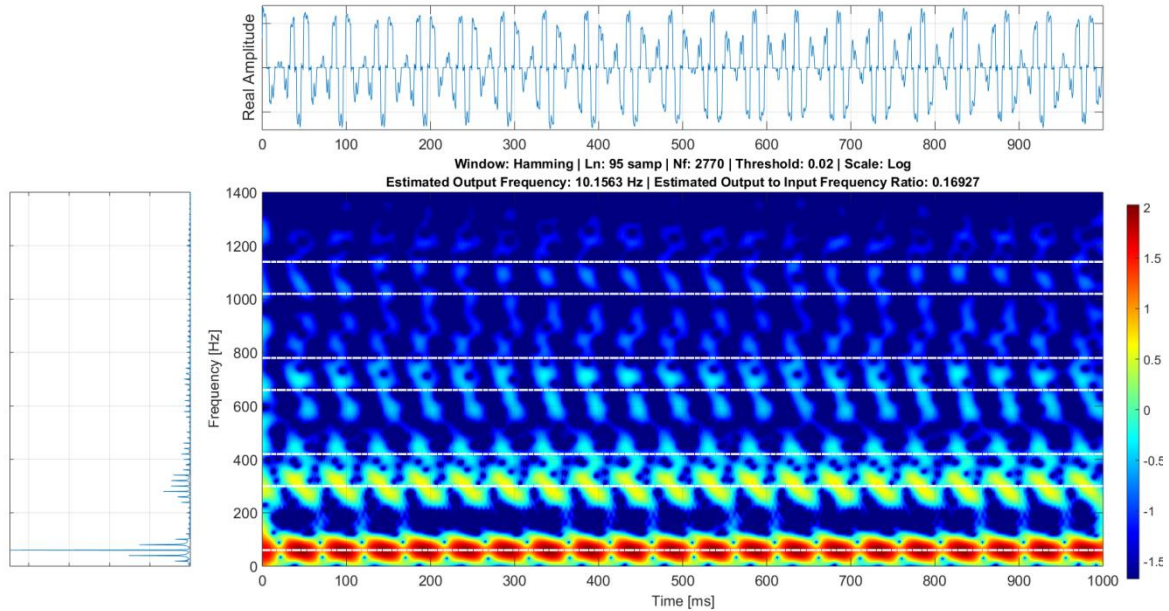


Figure 2-18. Frequency centers (white dotted lines) associated with each harmonic chirp for a loaded motor on F2 with ratio of approximately 0.1693.

The frequency centers for each harmonic are calculated and their differences from the expected frequency center of its corresponding harmonic are listed in Table 2-1. Frequency centers with a difference of greater than 10 Hz are highlighted in red. In general, frequency centers are poorly defined for the higher ratios and for the higher order harmonics with a close neighbor. As will be seen, this has an effect on the harmonic slope calculation as well. Note that some of the difference in Table 2-1 is the result of the resolution of the frequency bins of the Fourier transform in the discrete domain. As a consequence, there may not exist a frequency bin with exactly the frequencies of interest, so we must instead take the closest frequency bin to that value.

⁵ A higher order harmonic with a close neighbor will always refer to the 7th, 13th, and 19th harmonic.

Table 2-1. Differences in frequency centers of input current harmonics from the expected frequency centers for loaded datasets.

Fund. Freq (Hz)	60		Difference in Frequency Centers (Hz) for each Harmonic					
Output Frequency (Hz)	Notes	f_o/f_i	5 th	7 th	11 th	13 th	17 th	19 th
3.1250	F6	0.0521	0.67181	1.61357	1.06676	4.5575	2.81985	9.04592
4.6875	Damaged F1	0.0781	1.70182	4.61863	3.70852	6.8241	5.41532	13.574
5.0782	F1	0.0846	2.36066	5.89878	3.06556	3.4428	1.35837	8.48903
5.8900	F6	0.0982	0.44913	3.25143	4.99362	4.26692	1.47436	14.5271
6.2500	F1	0.1042	0.64128	0.77556	1.83172	4.90908	7.37214	6.36295
7.4219	F6	0.1237	0.69809	12.4981	2.06819	24.7826	15.0807	25.0718
8.5938	F6	0.1432	5.35541	13.8169	8.34823	28.1317	10.0451	35.8313
9.7657	F6	0.1628	2.05665	25.3822	0.16519	51.2453	1.7362	50.6884
10.1563	F2	0.1693	4.96555	31.8312	3.60641	60.0697	3.90778	63.3621

In previous spectrograms, the cycloconverter being analyzed is driving a loaded motor. One of the defining characteristics of the loaded motor is the sloping in time of the frequency content. Unloaded motors decidedly do not exhibit this characteristic, and their spectrograms are shown in Figure 2-19 and Figure 2-20. The reason for this is not explicitly known, and as there has been little research in this area, there is little background on which to establish a solid reason. Also of interest is the fact that as the output frequency rises, the frequency content of the spectrogram also rises. This can be seen by comparing Figure 2-19 and Figure 2-20 where the dotted white lines correspond to the expected locations of the frequency centers of each chirp. This was unexpected, but is shown soon to be linear. One might expect that the lack of frequency modulation for unloaded motors invalidates the reasoning provided earlier for the observance of frequency modulation for loaded motors. Rather though, it is thought that the same reason that causes the frequency centers to rise is responsible for the lack of change in frequency content over time. Indeed, equation (2-6) predicts the frequency content for loaded motors, but for unloaded motors this equation does not hold. However, if we examine Figure 2-21 during a transition from unloaded to loaded states, we find that the upper frequency content of the harmonic of the loaded motor approximately corresponds to the location of the frequency center for the unloaded motor. This helps explain the linear rise that will be shown shortly. As the rise is linear, it seems probable that the locations of the frequency centers of unloaded motors correspond, though not necessarily directly, to the upper frequency spread of each harmonic from the harmonic equation (2-6). While this fact may not aid in the development of the techniques proposed here, it is an interesting point potentially of importance in future work.

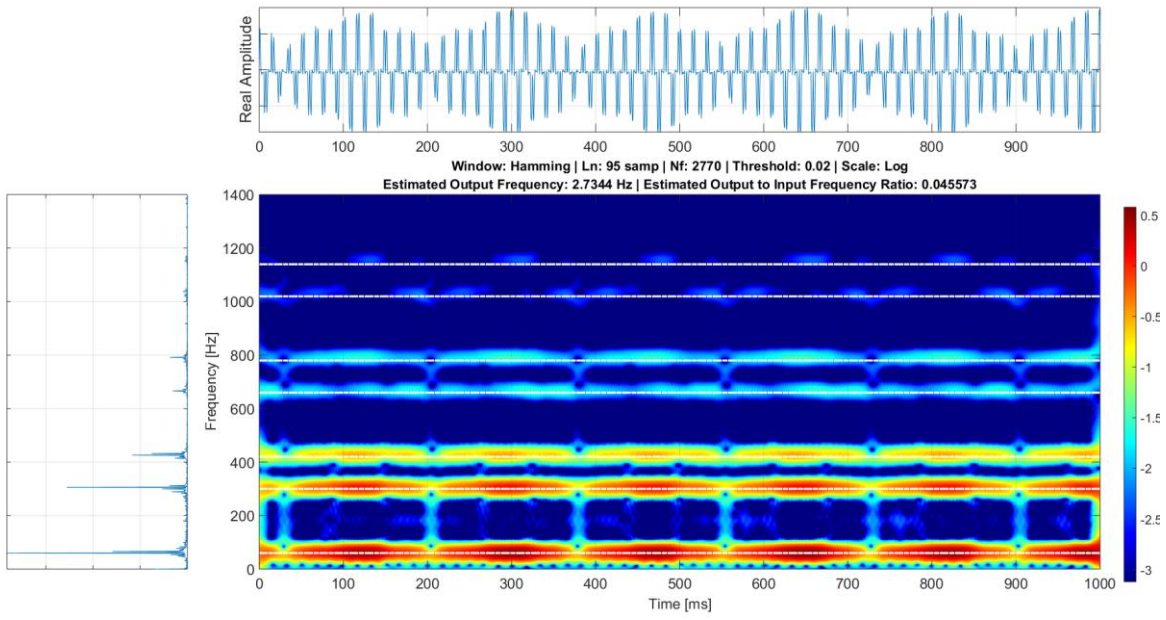


Figure 2-19. Frequency centers (white dotted lines) associated with each harmonic chirp for an unloaded motor on F1 with ratio of approximately 0.0456.

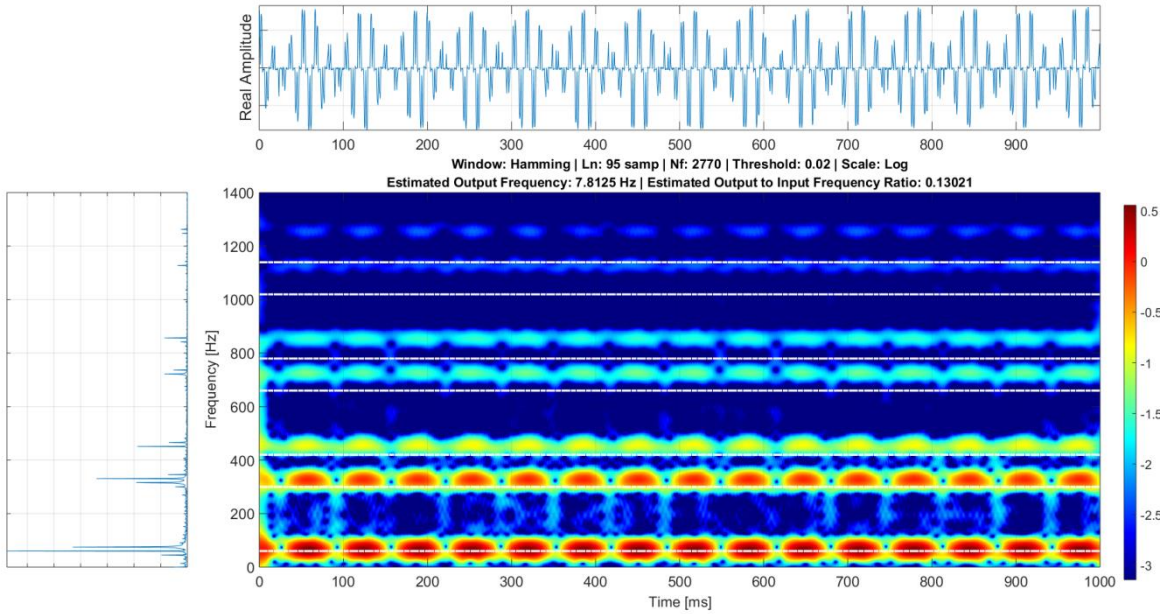


Figure 2-20. Frequency centers (white dotted lines) associated with each harmonic chirp for an unloaded motor on F1 with ratio of approximately 0.1302.

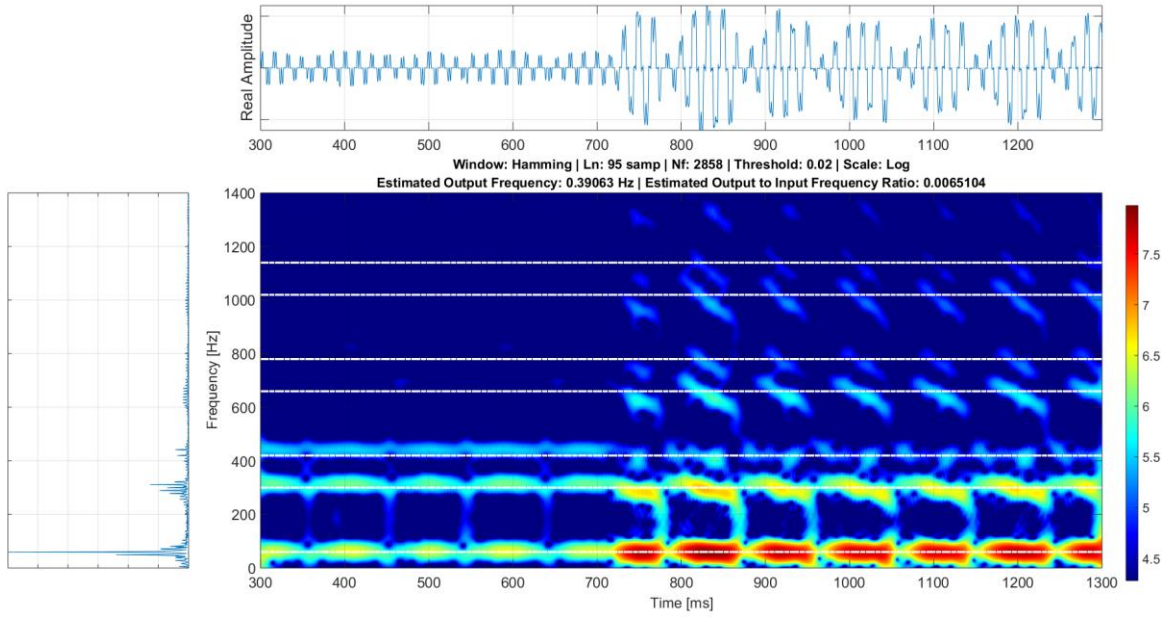


Figure 2-21. Transitional loading case for F6.

The same method for frequency center calculation of loaded motors was employed for those of unloaded motors. The resulting data is charted in Table 2-2.

Table 2-2. Frequency centers of input current harmonics for unloaded datasets.

Fund. Freq (Hz)	60	Frequency Centers (Hz) for each Harmonic								
Output Frequency (Hz)	Notes	f_o/f_i	1 st	5 th	7 th	11 th	13 th	17 th	19 th	
2.7344	F1	0.0456	61.3866	304.748	426.475	666.659	791.399	1028.72	1167.53	
2.7344	F2	0.0456	61.1906	304.22	427.181	665.306	791.56	1027.7	1155.58	
3.125	F6	0.0521	61.9667	305.409	427.245	666.929	792.952	1031.83	1167.61	
4.6875	F1	0.0781	62.0921	310.016	434.835	676.757	818.664	1052.51	1172.82	
5.0781	F6	0.0846	63.3391	313.103	439.498	688.539	830.172	1066.91	1209.55	
6.25	F6	0.1042	64.4496	314.176	445.506	705.341	839.348	1094.53	1219.01	
7.4219	F6	0.1237	66.791	326.33	451.01	717.439	856.179	1129.96	1253.63	
7.8125	F2	0.1302	64.6918	323.471	453.416	721.242	858.666	1145.3	1260.14	
8.5938	F6	0.1432	66.4499	328.885	457.599	729.928	866.812	1183.18	1272.74	
9.375	F6	0.1563	67.2197	331.607	463.253	742.134	875.432	1157.62	1287.49	

This data was then plotted, and a linear function was fit to each harmonic. It becomes evident that this rise in the frequency centers of harmonics is linear.

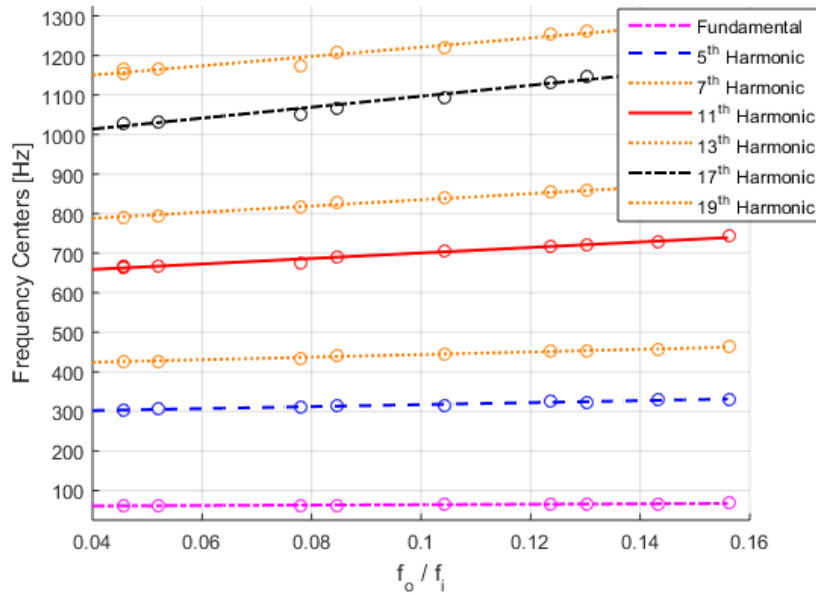


Figure 2-22. Frequency centers of input current harmonics for unloaded datasets.

The linear regression function for each harmonic is given by the following equation, though only the 5th, 11th, and 17th are used in this research.

$$\alpha_h \left(\frac{f_o}{f_i} \right) = a \left(\frac{f_o}{f_i} \right) + b \quad (2-16)$$

where α is the rise of the frequency center, h corresponds to either the 5th, 11th, or 17th harmonic, and the coefficients a and b are determined by Table 2-3.

Table 2-3. Coefficients for equation (2-16). $h = 1$ corresponds to the fundamental.

	Coefficient	
	a	b
<i>h</i>	1	53.427
	5	250.63
	7	327.43
	11	694.3
	13	780.54
	17	1384.7
	19	1175.9

2.3.4 Harmonic Slopes

The harmonic content present corresponds to those predicted by equation (2-6). The center of each of these harmonics corresponds to the solid red lines of Figure 2-5, and the spread about that center corresponds approximately to the dotted blue lines. Though it has

already been stated, every spectrogram for a loaded motor experiences a change in frequency over time when looking at a specific “island”. As was previously mentioned, an island is the ellipse in the spectrogram and corresponds to a single cycle, or hill, of the upper envelope in the time domain. Across the entire one second interval, the signal is stationary and can be considered in steady state, but as can be seen in the time-frequency domain, it is not strictly stationary across a single island. As the output frequency to input frequency ratio rises, the rate of change of the frequency content within an island becomes steeper. This is also expected because as seen in Figure 2-5, as the ratio increases the spread about the harmonic center becomes wider, but in the spectrogram a single island becomes shorter. Consequently, an increase in the rate of change of the frequency content in time is observed. We see however, that not only does the rate of change overall increase with an increase of the ratio, the rate of change of the energy content of higher order chirps also increase relative to chirps of lower order harmonics. This phenomenon is observed in Figure 2-10, Figure 2-11, Figure 2-12, Figure 2-17, and Figure 2-18. The rate of change of those frequencies is referred to hereon out as the harmonic slopes because they are the consistent rates of change which correspond to each chirp centered about a harmonic. Their determination is vital and what follows is a discussion of the technique utilized to extract the harmonic slopes. All of this analysis takes place over spectrograms of 1 second intervals.

Consider first the spectrogram of Figure 2-23. The white dotted lines correspond to the frequency centers of each chirp which correspond to the 5th, 7th, 11th, 13th, 17th, and 19th harmonics. First the chirp of interest is localized by simply ignoring everything with which we aren’t concerned. This is done by fitting a window about the chirp of interest with upper and lower limits of the windows dictated by equation (2-6). The maximum values along the x-axis are taken, similar to the output frequency estimation procedure. The dc component of these values, that which corresponds to the center of the limited window, is removed and the values are then filtered by a narrow single pole Butterworth filter with upper and lower cut-off frequencies are ± 4 Hz respectively of twice the output frequency. For well-defined chirps, this filter should have a smoothing effect on the maximum values because the dominant frequency in the maximum values should correspond directly to twice the output frequency, i.e., the frequency of the envelope of the time domain signal. If it does not then the signal will simply look like an attenuated noisy signal.

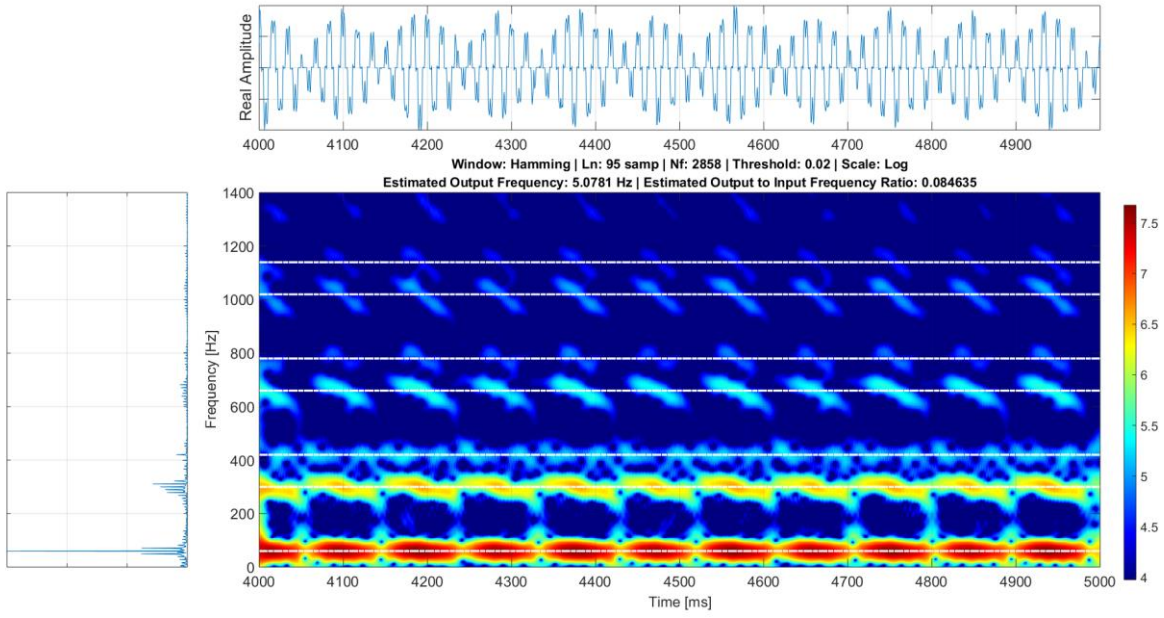


Figure 2-23. Spectrogram for a loaded motor on F6 with a ratio of approximately .0846.

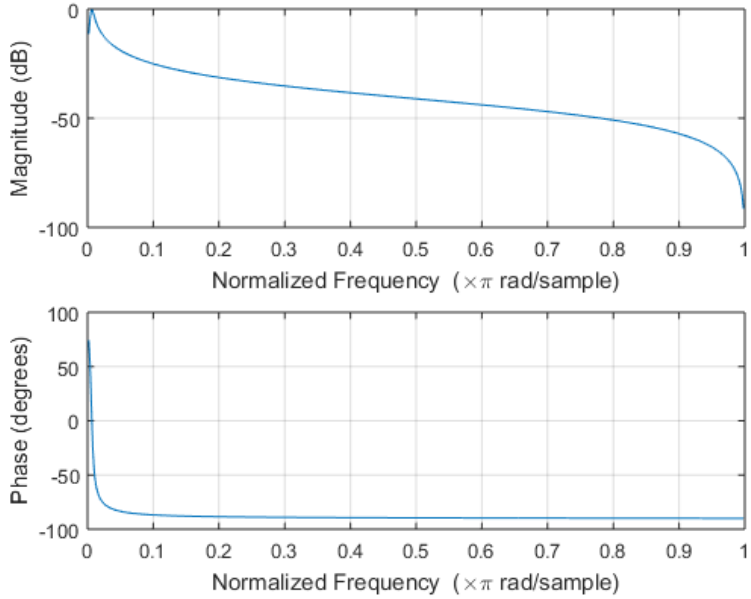


Figure 2-24. Bode for filtering maximum values in windows of interest. Here it corresponds to **Figure 2-23** and is centered about a frequency of 5.0781 Hz with a lower cut-off frequency of 1.0781 Hz and an upper cut-off frequency of 9.0781 Hz.

Once the maximum values along the x-axis of the window are extracted and filtered, a zero crossing method is implemented to detect the points where the sinusoid crosses the center of the window which corresponds to the center of the harmonic. We are only concerned here with the falling values, i.e. the ones that correspond to negative slopes, so we ignore the others. A line tangent to the sinusoid is then found at each of these zero crossing points and the slope of this line is taken. This value is a linear approximation of a curve because the

actual sloping energy content does not change exactly linearly. All of these slopes are then averaged. Typically the first and last slopes are ignored in the average as the filtering method sometimes causes attenuation in the first and last cycles of the filtered maximum value signal. This is seen in Figure 2-25 a.

Figure 2-25 through Figure 2-27 display this method for the slope calculation of each harmonic. Take for example Figure 2-25 a. and b. We have windowed the original spectrogram from Figure 2-23 about the 300 Hz (5th harmonic) frequency center. The blue lines here correspond to the raw maximum values, that is, the unfiltered maximum values in the spectrogram along the x-axis. The orange line corresponds to these values which have been filtered by the Butterworth filter of Figure 2-24. Note that they appear sinusoidal and match the original values very closely. Last, are the solid black lines which are the lines tangent to each of the zero crossing points; these are the slopes. Figure 2-25 a. demonstrates that these lines closely match the slopes seen in the background window. Figure 2-25 c. and Figure 2-25 d. show the same procedure about the 420 Hz (7th harmonic) frequency center. From Figure 2-23 however, it is evident that the 7th harmonic is not well defined in the spectrogram and consequently the harmonic slopes are not well defined. Indeed, the energy content of the spectrogram for this harmonic appears more as an artifact from the 5th harmonic than it does its own entity. This is especially true for the higher order harmonics with close neighbors. The problem only tends to worsen as the output to input frequency ratio rises.

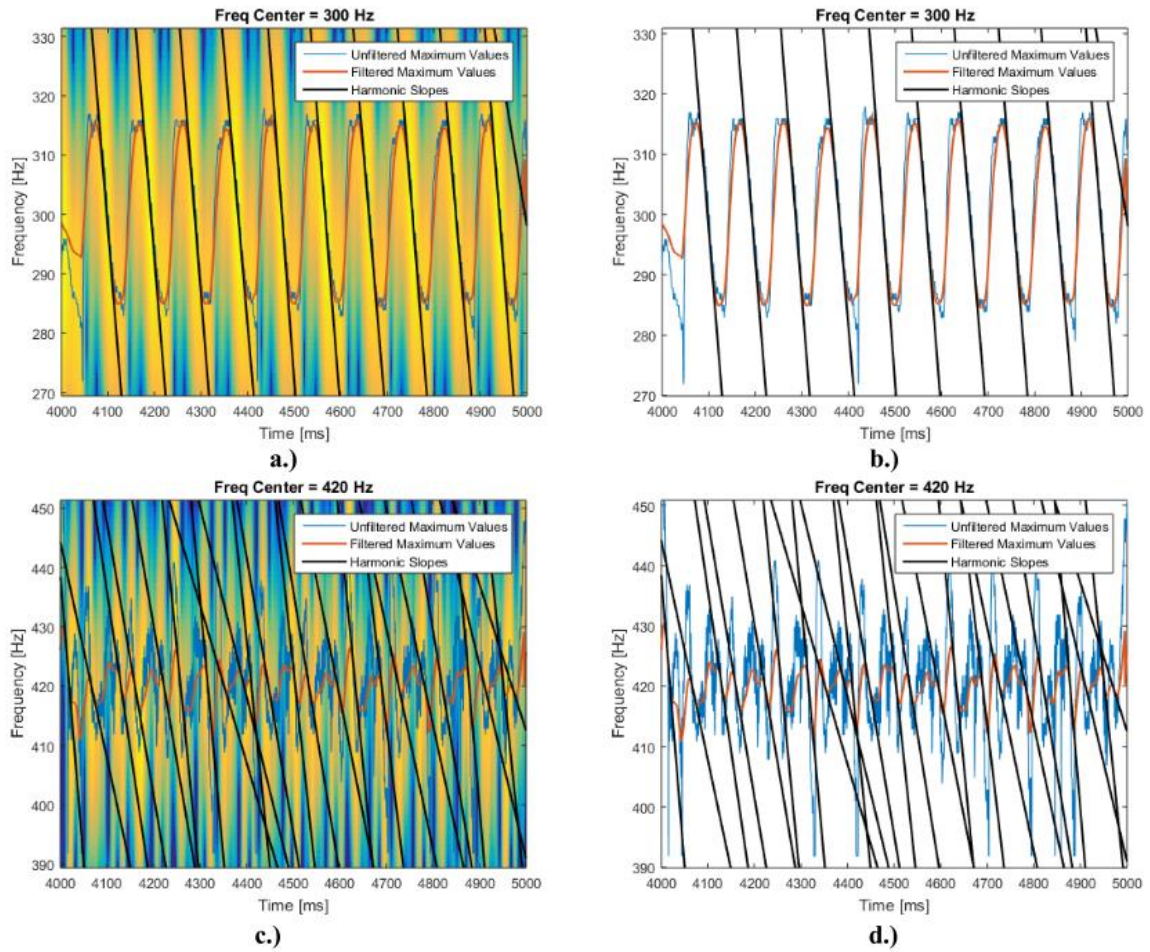


Figure 2-25. All images correspond to the spectrogram in Figure 2-23.

- a.) Window centered about the 5th harmonic (300 Hz) and the approximate slopes in the time-frequency domain. The window background is shown.
- b.) Window centered about the 5th harmonic (300 Hz) and the approximate slopes in the time-frequency domain. The window background is not shown.
- c.) and d.) The same but centered about the 7th harmonic (420 Hz).

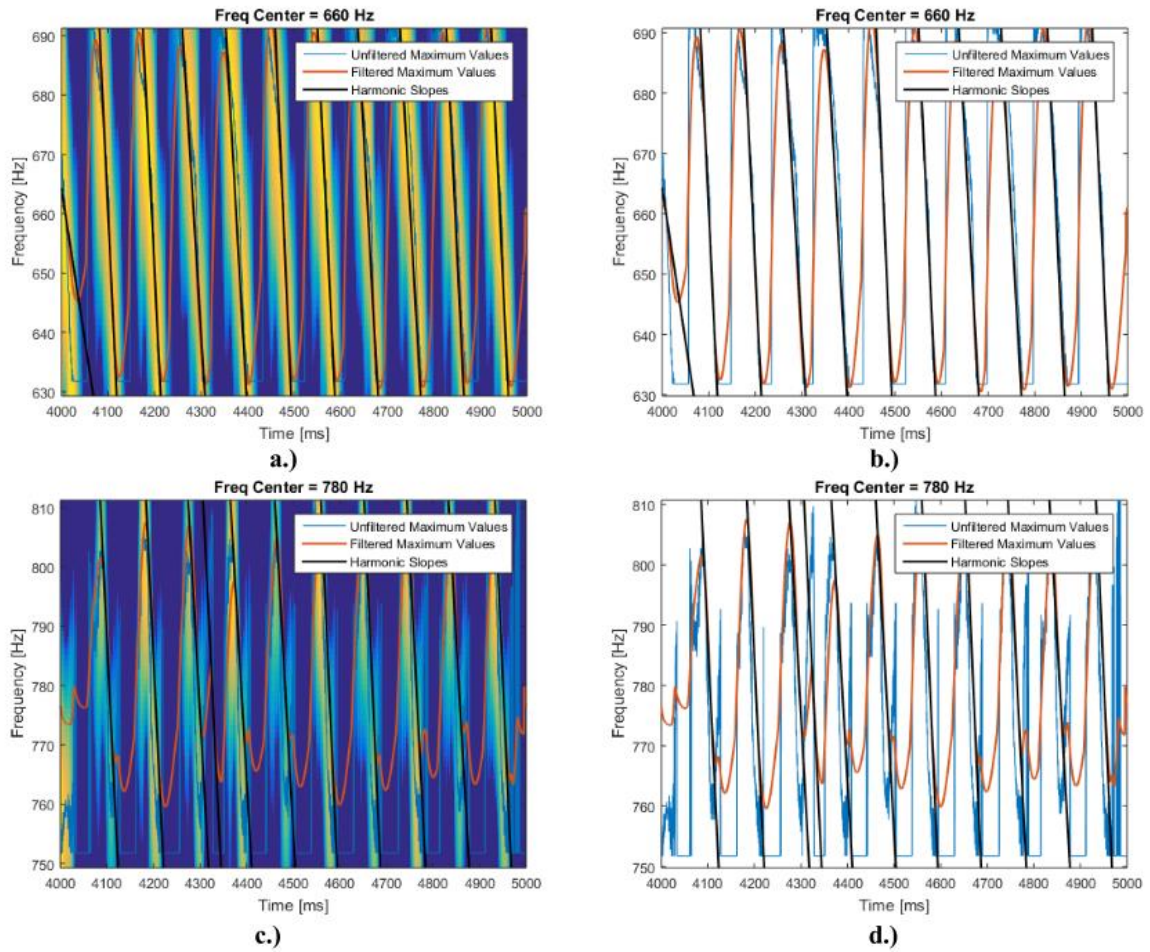


Figure 2-26. All images correspond to the spectrogram in Figure 2-23.

a.) Window centered about the 11th harmonic (660 Hz) and the approximate slopes in the time-frequency domain. The window background is shown.

b.) Window centered about the 11th harmonic (660 Hz) and the approximate slopes in the time-frequency domain. The window background is not shown.

c.) and d.) The same but centered about the 13th harmonic (780 Hz).

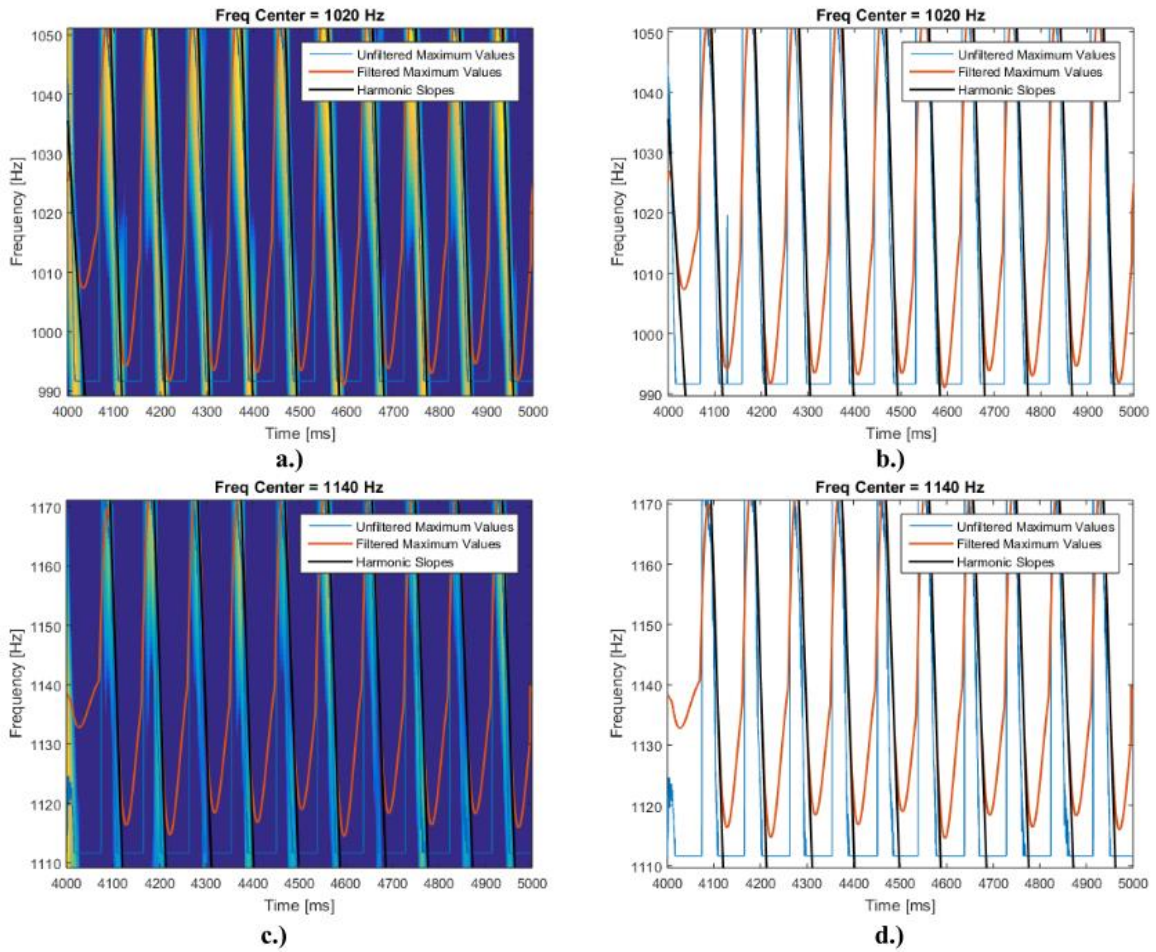


Figure 2-27. All images correspond to the spectrogram in Figure 2-23.

- a.) Window centered about the 17th harmonic (1020 Hz) and the approximate slopes in the time-frequency domain. The window background is shown.
- b.) Window centered about the 17th harmonic (1020 Hz) and the approximate slopes in the time-frequency domain. The window background is not shown.
- c.) and d.) The same but centered about the 19th harmonic (1140 Hz).

This type of analysis was performed on the various datasets provided and is tabulated in Table 2-4. For each dataset a qualitative assessment was made. Datasets which appear poorly defined are highlighted in red, suspect in yellow, and acceptable in green. Although this analysis is subjective, it is clear that for the 7th, 13th, and 19th harmonics the slopes are not consistently well enough defined to extract meaningful slope data. From Table 2-4 it can be seen that the values extracted for these slopes sometimes vary wildly. For the same reasons the frequency centers were not well-defined, the slopes are not well-defined, and for these two reasons these harmonics are ignored in the following sections of this study. Note that the slopes of the damaged dataset were included because in this case, the indicators of damage in the spectrogram do not affect the slope values. In Figure 2-28 the data in Table 2-4 was plotted and a 2nd order polynomial was then fit to the data.

Table 2-4. Harmonic slopes of input current harmonics for loaded datasets.

Fund. Freq (Hz)	60		Slopes ($1/s^2$) for each Harmonic						
Output Frequency (Hz)	Notes	f_o/f_i	5 th	7 th	11 th	13 th	17 th	19 th	
3.1250	F6	0.0521	-298.032	-413.164	-320.69	-417.907	-605.254	-942.754	
4.6875	Damaged F1	0.0781	-757.477	-1093.36	-1536.77	-1797.27	-2238.61	-2434.87	
5.0782	F1	0.0846	-966.963	-429.803	-1862.95	-2399.77	-3161.72	-2428.16	
5.8900	F6	0.0982	-1304.91	-1299.09	-2988.41	-2796.09	-4842.51	-2689.1	
6.2500	F1	0.1042	-1436.63	-2013.41	-3351.9	-3715.78	-5345.38	-2991.21	
7.4219	F6	0.1237	-2204.23	-1161.61	-5680.3	-3369.64	-9577.36	-3240.7	
8.5938	F6	0.1432	-3024.39	-1974.72	-7624.62	-2689.37	-12383	-8090.44	
9.7657	F6	0.1628	-4151.52	-1088.81	-10831	-8433.86	-14597.5	-8075.43	
10.1563	F2	0.1693	-3951.42	-1917.6	-8790.61	-8174.87	-13717.1	-5389.72	

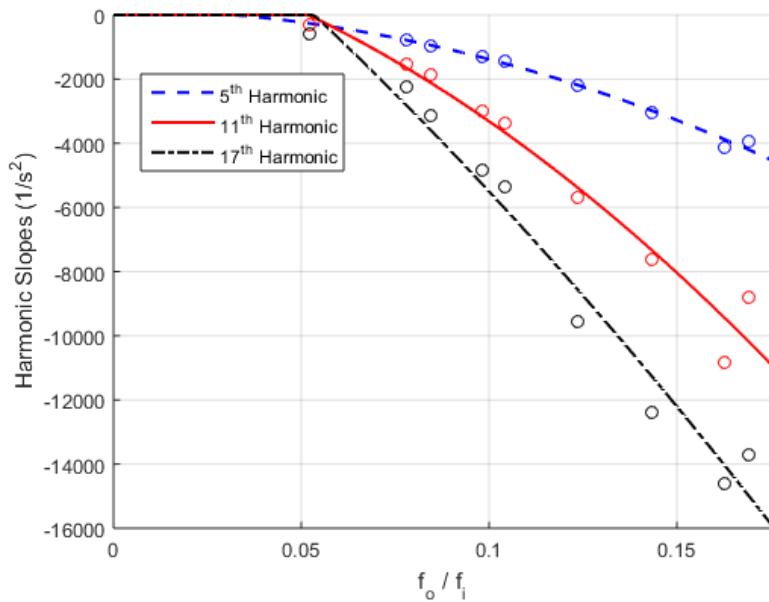


Figure 2-28. Harmonic slopes for the 5th, 11th, and 17th harmonics for loaded datasets.

The 2nd order nonlinear regression function for each harmonic is given by the following equation.

$$\gamma_h \left(\frac{f_o}{f_i} \right) = c \left(\frac{f_o}{f_i} \right)^2 + d \left(\frac{f_o}{f_i} \right) + e \quad (2-17)$$

where γ is the harmonic slope value determined empirically, h corresponds to either the 5th, 11th, or 17th harmonic, and the coefficients c , d , and e are determined by Table 2-5.

Table 2-5. Coefficients for equation (2-17). $h = 1$ corresponds to the fundamental.

		Coefficient		
		c	d	e
h	1	0	0	0
	5	-148466	-796.26	181.33
	11	-258957	-29639	2236.4
	17	-164832	-92806	5246.5

This method for the slope estimation of the harmonics is an approximation and it's possible that there exist more robust and adequate methods to extract this information. Despite this however, this method of extraction tends to provide a good estimation which can be used to create an acceptable model. Moreover, because the empirical data provided only covers a relatively limited range of ratios, equation (2-17) is not guaranteed to be accurate for very low or very high ratios. Cycloconverters tend to operate within a narrow band of output to input frequency ratios so it is not expected that this will prove significantly problematic. More empirical data would help refine equation (2-17) as well as the technique overall.

2.4 Modeling

It is the ultimate goal of this research to develop a method that allows for the diagnosis of the cycloconverter state based only on analysis of the input current data. To do this, it's beneficial to have some sort of reference to which it is possible to compare the real cycloconverter data. This reference is the model whose characteristics and development are discussed in this section.

2.4.1 Modeling Equation

Because we want to make a comparison of spectrograms in the time-frequency domain, we must create a time domain model whose spectrogram in the time-frequency domain exhibits the characteristics of a normal functioning cycloconverter; equation (2-18) is such an equation.

$$\begin{aligned}
 c_{model}(t) = & \\
 & \sin(2\pi f_o t) \sum_{n=0}^3 \left| \frac{1}{6n-1} \right| \sin \left(\left(\left(|6n-1| f_i (1-\eta) + \eta \alpha \left(\frac{f_o}{f_i} \right) \right) 2\pi t \right) \right. \\
 & \left. + \beta \left(\gamma_h \left(\frac{f_o}{f_i} \right) \right) |\sin(2\pi f_o t)| \right) \quad (2-18)
 \end{aligned}$$

$$\text{with } \eta = \frac{\operatorname{sgn} \left(\max \left(-1, \alpha_h \left(\frac{f_o}{f_i} \right) - 1 \right) \right) + 1}{2}$$

where f_o is the output frequency of the cycloconverter, f_i is the input frequency, and $h = |6n - 1|$ and is the harmonic of interest. Equation (2-18) is inspired by equation (2-7). Note that the first term, $\sin(2\pi f_o t)$, of (2-7) is very similar to that of equation (2-18). It is this that gives the time domain its characteristic amplitude modulation which corresponds directly to the output frequency. The sinusoidal term within the summation is also inspired by (2-7) and is designed to model the characteristics in the time-frequency domain. $|6n - 1|$ ensures that only the Fundamental, 5th, 11th, and 19th harmonics are included in the model but no others.

$\left|\frac{1}{6n-1}\right|$ follows from the Fourier series expansion of a square wave where the amplitude of the odd terms of increasing order are decreased by the reciprocal of their order. Section 2.1.3 mentions that the amplitudes of each harmonic are independent of the frequencies present, but consistently decrease as the harmonic order increases. This term causes the same effect, but it does not correspond directly to the qualitative data provided by Pelly. It will be shown however that this decision proves to be appropriate, though holds better for loaded motors.

Next is the choice of $\beta \left(\gamma_h \left(\frac{f_o}{f_i} \right) \right) |\sin(2\pi f_o t)|$. This function modulates each harmonic in time and is inspired by the $f(\theta_o)$ term of equation (2-7). Like $f(\theta_o)$, it is modulated sinusoidally where $\beta \left(\gamma_h \left(\frac{f_o}{f_i} \right) \right)$ controls the peak value of the modulation. Note however that it is not a pure sinusoidal term; it is instead the absolute value of the sinusoid.

$\alpha_h \left(\frac{f_o}{f_i} \right)$ controls the frequency center of each harmonic, and is a direct calculation from (2-16) and for cycloconverters driving loaded motors, is always zero. η is either 0 or 1 (except in the impossible case where $\alpha = 1$) and has the effect of zeroing out the effect of α_h if the motor is loaded. The value of $\alpha_h \left(\frac{f_o}{f_i} \right)$ corresponds to the linear rise of the frequency centers. For unloaded motors, β is always zero as there is no modulation in the frequency domain.

$\beta \left(\gamma_h \left(\frac{f_o}{f_i} \right) \right)$ is more complicated. By equation (2-5) and equation (2-7) we know that the frequency modulation term we chose to modify the phase of each harmonic in time must be sinusoidal. Among other problems, from equation (2-5) we know that the term is dependent on the value of r , however, not knowing r makes it impossible to explicitly use equation (2-5). Moreover we know that the phase of the switching function is modulated sinusoidally, and this is likely the cause of the change in frequency over time observed, but this does not guarantee that this is the only explicit source of this characteristic. We do know however that the instantaneous frequency, which is given by the spectrogram, is the derivative of the phase. Knowing this then we can observe the spectrogram for characteristics that will provide insight into the appropriate choice of a frequency modulation function in part by inspection. We consider the frequency modulation function $\phi(t) = |\sin(2\pi f_o t)|$ where $\phi(t)$ is the phase being modulated. Let $f_o = 1 \text{ Hz}$; this is shown in Figure 2-29. Its derivative is then the instantaneous frequency which is given in the time-frequency domain. This functions graph is shown in Figure 2-30. Note that this function has a sloping that is characteristic of the harmonic slopes exhibited in the time-frequency domain. If we can then multiply the original modulating function $\phi(t)$ by some constant, then we can control the slope of its 2nd derivative which will correspond to our empirically calculated γ_h from the previous section. Lastly, we know that the derivative of the $\phi'(t)$ directly relates to its slope, therefore if we

specify the peak of $\phi''(t)$ then we can control the required term β by which we must scale $\phi(t)$ so that the slope of its derivate when it crosses the x-axis corresponds to the value predicted by γ_h . The 2nd derivative $\phi''(t)$ is graphed in Figure 2-31. The derivatives of $\phi(t)$ were all calculated and checked in MATLAB symbolically and numerically.

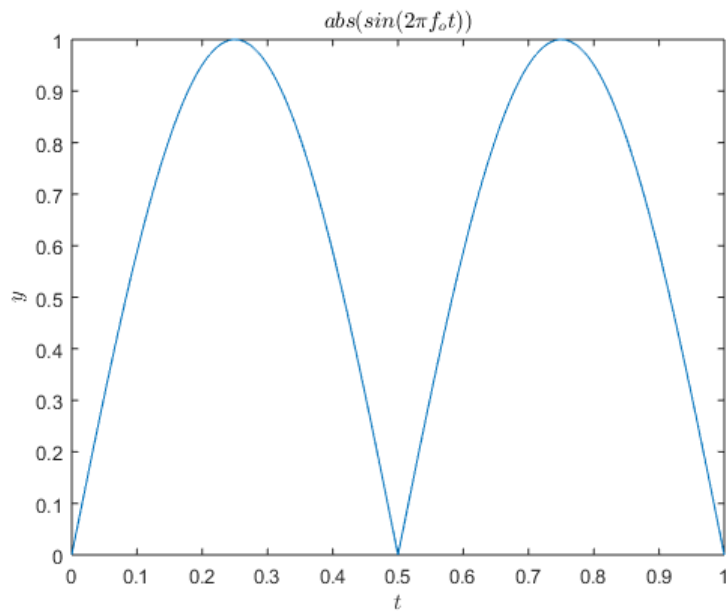


Figure 2-29. $\phi(t)$, the frequency modulation function.

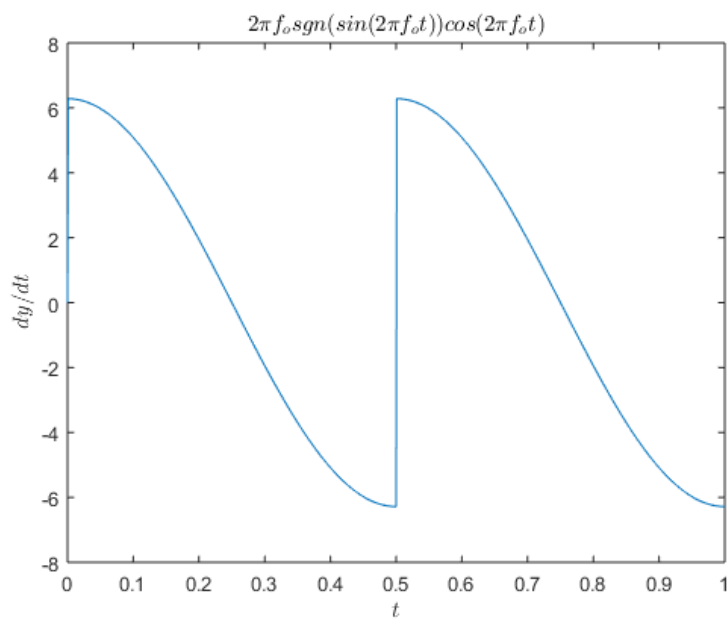


Figure 2-30. $\phi'(t)$, the derivative of frequency modulation function.

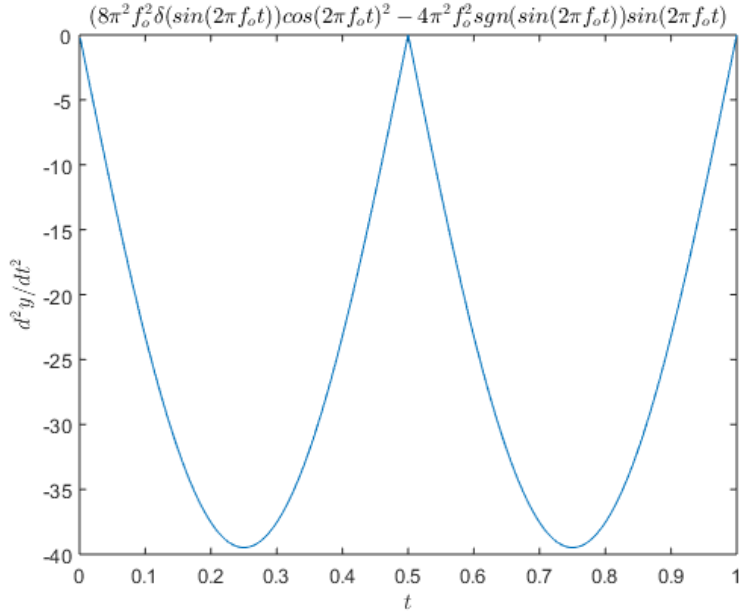


Figure 2-31. $\phi''(t)$, the 2nd derivative of frequency modulation function.

If we know that the peak value of $\phi''(t)$ relates to the expected slope $\gamma_h \left(\frac{f_o}{f_i} \right)$ then we must find a value β that scales $\phi(t)$ appropriately. We recognize that there are always 2 peak values of $\phi''(t)$ centered at $\frac{1}{4}$ and $\frac{3}{4}$ the period. Thus, if we want the peak of $\phi''(t)$ then we need to analyze it at $\phi'' \left(\frac{1}{4} T_o \right)$ where T_o is the output period. Because as f_o increases, the function $\phi''(t)$ gets “squished” in the time domain, it’s required that we multiply by f_o as a scaling factor so that it increases proportionally in height to its decrease in width. The full equation for $\beta \left(\gamma_h \left(\frac{f_o}{f_i} \right) \right)$ is given by equation (2-19) and is simplified through (2-20) into (2-21).

$$\beta \left(\gamma_h \left(\frac{f_o}{f_i} \right) \right) = \frac{\gamma_h \left(\frac{f_o}{f_i} \right) f_o}{\phi'' \left(\frac{1}{4} T_o \right)} \quad (2-19)$$

$$\begin{aligned} \beta \left(\gamma_h \left(\frac{f_o}{f_i} \right) \right) &= \frac{\gamma_h \left(\frac{f_o}{f_i} \right) f_o}{8 \pi^2 f_o^2 \delta \left(\sin \left(2\pi f_o \frac{1}{4f_o} \right) \right) \cos^2 \left(2\pi f_o \frac{1}{4f_o} \right)} \\ &\quad - 4 \pi^2 f_o^2 \operatorname{sgn} \left(\sin \left(2\pi f_o \frac{1}{4f_o} \right) \right) \sin \left(2\pi f_o \frac{1}{4f_o} \right) \end{aligned} \quad (2-20)$$

$$\beta \left(\gamma_h \left(\frac{f_o}{f_i} \right) \right) = \frac{\gamma_h \left(\frac{f_o}{f_i} \right)}{4 \pi^2 f_o \left(2\delta \left(\sin \left(\frac{\pi}{2} \right) \right) \cos \left(\frac{\pi}{2} \right)^2 - \operatorname{sgn} \left(\sin \left(\frac{\pi}{2} \right) \sin \left(\frac{\pi}{2} \right) \right) \right)} \quad (2-21)$$

The time domain signal and their spectrograms generated by modeling equation (2-18) are given below. It will be discussed in the next section, but it is notable that these models are filtered just by the same technique used to remove the 7th, 13th, and 19th harmonics.

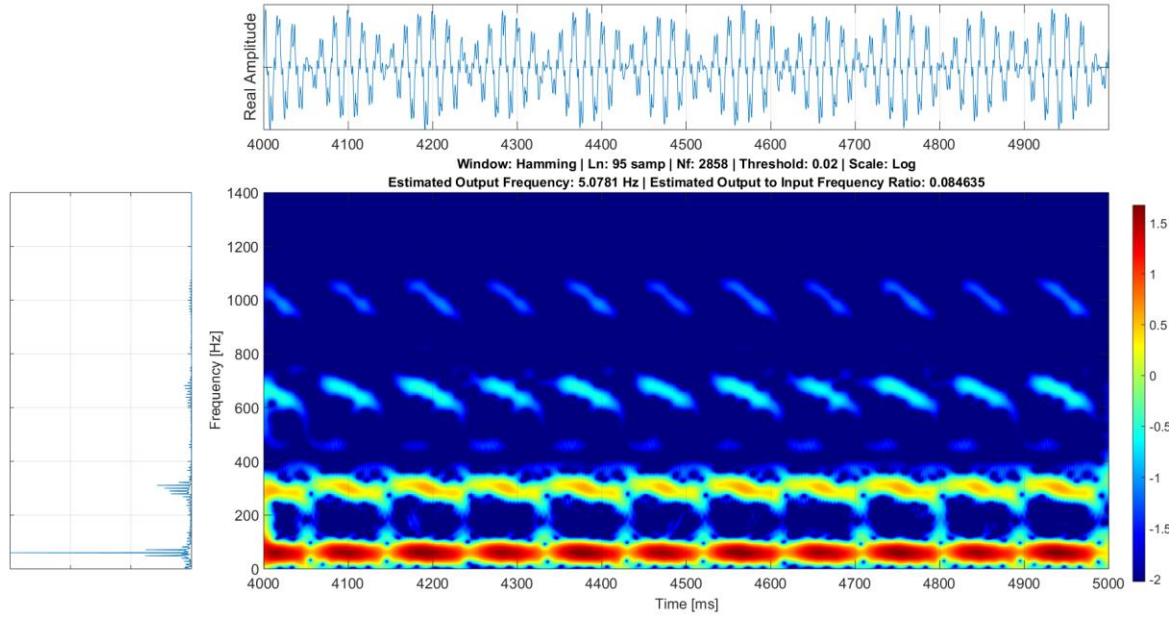


Figure 2-32. Spectrogram of real filtered input current for a loaded cycloconverter with ratio of approximately .084635.

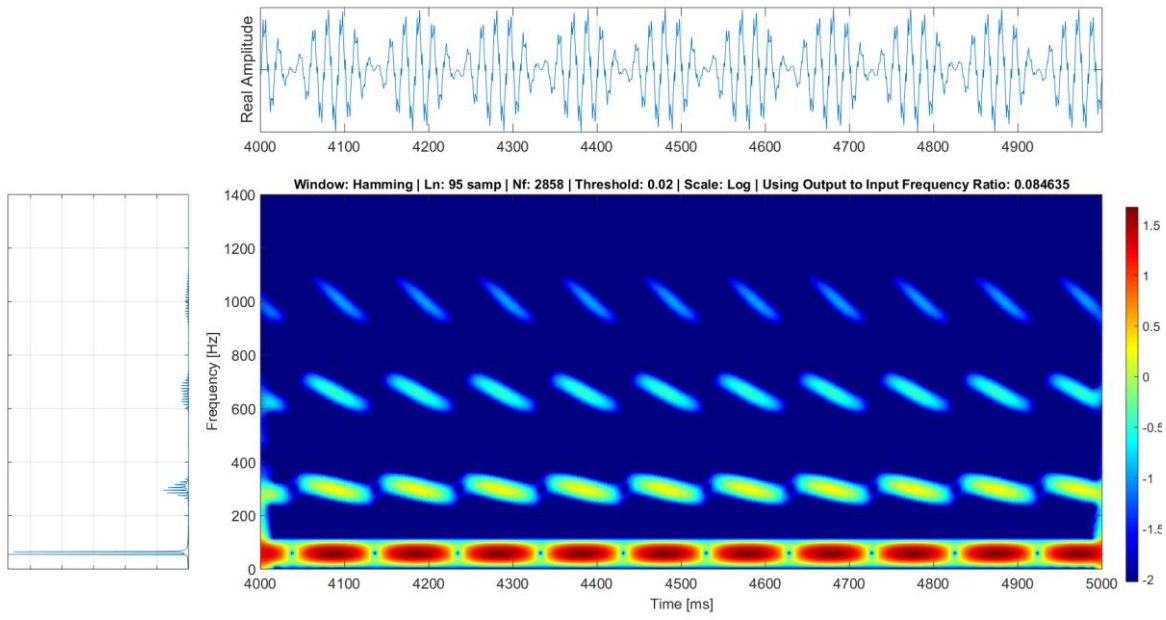


Figure 2-33. Spectrogram of modeled and filtered input current for a loaded cycloconverter with ratio of approximately .084635.

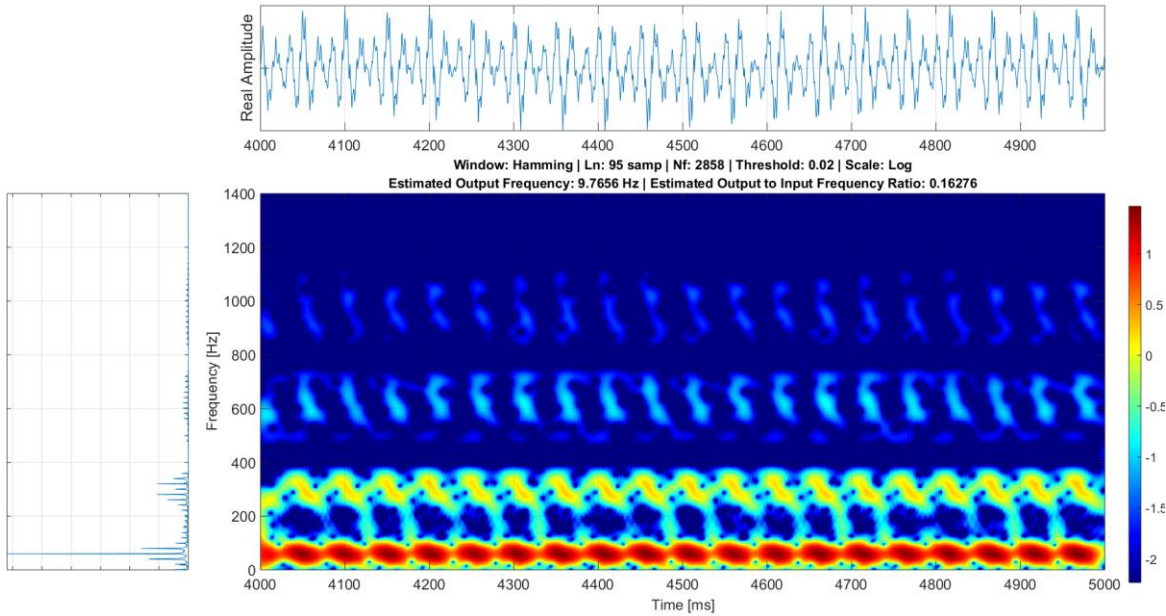


Figure 2-34. Spectrogram of real filtered input current for a loaded cycloconverter with ratio of approximately 0.16276.

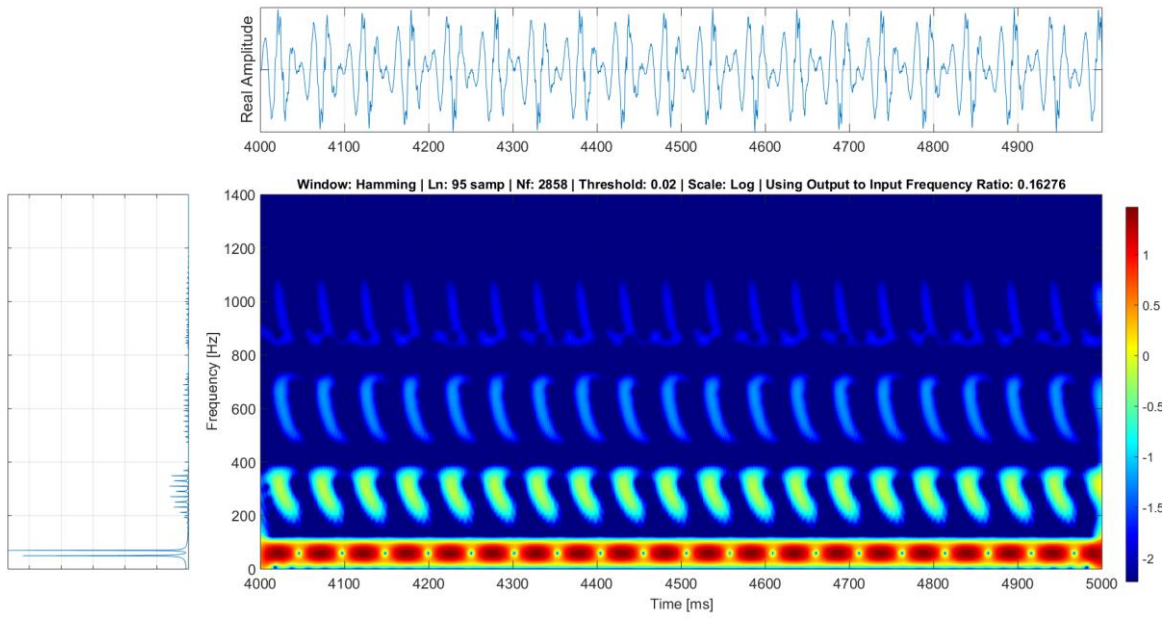


Figure 2-35. Spectrogram of modeled and filtered input current for a loaded cycloconverter with ratio of approximately 0.16276.

Specifically included are the spectrograms at a lower ratio as well as those at a higher ratio. While the model for loaded motors is relatively robust, at higher ratios the slopes become much steeper and the model tends to become less accurate. This is in part due to limitations in the harmonic slope extraction technique. As the slopes become less well defined at higher speeds, the estimation by the method of section 2.3.4 becomes less reliable and the model becomes less accurate. Cycloconverters are however typically run at very low output frequencies.

Note that the input current data and its corresponding model are not in phase. This is not of importance as the entire spectrogram over the entire interval of time is not compared directly. Instead a single reference window is extracted which is then used in this research for comparison across the entire spectrogram and in actual use should be used to make in phase comparisons in real time. The reference window extracted from Figure 2-33 is shown in Figure 2-36.

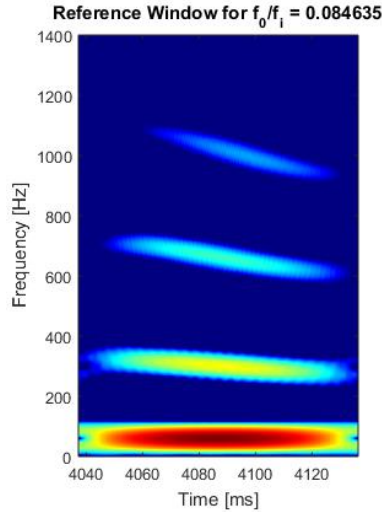


Figure 2-36. Reference window for the loaded motor of Figure 2-33 at a ratio of 0.084635.

2.4.2 Filtering Undesired Harmonic Components and Normalizing Data

It's already been stated explicitly, but the 7th, 13th, and 19th harmonics must be removed in order to compare our model and real data because they are not consistently well defined in the time-frequency domain. The filtering is performed by a 6th order Butterworth filter with cut-off frequencies passed by equation (2-6) and an attenuation of 150 dB. This was chosen after several iterations of other filters and it tended to offer the best performance.

Although unintuitive, we must filter both the input current model and the real input current data. Filtering the real input current data, especially as the output to input frequency ratio rises, causes the cut-off frequencies to start to slightly affect the harmonics of interest (i.e. the 5th, 11th, and 17th). These effects can be seen in Figure 2-34 as the scattering of the energy content on the edges of each harmonic slope. Even though the model does not contain the frequencies of interest, filtering it with the same filter provides a similar effect on the frequencies that are present. In order to make a more accurate comparison then, it's best to filter both so that the affect is realized in each case.

In addition to the filtering, the model window and reference window must be normalized such that their maximum and minimum amplitudes are the same. Their relative amplitudes within this range are the values of importance. If there is an exceptionally high error contained within some portion of the input data spectrogram, then this error will stand out when compared to the reference model.

2.4.3 Model Definition

Finally, the total system that diagnoses the status can be introduced. This entire model is shown in Figure 2-37. Note that the model at this stage is a framework on which to build and is only representative. It does not, at the time of writing this thesis, provide real-time support. It's important however to understand its role and the function of each part.

The top portion of Figure 2-37 is now considered. First the input data must be down sampled to a lower sampling rate. This is the role of the “Downsampler” block, and while not strictly required typical sampling rates provided are very high and thus analysis is computationally intensive; the decimation is done with respect to the maximum frequency content of interest. That time domain data must then be filtered by the “Butterworth Harmonic Filter” blocks in order to remove the harmonics (7th, 13th, and 19th) which are not of interest. The cut-off frequencies for these filters are given by equation (2-6) and are calculated in the “Cycloconverter Harmonic Frequency Bands” block. This block takes as its input arguments the drive pulse number, the input frequency, and the output frequency of the cycloconverter. Last, the model itself must be created in the “Ideal Half-Cycle Model Signal Window” block. This block creates the window to which real world data will be compared and uses the modeling equation of (2-18). It requires as its arguments the input and output frequencies of the cycloconverter, the sampling rate of the real data, and the loaded state of the cycloconverter. That concludes the top portion of the model in Figure 2-37.

The bottom portion includes the signal normalizer for each signal. As was mentioned, this is to ensure that the model and real data are referenced to the same scales, but the values within these scaled models are still relative to each other. The short-time Fourier transform (STFT) is then taken, with a specified windowing function, and its magnitude squared to produce the time-frequency spectrogram. Both the spectrogram of the model and the spectrogram of the representative data are fed into the “In-Phase Window Comparison” block which makes a decision about the status of the cycloconverter; also included as inputs to this block are the cycloconverter output frequency reference and a measurement of the actual output frequency. These values aren’t required, but could be of later use and for this reason are included here. This block also must include a 2 dimensional buffer that is the size of the expected reference window. The buffer should be filled with the spectrogram of the real time input current data and a comparison should be made when the buffer is full; a full buffer should represent one half-cycle of input current data with the peak centered at the center of this buffer. This will correspond to an in-phase comparison. As will be shown in the next section, the 2 dimensional matrix that defines the spectrogram of the reference window must be compared in phase with the 2 dimensional matrix that defines the spectrogram of the real data in order to make a diagnosis decision based on the mean squared error (MSE), thus two comparisons will be made per period of the output frequency. This necessitates that a phase locked loop is used that extracts the phase of the real time input current data. Because the peaks of the upper envelope of the signal align with the peaks in the spectrogram, the phase information can be extracted from here and utilized to ensure that the reference window and real data window are compared in phase.

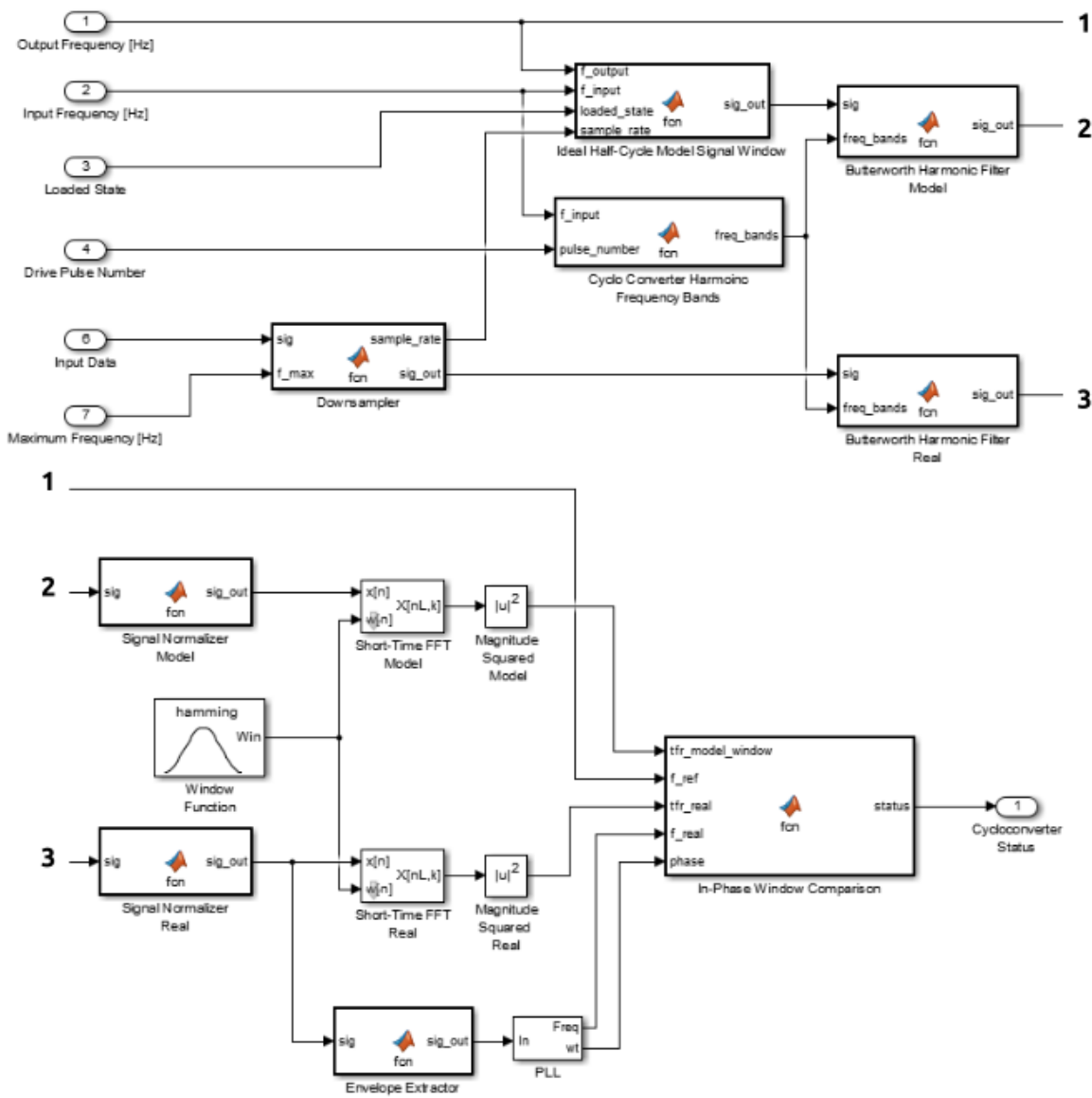


Figure 2-37. Proposed Cycloconverter Status Diagnosis Model.

3. OPERATING STATUS DECISION BOUNDARY

3.1 Analysis in the Time-Frequency

Before a discussion of the error is made, it is beneficial to first analyze a time domain signal of damaged cycloconverter input data. Such a signal is given in Figure 3-1. Note the consistent spikes in the current. The motor of this cycloconverter experienced damage that caused it to trip intermittently; while the current may spike in the time domain, it may or may not reach the threshold required to trip a breaker in the protection system, in which case the cycloconverter could continue functioning; potentially allowing for further damage to occur.

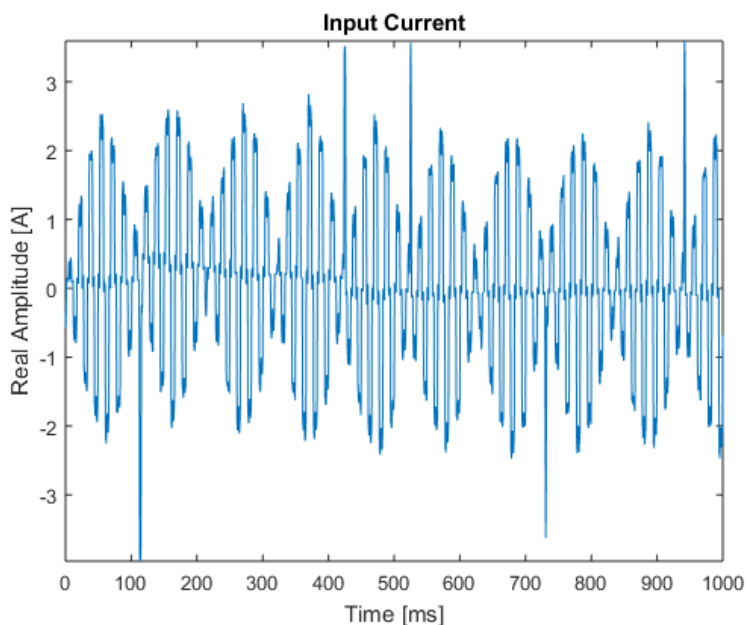


Figure 3-1. Input current for a damaged F1.

Looking at the input current data in the time-frequency domain in Figure 3-2, it can be seen that there is significant inter-harmonic energy content, that is, energy content found between harmonics. By comparing our reference window to this real world data then, these spikes become very evident. Certain tendencies in the time domain, which may not be registered as events, might become more defined in the time-frequency domain, and it is with this hunch that we hope to utilize these facts to diagnose the system.

If we can observe functioning cycloconverters and gain an intuition about what sort of quantized error constitutes normal operation, then we can begin to design a decision boundary such that we can dichotomize between normal and abnormal operation, thus diagnosing the cycloconverter. What follows now is data analysis and a quantized decision boundary defined statistically for the loaded and unloaded cycloconverters.

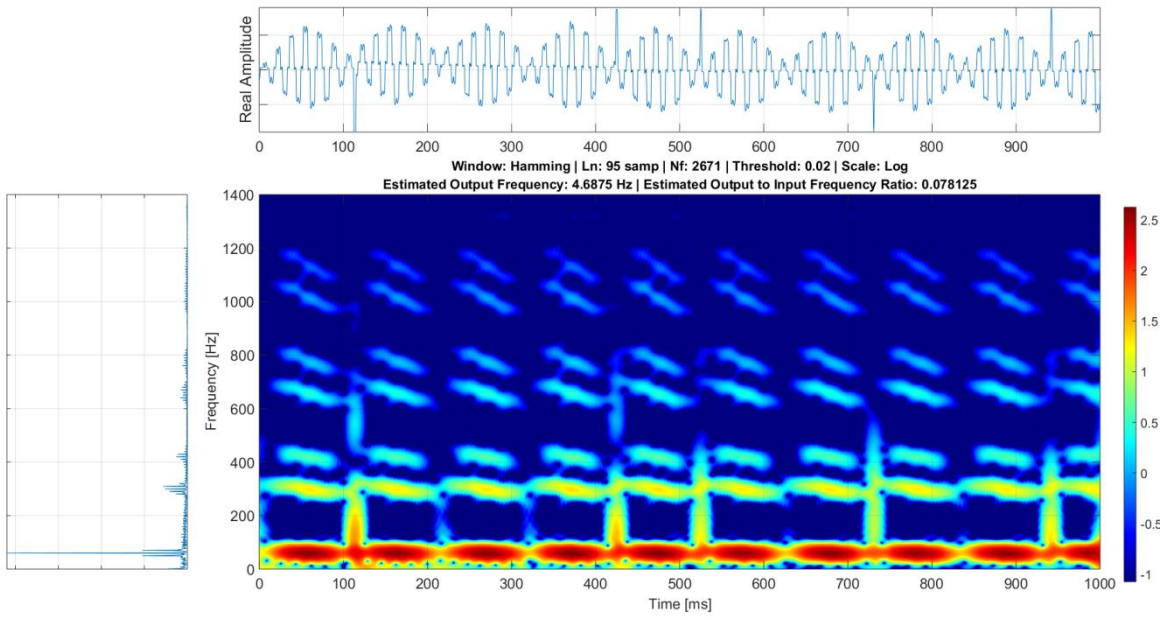


Figure 3-2. Spectrogram of input current for a damaged and loaded F1.

3.2 Error Analysis Technique

3.2.1 Error Analysis for Damaged Cycloconverters Driving Loaded Motors

Let us first consider the case of the damaged and loaded cycloconverter. Of importance is the technique utilized to make the statistical decision boundary of interest. From the discussion of the model in sections 2.4.2 and 2.4.3, we know that we must filter the data in order to make a valid comparison because we have chosen to ignore the 7th, 13th, and 19th harmonics. The filtered data is shown in Figure 3-3.

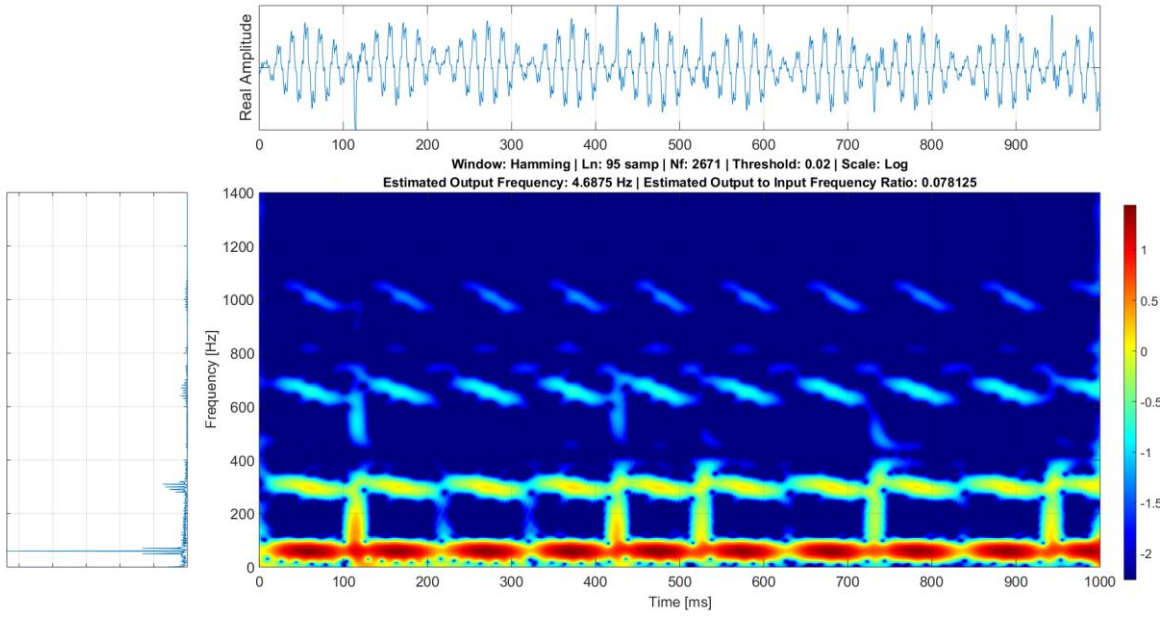


Figure 3-3. Spectrogram of filtered input current for a damaged and loaded F1.

We can then take our reference window as shown in Figure 3-4 and discussed at the end of section 2.4.1. The time axis of this window is not important, only that this time is the same as half the period of the output frequency. Again, this is important because the reference window is compared to spectrogram of the real filtered data and as will be shown for a valid comparison we want the reference window to align in phase with the filtered data.

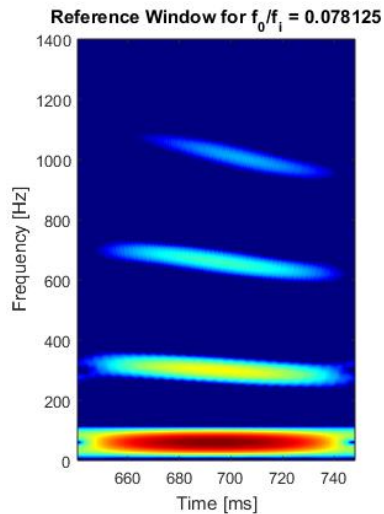


Figure 3-4. Reference window for a loaded motor at a ratio of 0.078125.

In actual real time utilization, this comparison would occur only whenever the reference window is in phase with the data. Here however, to garner an understanding, the reference window is slid through real data column by column. In this case, the row-column dimension of the spectrogram matrix is 2770x2770 and the reference window has dimensions of 2770x337. The entire window is always compared, so in the first iteration, the reference

window is placed on top of the filtered data with both of their left most columns aligned and is moved through the spectrogram until the last iteration when their right most columns align. This means that there are 2096 iterations⁶. At every iteration, the square of the absolute value of the difference between each point in the reference window and the corresponding point in the filtered data window is taken; equation (3-1) shows this. This produces a window of the same size as the reference window, but emphasizes the differences between the reference and real data. Three samples of these windows are shown in Figure 3-5.

$$C_{error}[n, m] = |C_{reference}[n, m] - C_{real}[n, m]|^2 \quad (3-1)$$

where n and m correspond to the row and column coordinates of the matrix which defines each window.

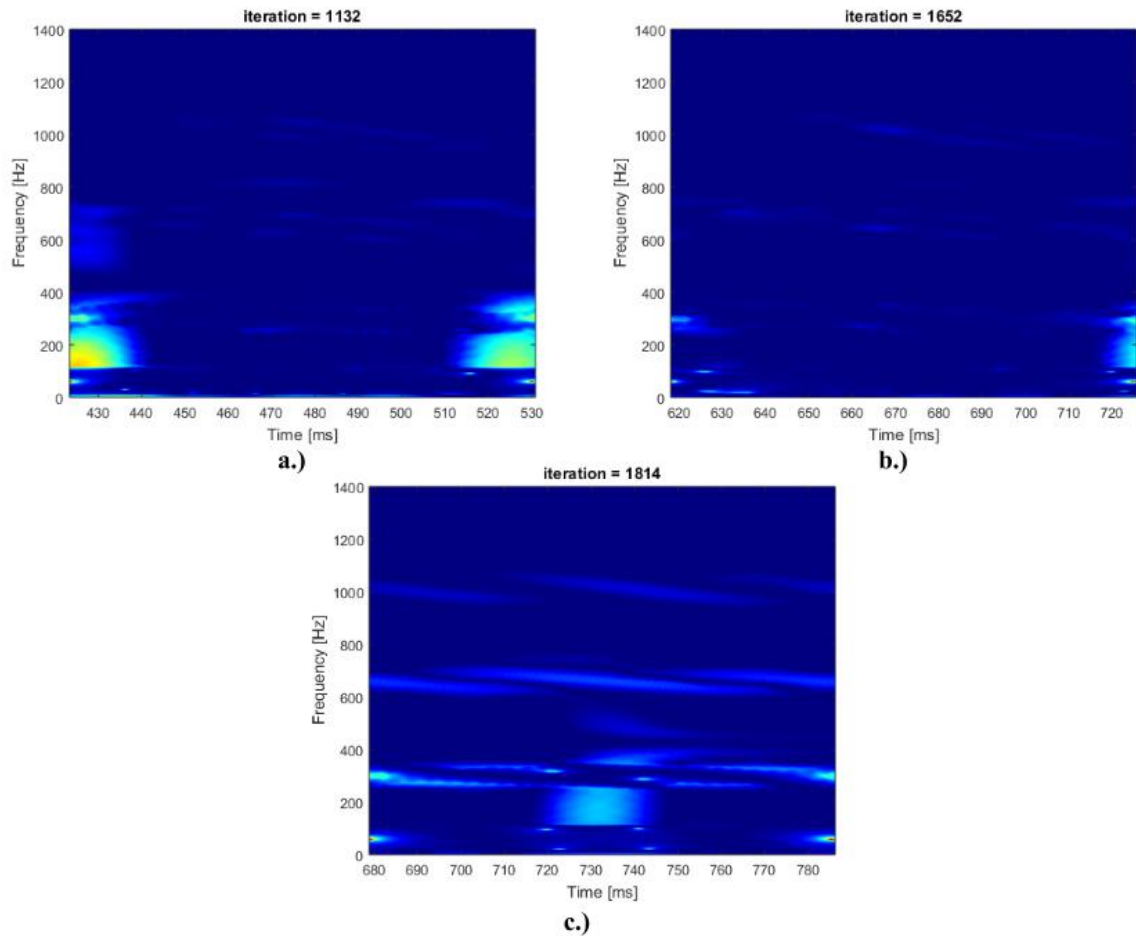


Figure 3-5. Error window between reference and real filtered data for a damaged and loaded cycloconverter F1.

a.) In phase high error. **b.)** In phase low error. **c.)** Out of phase high error.

⁶ $2096 = 2770 - (2 * 337)$

The mean square error of each of these windows is then taken and plotted against its iteration number. The mean square error for a two dimensional window such as those in Figure 3-5 is given by

$$MSE = \frac{1}{N \cdot M} \sum_{n=1}^N \sum_{m=1}^M |C_{reference}[n, m] - C_{real}[n, m]|^2 \quad (3-2)$$

where N and M are the row and column heights of the window respectively. The MSE for each iteration was then plotted and is shown in Figure 3-6. Also plotted are the differences between the local minima, or valleys of this function. The valleys of this function correspond to iterations where the reference window was in phase, or lined up, with the real filtered data. Whenever the reference window sits between two peaks in the spectrogram, the error is the greatest. Figure 3-5 a. and b. show the error window when the reference window was in phase. For the damaged cycloconverter there is significant interharmonic energy content present even when compared in phase. This corresponds to the current spikes seen in Figure 3-1 and seen in the spectrogram in Figure 3-2.

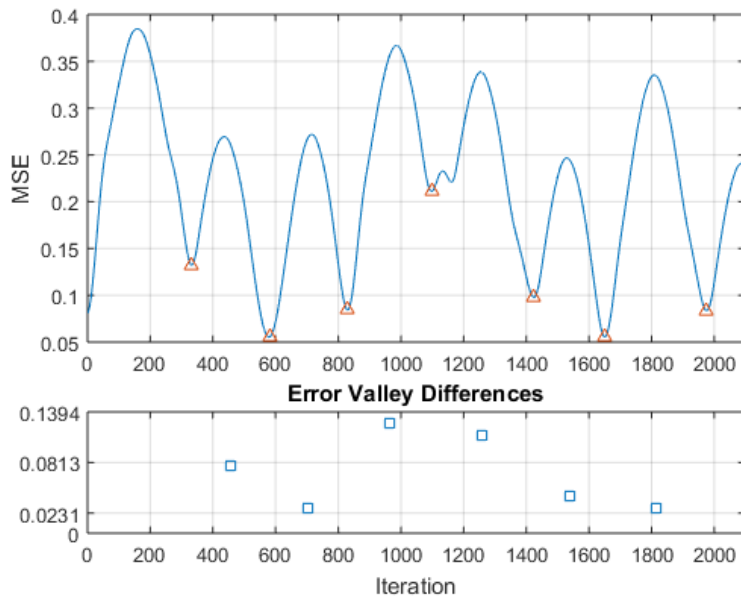


Figure 3-6. MSE and error differences for an undamaged and loaded F1.

Ideally, the values of the valleys of the MSE should all be close; however, it is clear from the differences between them that this is not the case. This is a strong indicator of a problem with the cycloconverter. We record the values of the local minima and the differences between them for statistical analysis later but we do not utilize them to characterize a functioning cycloconverter.

3.2.2 Error Analysis for Undamaged Cycloconverters Driving Loaded Motors

For comparison to the previous section, we consider the repaired cycloconverter F1. Figure 3-7 shows the filtered spectrogram for this condition; note the lack of current spikes as well as lack of 7th, 13th, and 19th harmonic content.

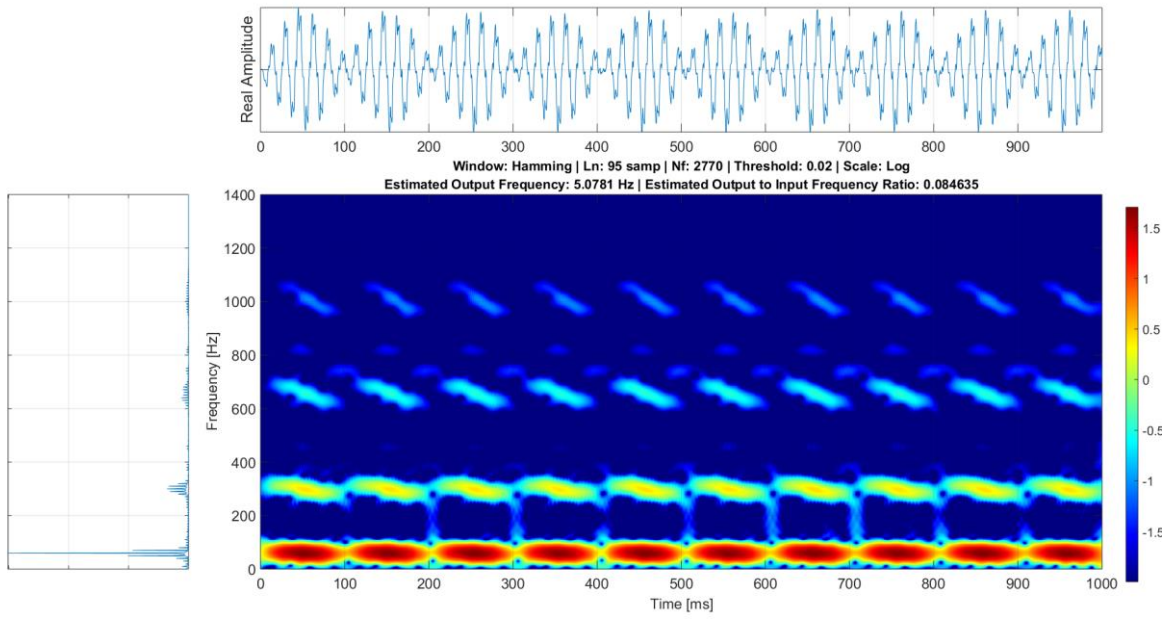


Figure 3-7. Spectrogram of filtered input current for an undamaged and loaded F1.

The reference window (not pictured here), is then slid through this spectrogram to produce the MSE function of Figure 3-8. Here the errors and their differences between the valleys are more consistent. These two are recorded for statistical analysis and unlike the case of the damaged cycloconverter, these values are used to characterize the normal operating condition.

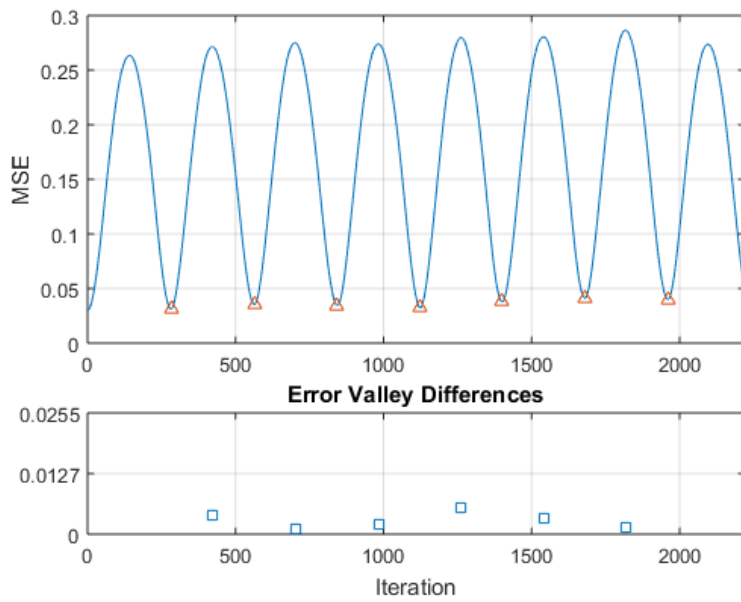


Figure 3-8. MSE and error differences for an undamaged and loaded F1.

3.2.3 Error Analysis for Undamaged Cycloconverters Driving Unloaded Motors

Finally let us consider the case of the unloaded and undamaged motor⁷. Its filtered spectrogram and the corresponding reference window are depicted in Figure 3-9 and Figure 3-10 respectively. A very important point here is that the amplitudes in the time-frequency domain of the real data do not correspond very well to those of the reference window. Because of the earlier assumption that the magnitudes decrease with harmonic order, the amplitudes of the magnitudes of the reference window here follow from that assumption. However, for unloaded motors this assumption is less accurate. Indeed, the 5th order harmonic amplitude of Figure 3-9 is still very high relative to the fundamental, unlike the case of the loaded motor. As can be seen in Figure 3-11, this causes the MSE to be consistently high. Also, higher order harmonics for unloaded motors tend to string together and are not as consistently confined to their respective island. This causes the in-phase error to vary which means their differences are not consistent like those for loaded motors. As a consequence of this, this modeling technique does not hold as well for unloaded motors. As will be seen however, a decision boundary can still be found and intuition made even though there exists a less strong case for its status diagnosis ability with respect to unloaded motors.

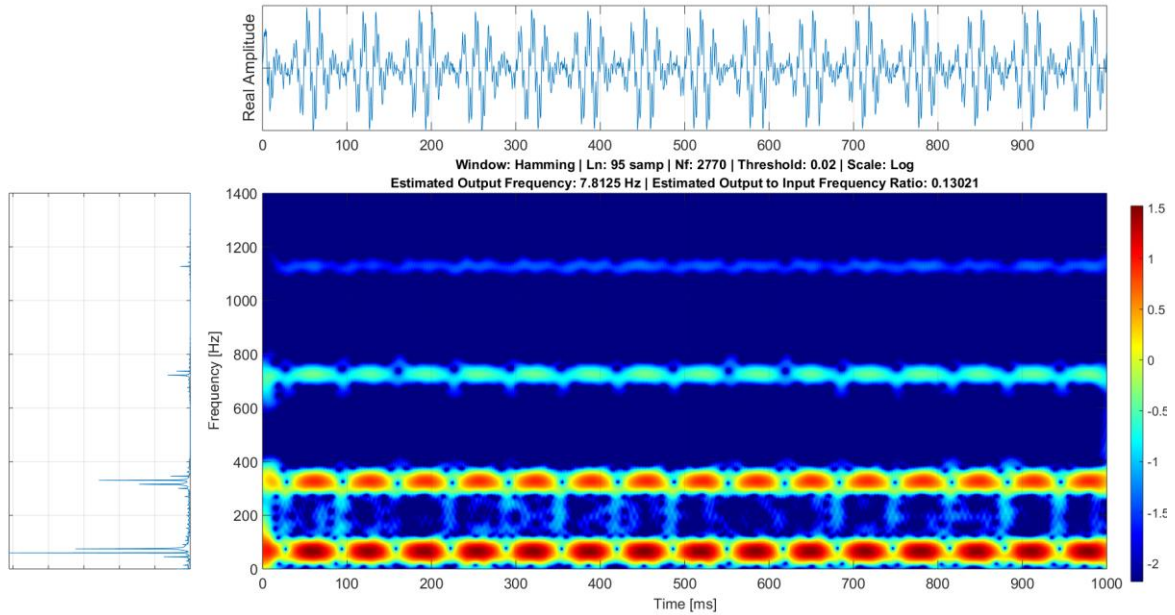


Figure 3-9. Spectrogram of filtered input current for an undamaged and unloaded F2.

⁷ No input current data was available for both damaged and unloaded cycloconverter so it is not considered here.

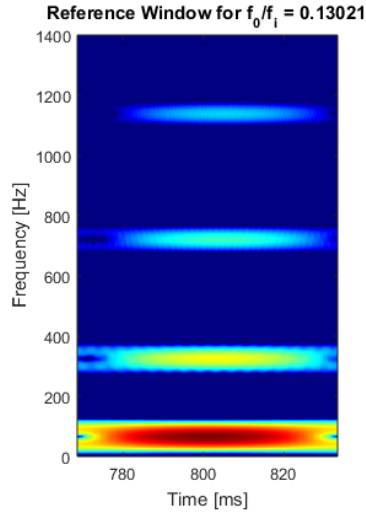


Figure 3-10. Reference window for a loaded motor at a ratio of 0.13021.

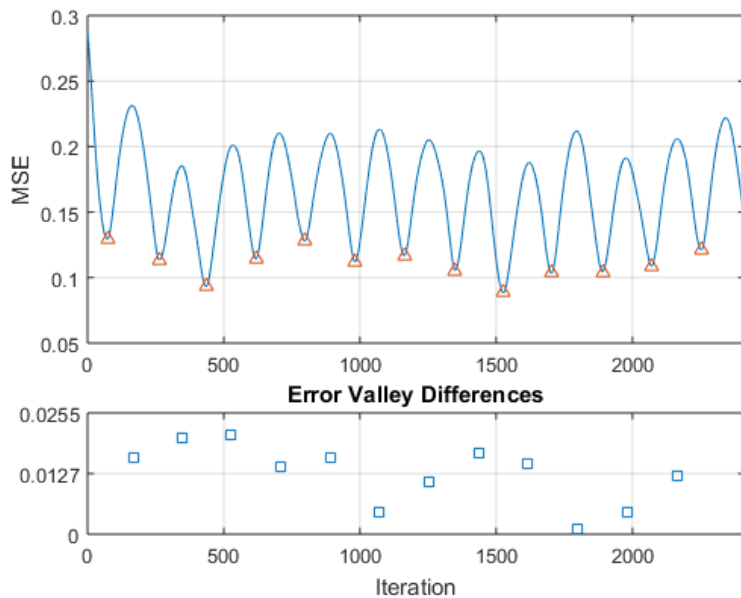


Figure 3-11. MSE and error differences for an undamaged and unloaded F2.

3.3 Loaded Motors Error Analysis

For each every dataset, the MSE valleys and the corresponding difference in those valleys was found. A statistical analysis was then performed on this data with the hope of identifying statistical indicators to distinguish between the functioning and non-functioning cycloconverter, ideally, regardless of the loaded condition. It's important that we consider both the MSE in-phase error values (local minima) and the differences between those minima. As will be shown, the differences provide a clear indicator of damage, but we cannot only rely on the differences, because a consistent error may be present. We must also then be able to recognize error as a function of the ratio that is abnormal. Using both should give good

indicators. This only applies to loaded motors however. As was discussed previously, and as will be shown statistically, the error differences for unloaded motors is unreliable. Near to the writing of this thesis, Nucor was gracious enough to provide another dataset for the loaded motor. For this reason the data that follows includes an extra data point that was not included in the slope analysis for loaded motors.

3.3.1 Local Minima Values for Loaded Motors

All of the local minima values for the various loaded motor datasets are shown in Table 3-1. As the frequency increases, the number of local minima in the MSE graph also increases. Because only one second of data is analyzed in this research, it follows that there are less data points on which to compute averages for the local minima associated with each output to input frequency ratio. Despite this though, a statistical relevance can still be seen in the data. Note also that while the number of peaks should be always increasing, the local minima detector sometimes misses local minima located near the edges because the reference window must start and end completely within the window. If the signal to be analyzed then starts out of phase with the reference window, then it will not include those minima because they don't look like minima in the MSE plot. Also, it's possible that the frequency estimator is not exact; therefore the reference window generated is not exactly the same size as that to which it is being compared. This will cause the error in general to be higher, but can also cause the local minima detector to exclude values. This is because the local minima detector utilizes a threshold in time that ensures the peaks do not fall too close together and thus avoids mistakenly identifying non-local minima as such. This threshold corresponds to twice the period of the output frequency. If the frequency is artificially slightly too high however, then this threshold lies too far apart and some local minima may be missed. These limitations however only affect the statistical MSE analysis and thus only minimally influence the model in that the decision boundary for status dichotomization is dependent on the results reached by this statistical analysis.

Table 3-1. Loaded Motor Local Minima MSE.

Fund. Freq (Hz)	60	Loaded Motor Local Minima MSE																				
Output Frequency (Hz)	Notes	f_o/f_i	Mean	Std.	0.065	0.071	0.065	0.072	0.098	0.056	0.084	0.098	0.056	0.084	0.098	0.056	0.084	0.098	0.056	0.084		
3.1250	F6	0.0521	0.0681	0.0033	0.065	0.071	0.065	0.072	0.098	0.056	0.084	0.098	0.056	0.084	0.098	0.056	0.084	0.098	0.056	0.084		
4.6875	Damaged F1	0.0781	0.1029	0.0505	0.132	0.055	0.084	0.211	0.098	0.056	0.084	0.098	0.056	0.084	0.098	0.056	0.084	0.098	0.056	0.084		
5.0781	F6	0.0846	0.0836	0.0048	0.085	0.079	0.08	0.083	0.088	0.079	0.082	0.094	0.056	0.084	0.098	0.056	0.084	0.098	0.056	0.084		
5.0781	F1	0.0846	0.0360	0.0035	0.031	0.035	0.034	0.032	0.038	0.041	0.04	0.098	0.056	0.084	0.098	0.056	0.084	0.098	0.056	0.084		
5.8594	F1	0.0977	0.0966	0.0057	0.098	0.081	0.1	0.1	0.092	0.098	0.098	0.101	0.096	0.101	0.098	0.056	0.084	0.098	0.056	0.084		
6.2500	F6	0.1042	0.0634	0.0033	0.066	0.066	0.065	0.062	0.069	0.065	0.061	0.063	0.061	0.056	0.084	0.098	0.056	0.084	0.098	0.056	0.084	
7.4219	F6	0.1237	0.1385	0.0066	0.124	0.132	0.138	0.138	0.134	0.139	0.137	0.137	0.146	0.152	0.145	0.141	0.137	0.141	0.152	0.145	0.141	
8.5938	F6	0.1432	0.1373	0.0140	0.137	0.138	0.15	0.146	0.149	0.142	0.152	0.145	0.152	0.139	0.137	0.13	0.129	0.109	0.104	0.145	0.137	
9.7656	F2	0.1628	0.1651	0.0081	0.16	0.161	0.17	0.154	0.156	0.172	0.163	0.168	0.172	0.173	0.152	0.154	0.177	0.178	0.169	0.159	0.16	0.174
10.1563	F2	0.1693	0.1141	0.0037	0.119	0.113	0.104	0.111	0.113	0.118	0.121	0.117	0.115	0.113	0.116	0.112	0.11	0.113	0.115	0.117	0.115	0.112

All of the raw data from Table 3-1 is plotted in Figure 3-12. A linear function was fit to the means of the local minima. The mean and standard deviation was excluded in the linear regression function because those MSE values are not representative of the normally functioning cycloconverter. This mean does not appear strictly linear but there does exist a tendency for the error to rise with the output to input frequency ratio. It is believed that this is a limitation of the modeling technique utilized, the uniqueness of each cycloconverters energy content, and lastly of only having access to a relatively limited number of datasets.

That said however, it's clear that the damaged cycloconverter contains error values that are significantly different than those of a normal cycloconverter. Figure 3-13 shows the standard deviations of the data and the linear function that was fit to them. While this data does tend to move up with the ratio, the linear fit is only an approximation and at such a small scale do not appear strictly linear. The fact that they tend to be small however is good as it means the means are clustered together.

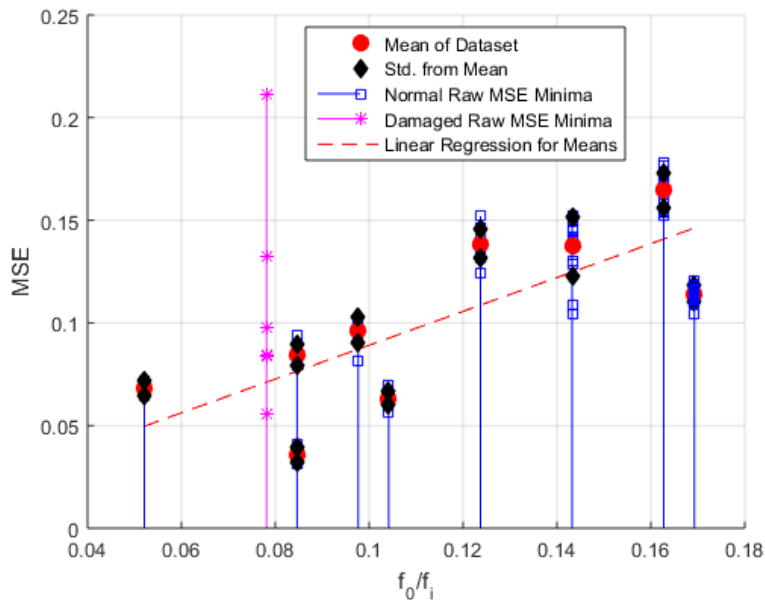


Figure 3-12. MSE data and associated linear regression from Table 3-1.

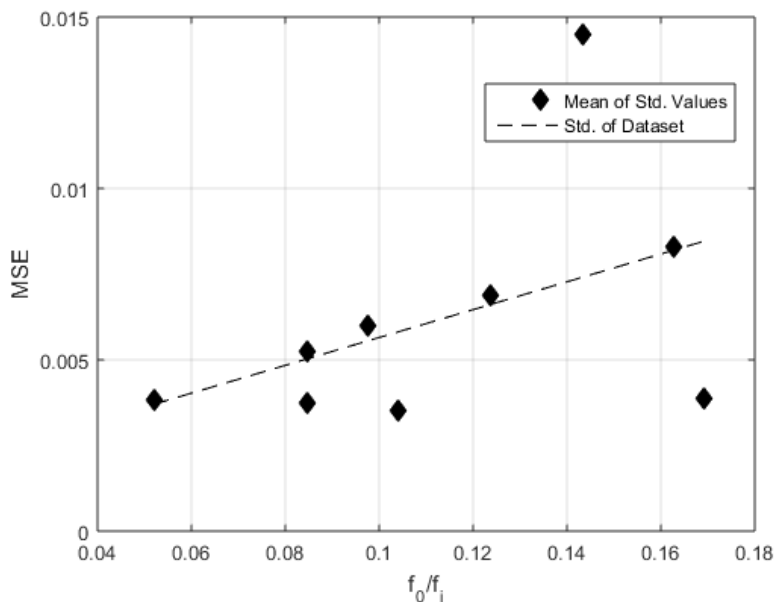


Figure 3-13. Standard deviation of MSE data and associated linear regression from Table 3-1.

The regression lines in Figure 3-12 and Figure 3-13 are simply the equation of a straight line as given by equation (3-3) with coefficients given in Table 3-2.

$$MSE_{\mu \text{ or } \sigma} \left(\frac{f_o}{f_i} \right) = m \left(\frac{f_o}{f_i} \right) + b \quad (3-3)$$

Table 3-2. Coefficients for equation (3-3) corresponding to Figure 3-12 and Figure 3-13.

	Coefficient	
	m	b
μ	0.8238	0.0068
σ	0.0406	0.0016

We hope to visualize the data from Figure 3-12 to better see a difference between the damaged and undamaged loaded cycloconverters. Using the linear approximations of the mean and standard deviations, we can create a normal probability distribution for the MSE of each output to input ratio $\frac{f_o}{f_i}$ according to equation (3-4)

$$PDF \left(MSE \left(\frac{f_o}{f_i} \right) \middle| \mu, \sigma \right) = \frac{1}{\sigma \sqrt{2\pi}} e^{\frac{-\left(MSE \left(\frac{f_o}{f_i} \right) - \mu \right)^2}{2\sigma^2}} \quad (3-4)$$

where μ is the mean from Figure 3-12 and σ is the standard deviation from Figure 3-13. These PDFs are shown in Figure 3-14, Figure 3-15, and Figure 3-16.

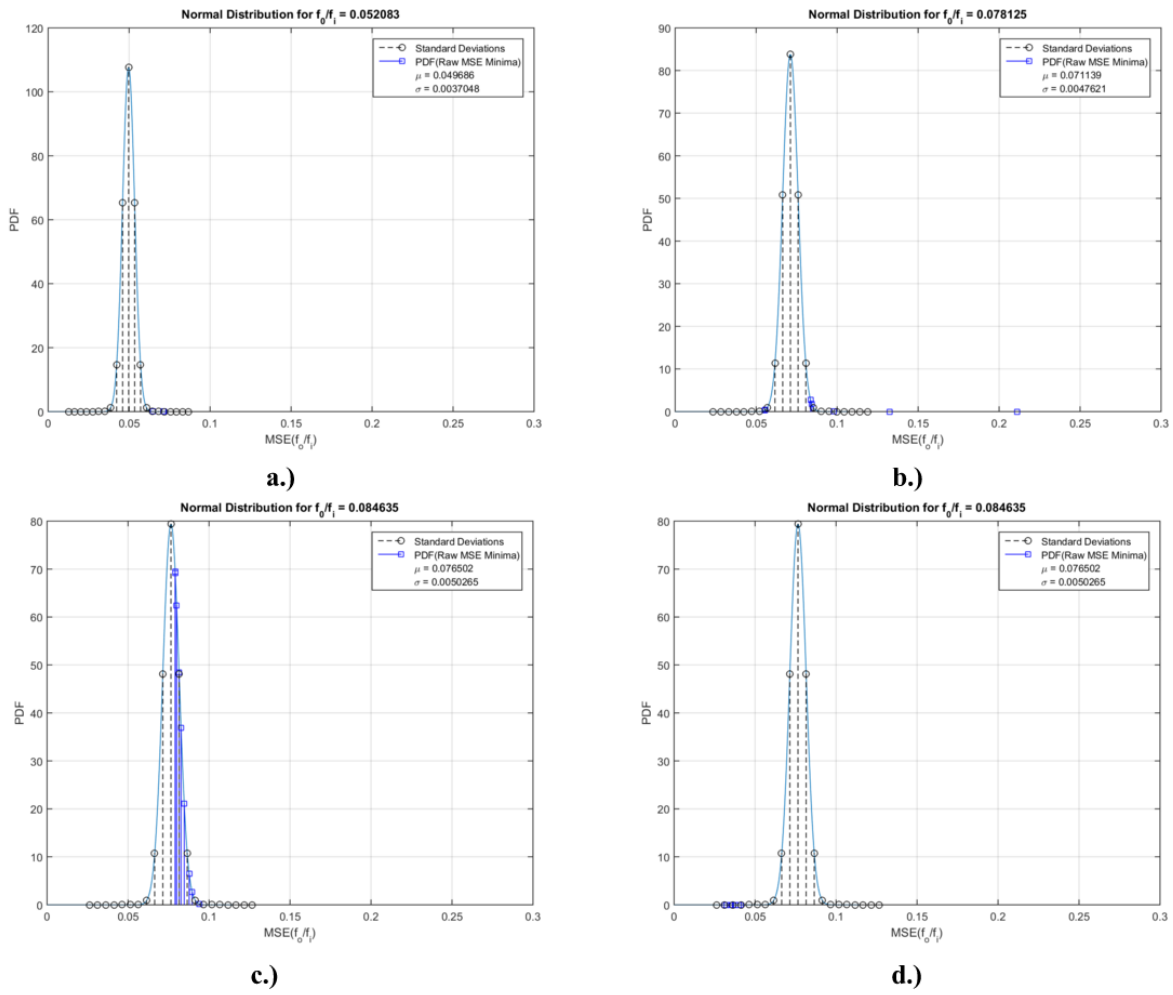


Figure 3-14. Probability distribution functions created by (3-4) with data from Figure 3-12.
Image b. corresponds to the damaged cycloconverter data.

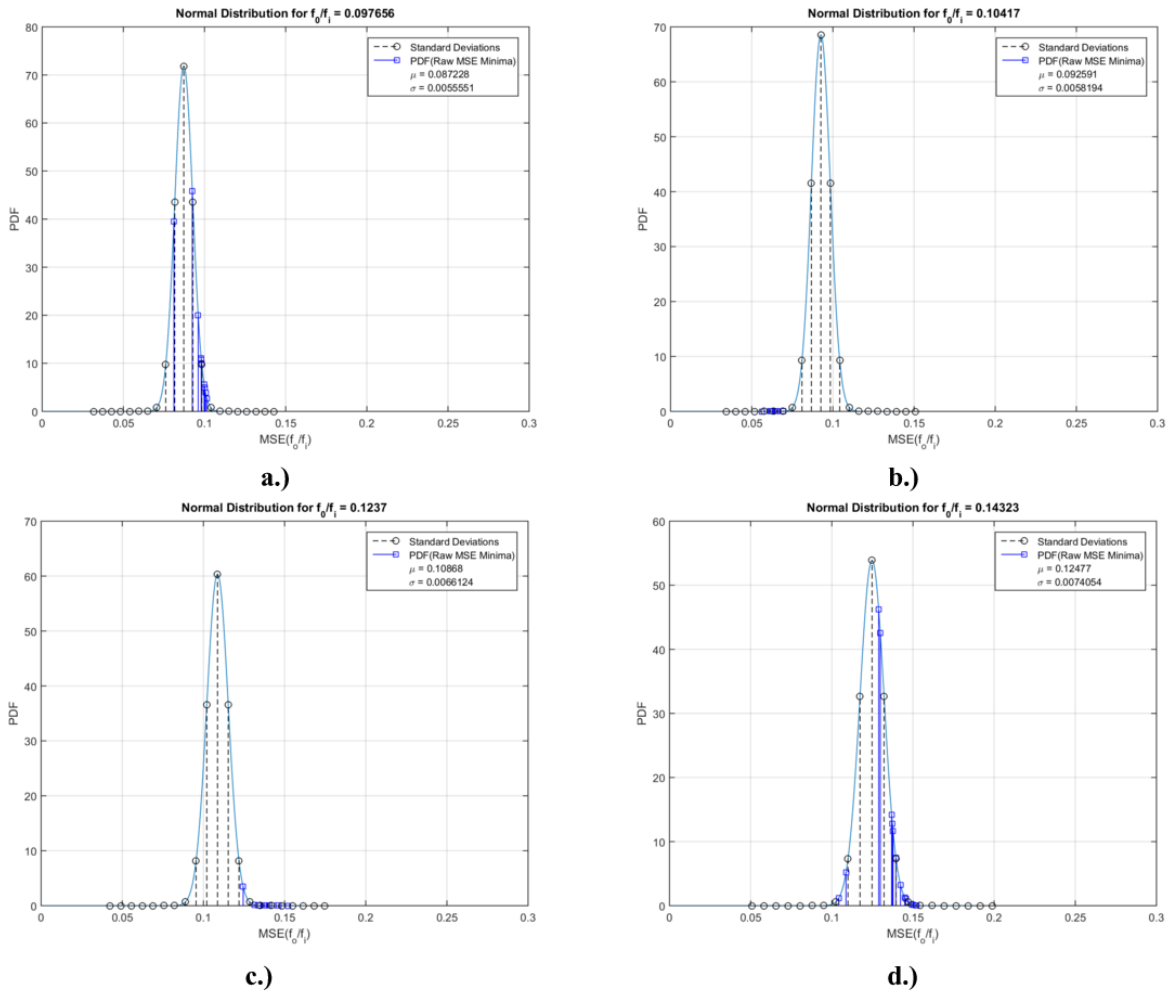


Figure 3-15. Probability distribution functions created by (3-4) with data from Figure 3-12.

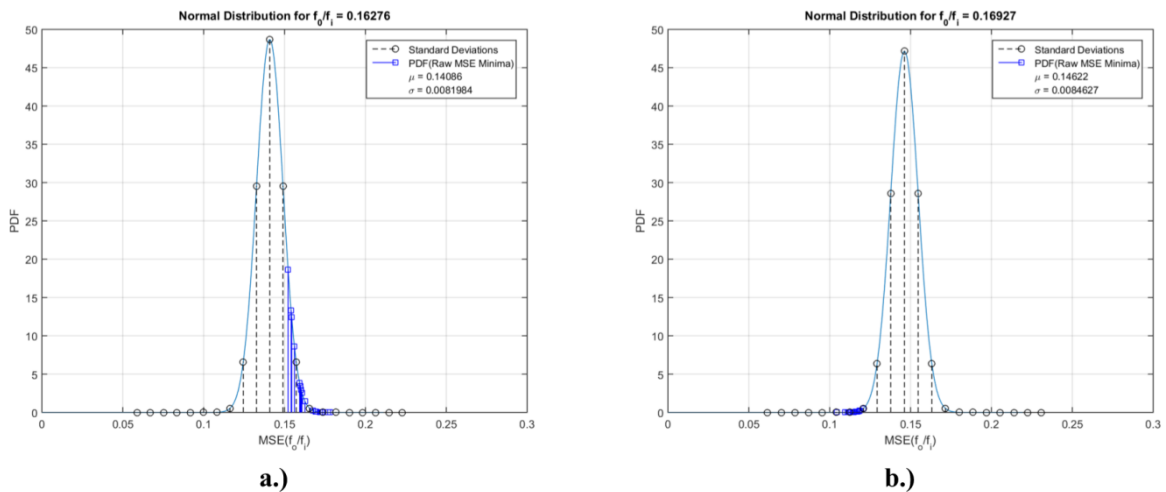


Figure 3-16. Probability distribution functions created by (3-4) with data from Figure 3-12.

The centers of each of these PDFs come from the linear mean of Figure 3-12. The data associated with each output to input ratio and their value given by the PDF is plotted on its own probability distribution. 10 standard deviations from the mean in both directions are shown. This is a very large range and is the result of the large scattering of data in Figure 3-12. MSE values that lie below the mean of their pdf are not of concern, because a value below the mean indicates a low error value. These values are disregarded. Of particular importance are values that lie at or above the mean. All of these fall within 10 standard deviations, most well within this range except for the data of the damaged cycloconverter. Figure 3-14 b. is that of the damaged cycloconverter and has data values that lie very far away from the statistical mean associated with its PDF. Having defined a statistical threshold, we can say that anything that falls further than 10 standard deviations away from the mean associated with its output to input frequency ratio is criteria for abnormal cycloconverter operation.

All data for loaded motors with PDF values that lie above the statistical mean of their output to input frequency ratio are plotted in Figure 3-17. Because the PDF is exponential, the natural logarithm of each data point is taken so that it scales more linearly. The negative of these values are taken so that the graph scales positively. These two modifications are purely for visual clarification. We can take 10 standard deviations of PDF value of each ratio away from the mean as one of the decision boundaries we use to diagnose the motor.

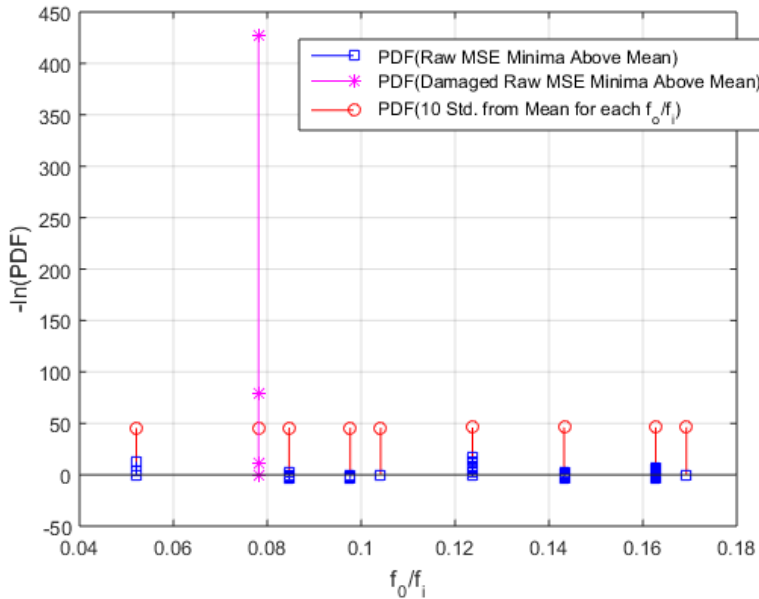


Figure 3-17. PDF of MSE data and threshold from Table 3-1 and Figure 3-12.

3.3.2 Local Minima Differences for Loaded Motors

Table 3-3 is all of the absolute value of the differences between local minima from Table 3-1. This table therefore has one less column. The differences between any two peaks for loaded motors should not vary greatly. The data is plotted in Figure 3-18 and a similar PDF analysis as that in section 3.3.1 is performed. The primary difference here is that because the differences should always ideally be zero, there is no linearly changing mean. There is, therefore, only a single mean and only a single PDF. The average of the differences at each

ratio was taken and plotted, and then the mean of these means (excluding the damaged data point) was found and plotted as well. These values are given in Figure 3-18.

Table 3-3. Loaded Motor Local Minima MSE Differences.

Fund. Freq (Hz)	60	Loaded Motor Local Minima MSE Differences																			
Output Frequency (Hz)	Notes	f_o/f_i	Mean	Std.	0.006	0.006	0.007														
3.1250	F6	0.0521	0.0066	0.0002	0.006	0.006	0.007														
4.6875	Damaged F1	0.0781	0.0694	0.0394	0.077	0.029	0.127	0.113	0.042	0.028											
5.0781	F6	0.0846	0.0054	0.0038	0.006	8E-04	0.003	0.005	0.009	0.002	0.013										
5.8594	F1	0.0977	0.0069	0.0063	0.017	0.019	3E-04	0.008	0.006	9E-05	0.003	0.005	0.005								
6.2500	F6	0.1042	0.0030	0.0022	3E-04	0.001	0.003	0.007	0.005	0.003	0.001	0.001	0.005								
7.4219	F6	0.1237	0.0045	0.0026	0.007	0.006	3E-04	0.004	0.005	0.002	3E-04	0.009	0.006	0.007	0.005	0.005	0.003				
8.5938	F6	0.1432	0.0071	0.0051	4E-04	0.012	0.005	0.004	0.007	0.01	0.007	0.007	0.012	0.003	0.007	1E-03	0.02	0.004			
9.7656	F2	0.1628	0.0084	0.0069	1E-03	0.009	0.015	0.002	0.016	0.009	0.005	0.004	0.001	0.021	0.002	0.022	0.001	0.009	0.01	9E-04	0.013
10.1563	F2	0.1693	0.0035	0.0021	0.005	0.009	0.007	0.001	0.006	0.003	0.004	0.003	0.001	0.003	0.004	0.002	0.004	0.001	0.002	0.002	0.003

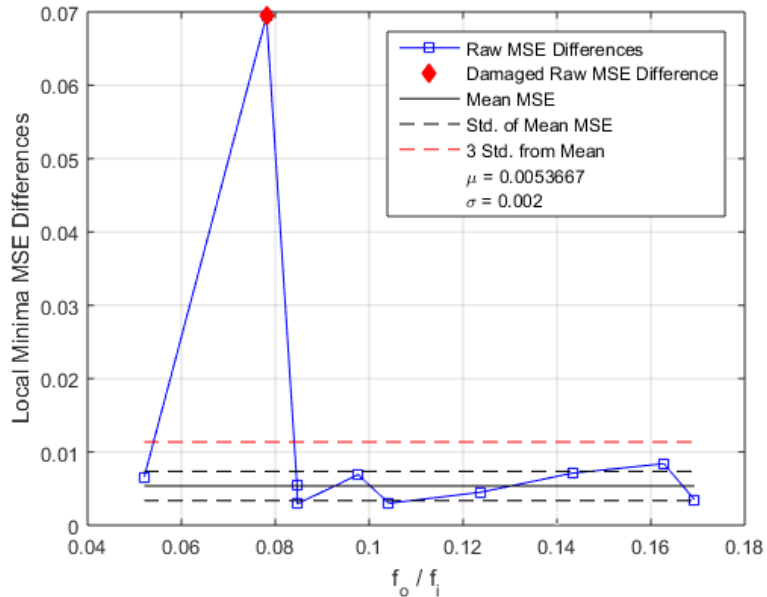


Figure 3-18. MSE differences, mean, and standard deviation from Table 3-3.

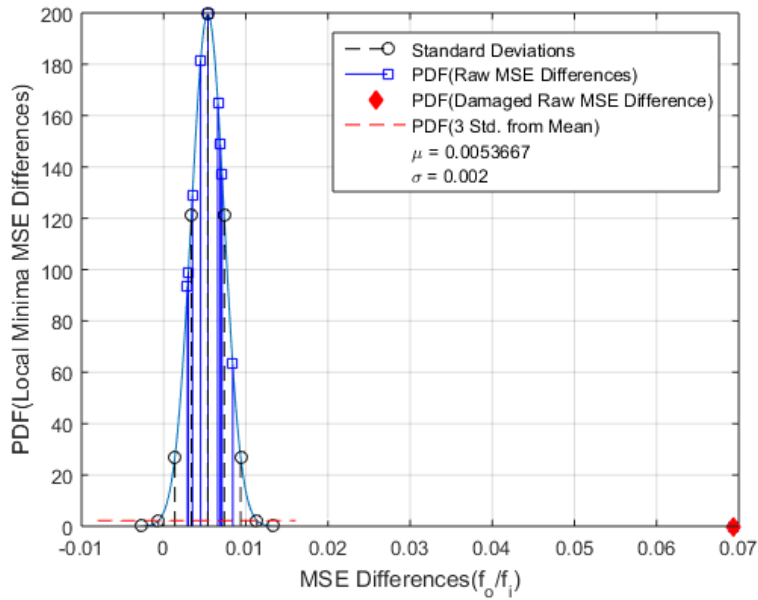


Figure 3-19. Probability distribution function created by (3-4) with data from Figure 3-18.

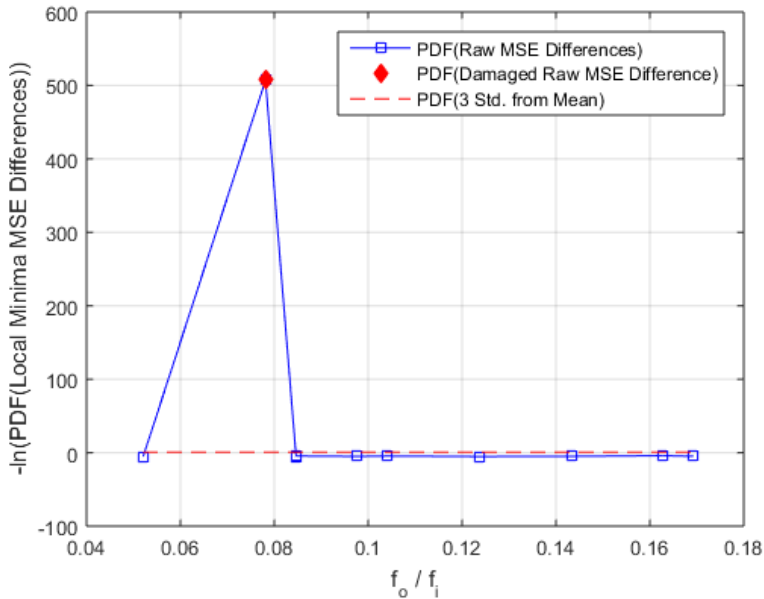


Figure 3-20. PDF of MSE differences and threshold.

From Figure 3-19, the damaged data value clearly lies very far outside of the statistical mean of the PDF while the rest fall well within 2 standard deviations. This is good because it establishes a very clear indicator that for any loaded cycloconverter, the differences between peaks should be consistent. The decision boundary for differences between peaks should be, statistically speaking, within at least 3 standard deviations from the mean (2 standard deviations is a very tight window). Again to provide a perhaps more intuitive visualization, Figure 3-20 shows the PDF values of undamaged and damaged MSE differences plotted on a

negative natural logarithmic scale. It's also clear here how far away the damaged data differences lie from the acceptable mean.

3.4 Unloaded Motors Error Analysis

3.4.1 Local Minima Values for Unloaded Motors

The exact same type of analysis performed in section 3.3.1 for loaded motors is performed for unloaded motors. All of the data is plotted in Table 3-5. Though the errors are relatively clustered and do tend to increase with output to input frequency, the lowest error for unloaded motors is still near the greatest error for those of loaded motors. This is because the model does not hold nearly as well for unloaded motors. Moreover, because there is no damaged unloaded motor to which we can compare, it's difficult to determine what constitutes a bad data value. That said, performing the same type of analysis produces useful results. The analysis follows in Figure 3-21 through Figure 3-26. All PDFs are made with equation (3-4). Equation (3-3) gives the linear functions for the regressions in Figure 3-21 and Figure 3-22. The coefficients for these functions are given in Table 3-4.

Table 3-4. Coefficients for equation (3-3) corresponding to Figure 3-21 and Figure 3-22.

	<i>Coefficient</i>	
	<i>m</i>	<i>b</i>
<i>μ</i>	0.4354	0.1508
<i>σ</i>	0.0589	0.0053

Table 3-5. Unloaded Motor Local Minima MSE.

Fund. Freq (Hz)	60	Unloaded Motor Local Minima MSE																	
Output Frequency (Hz)	Notes	f_o/f_i	Mean	Std.	0.171	0.164	0.172	0.163	0.152	0.145	0.138	0.131	0.124	0.117	0.110	0.103	0.096	0.089	0.082
2.7344	F1	0.0456	0.1676	0.0040	0.171	0.164	0.172	0.163	0.152	0.145	0.138	0.131	0.124	0.117	0.110	0.103	0.096	0.089	0.082
2.7344	F2	0.0456	0.1328	0.0015	0.132	0.135	0.131												
3.1250	F6	0.0521	0.1824	0.0059	0.175	0.19	0.182												
4.6875	F1	0.0781	0.2185	0.0113	0.232	0.228	0.214	0.233	0.212	0.203	0.208								
5.0781	F6	0.0846	0.2468	0.0172	0.242	0.222	0.237	0.265	0.267										
6.2500	F6	0.1042	0.2233	0.0097	0.223	0.22	0.239	0.212											
7.0313	F6	0.1172	0.2051	0.0058	0.203	0.202	0.21	0.197	0.213										
7.8125	F2	0.1302	0.1620	0.0118	0.18	0.167	0.145	0.167	0.181	0.163	0.167	0.154	0.139	0.157	0.156	0.158	0.172		
8.5938	F6	0.1432	0.1904	0.0172	0.178	0.164	0.192	0.179	0.202	0.184	0.238	0.19	0.202	0.205	0.203	0.184	0.185	0.176	
9.375	F6	0.1563	0.1947	0.0157	0.196	0.18	0.161	0.166	0.212	0.207	0.206	0.204	0.208	0.189	0.205	0.198	0.201		

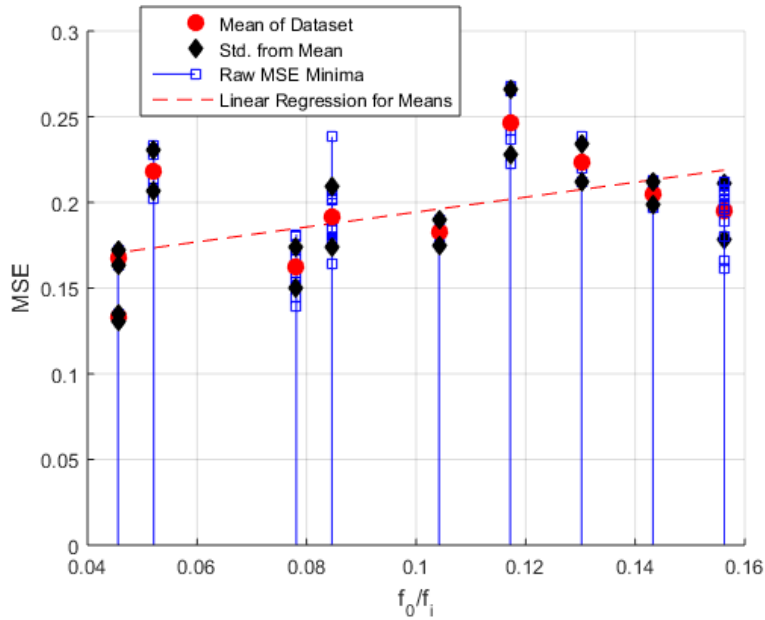


Figure 3-21. MSE data and associated linear regression from Table 3-5.

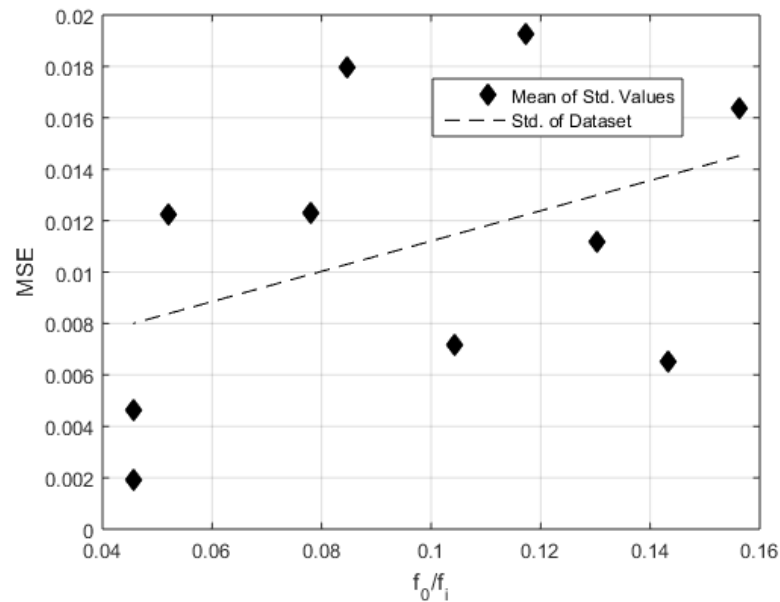


Figure 3-22. Standard deviation of MSE data and associated linear regression from Table 3-5.

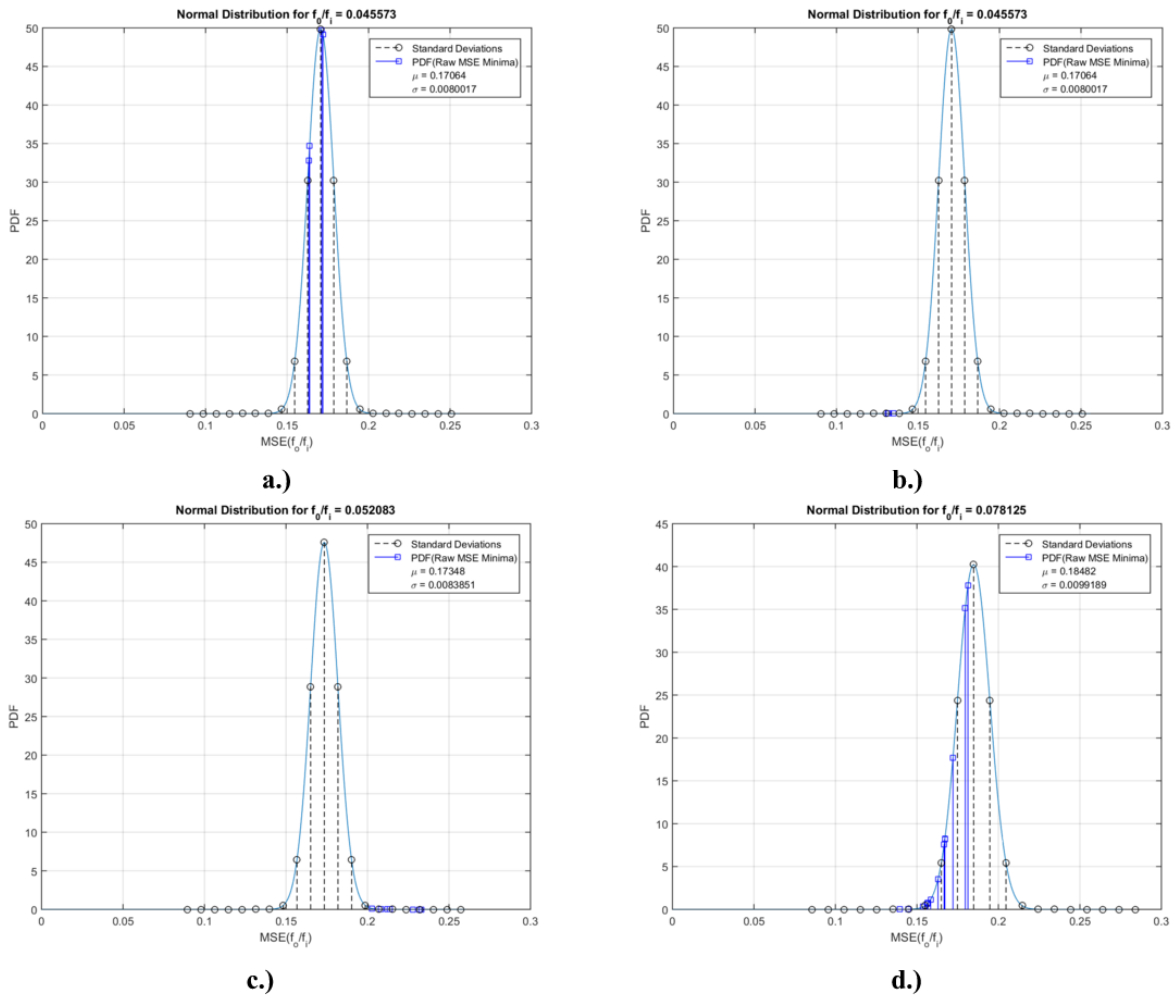


Figure 3-23. Probability distribution functions created by (3-4) with data from Figure 3-21.

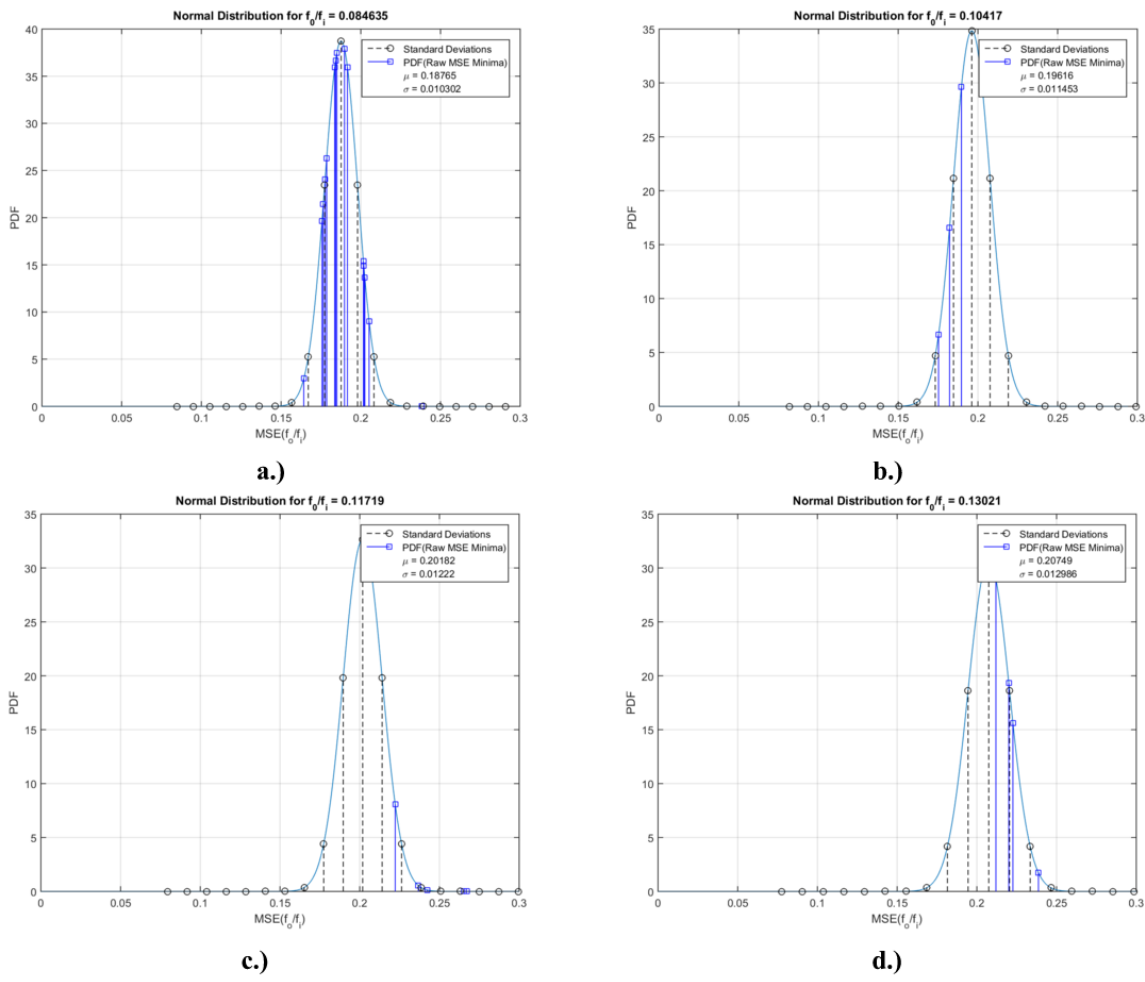


Figure 3-24. Probability distribution functions created by (3-4) with data from Figure 3-21.

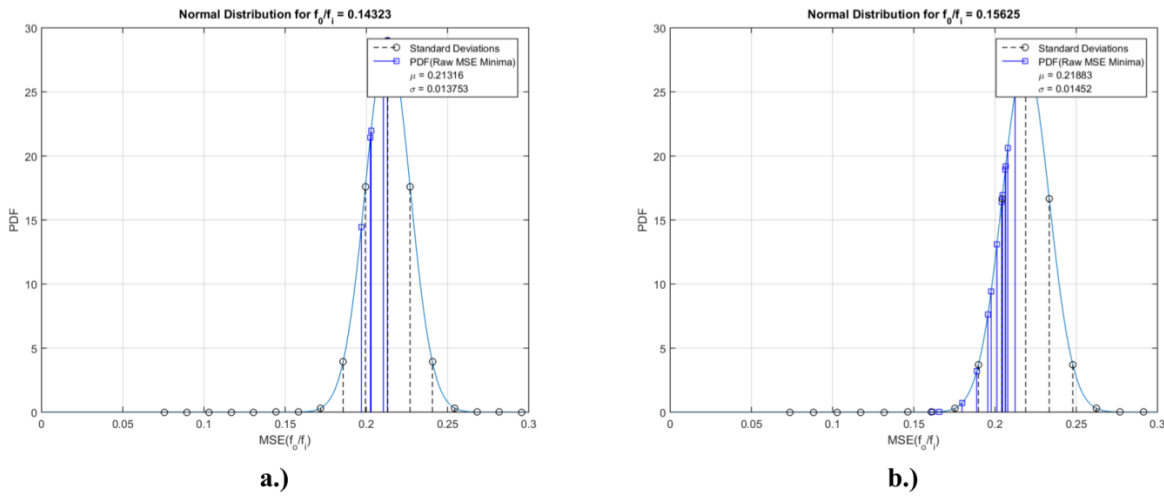


Figure 3-25. Probability distribution functions created by (3-4) with data from Figure 3-21.

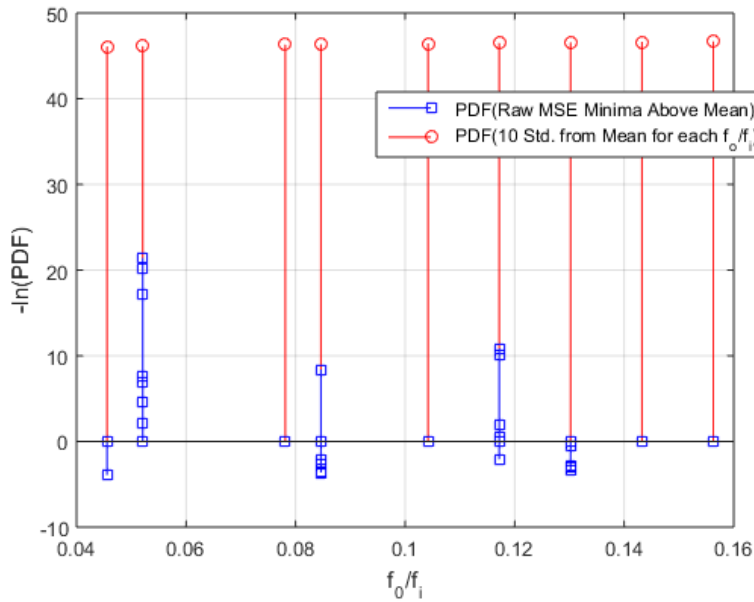


Figure 3-26. PDF of MSE data and threshold from Table 3-5 and Figure 3-21.

All of the data values fall within 8 standard deviations from the mean. The 10th standard deviation is shown in Figure 3-26 so that a comparison can be made to Figure 3-17 for the case of the loaded motor. The PDF of these values tend to be of similar or slightly greater values than their loaded counterparts. However, we can surmise that if we had a damaged cycloconverter similar to the case of the loaded motor, this value would likely fall outside of the 10 standard deviation threshold like it does for loaded motors. This type of statistical analysis then for unloaded motors proves valuable though untested.

3.5 Decision Boundary Thresholds

From the analysis in the previous sections, statistical thresholds can be set that dichotomize between normal and abnormal functioning of the cycloconverter. These are summarized in Table 3-6. Decision Boundary Status Diagnosis For in-phase MSE comparisons of both loaded and unloaded motors, the corresponding PDF function must be taken as a function of the mean and standard deviations which are themselves functions of the output to input frequency ratio. If the PDF of this value lies outside of 10 standard deviations then these values are nearly certain; based on the assessments made here, to represent a damaged cycloconverter. For loaded motors, the difference between the current MSE and the previous MSE must lie within three standard deviations of the mean of the PDF defined for loaded motor frequency differences. Obviously the difference can only be taken after the very first MSE has been found because there must be a previous value from which to subtract.

Table 3-6. Decision Boundary Status Diagnosis.

Error Type	State	PDF μ	PDF σ	Standard Deviatinon Threshold
In-Phase MSE	Loaded	Equation (3-3) with Table 3-2	Equation (3-3) with Table 3-2	10
	Unloaded	Equation (3-3) with Table 3-4	Equation (3-3) with Table 3-4	10
In-Phase MSE Differences	Loaded	0.0053	0.002	3
	Unloaded	N/A	N/A	N/A

The decision tree corresponding to Table 3-6 is shown in Figure 3-27. These represent the same information in two different formats. In practice, it would be placed in the comparison block of the model in order to diagnose the drive. With these decision boundary thresholds, a real time system should have the ability to distinguish between normal and abnormal cycloconverter operation.

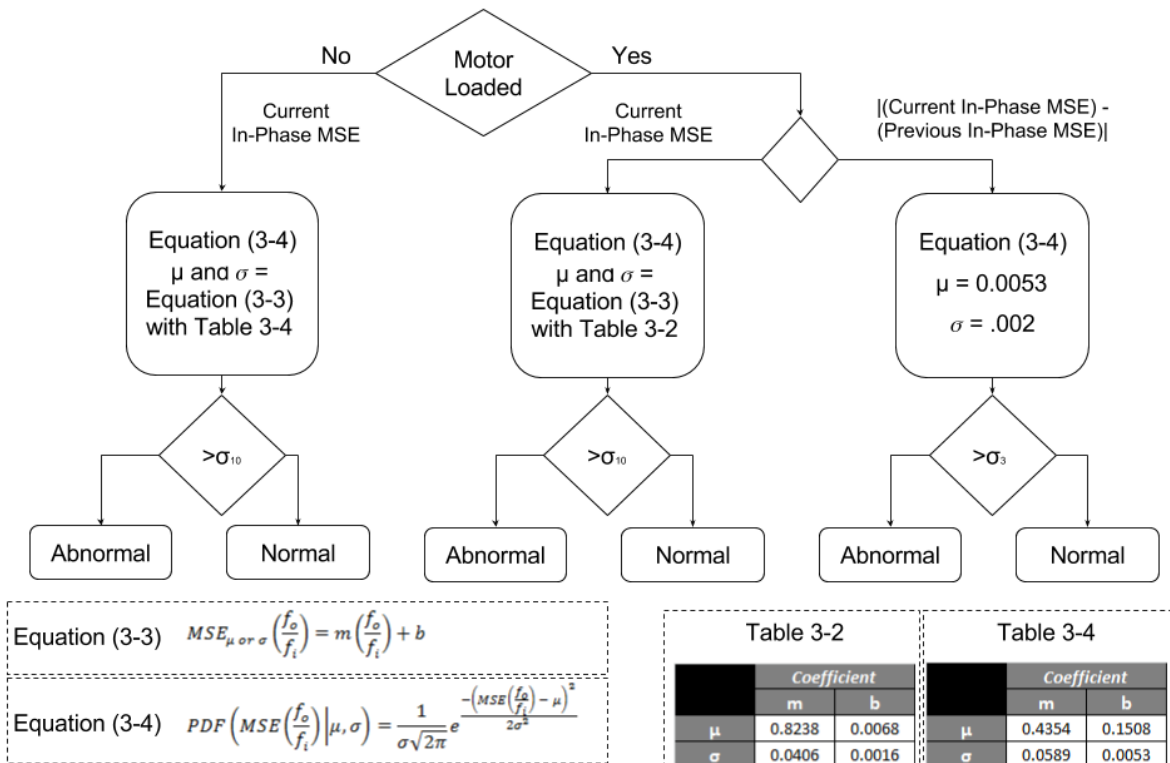


Figure 3-27. Cycloconverter Status Decision Tree.

4. SUMMARY

The parameters for a novel system have been introduced that should be able to diagnosis the cycloconverter as either operating normally or abnormally. The model framework for such a system was also introduced and formed the basis for many of the steps taken in this research. At the time of publication, the model itself has not yet been implemented in real-time; however, this thesis forms the groundwork on which the modeling technique can be built and expanded. This technique has two chief advantages. First is the fact that it requires only analysis of the input current data, ideally on each of the three phases but only necessarily on one, and requires only the drive pulse number, input frequency, and output frequency of the drive as references. Second is that it utilizes time-frequency signature analysis. This technique provides the unique ability to analyze data in two domains simultaneously. It is then likely possible to emphasize abnormalities that may not be caught by other systems.

Real input current data was utilized in conjunction with cycloconverter drive theory to form a model that approximates a normal functioning cycloconverter's input current. The time-frequency distribution known as the spectrogram is then used to transform both the model and real input current data of interest. The representation by the spectrogram is composed of a 2 dimensional discrete matrix. The model in the time-frequency domain consists of a reference window whose width corresponds to the half of the period of the specified output frequency of the cycloconverter. In practice input current data should be fed into the model, but for this research, one second datasets were analyzed in order to define characteristics for the model that allow for the status diagnosis of the cycloconverter.

The mean squared error (MSE) between the reference window and the real data can be found. Based on the datasets provided, a statistical analysis was performed that defines decision boundary thresholds for the cycloconverter status.

4.1 *Method Shortcomings and Potential Improvements*

By this point it should be clear that the methods discussed here introduce a powerful new technique that can hopefully be of use to diagnosis cycloconverter drives. Because research with respect to the use of time-frequency analysis to diagnosis drives is limited, this research should be considered preliminary. Though it has been shown that this method is adequate, there clearly exist a number of improvements that can be made.

Many of the shortcomings of this method are the result of the model used for comparison. The modeling equation design is the result of analysis of the cycloconverter input harmonic equation as seen in literature. Of particular concern in this equation is the frequency modulation term. The choice that was made is not necessarily the best choice, though it proved itself adequate in this context. Perhaps a more robust equation can be designed if there exists a more representative frequency modulation term that can be utilized.

As was seen in previous sections, as the output frequency of the cycloconverter increases so does the error. While this is in part due to the frequency modulation term, it is also due to

inaccuracies in the harmonic slope estimation method. The method can potentially be modified so that it has the ability to detect harmonic slopes more accurately for a wider range of output frequencies.

In addition to the methods themselves, if more data can be obtained then both the harmonic slopes and error analysis can be improved. Of particular interest is data for the damaged cycloconverter. Of course, this is difficult to obtain because data is not always recorded and one cannot simply request that the cycloconverter malfunctions so as to provide helpful data. Once the technique is honed however, it should be possible to simulate failure and see how the model responds.

It bears mentioning again that the output frequency of the cycloconverter was estimated from the data provided. While the estimation is decent, it is not perfect. It has been observed that for some datasets, the frequency estimation is slightly too high therefore in the data to model comparison there is a persistent error. This has also been checked by cross correlating the reference window and real data. For trials with an incorrect frequency estimation it is observed that the cross correlation term is less correlated than it should be. In practical usage however this frequency value would simply be passed to the model, ideally, but in order to better analyze the data provided, if the output frequency is not provided with the dataset, then it is worthwhile to improve the frequency estimator.

Last is a note about the computation time associated with time-frequency analysis. Though this has been hinted at throughout this document, it should be explicated stated here that time-frequency signature analysis is computationally intensive. Therefore implementation of a model such as the one proposed here may require significant computing power if the sampling frequency is high.

4.2 *Future Work*

In addition to the items of improvement included above, the next step in this research is the implementation of the real time model. Ideally this should be performed in SIMULINK, as the majority of the analysis has already been performed in MATLAB. The construction of the simulation however necessitates the design of function blocks which do not exist, therefore care must be taken to ensure that these function blocks perform appropriately. Even with a working model however, it is very important to ensure that the decision boundaries are accurate, therefore it is also important to gather more data and refine the model and analysis techniques proposed here.

It can be said that this research consists of two large parts. Data analysis that hopes to define the normal cycloconverter and provide some parameters on which decisions can be made that define the cycloconverter status, and the implementation of a system that uses those parameters. Future work should be sure to consider this principle when refining and then implementing these methods.

5. CONCLUSION

This document represents the careful and thorough attempt to begin the introduction of a new method of motor drive monitoring, specifically that of the cycloconverter. While there are already some methods available for variable frequency drive status diagnosis, none utilize the concepts discussed here to achieve that goal, especially not with respect to the cycloconverter. For this reason, this investigation is indeed very novel. While there are surely improvements that can be made, a strong case has been presented here that this technique is a very powerful and useful approach. It forms a solid base from which this method and those similar to it can improve, expand, and evolve.

The principles of the methods discussed here are not limited solely to cycloconverter or just to drive diagnosis. Digital signal processing plays an increasingly vital role in all manner things technological and consequently, clever methodologies will be developed that better help us control the rapidly expanding technological world around us.

6. REFERENCES

- [1] B. R. Pelly, *Thyristor Phase-Controlled Converters and Cycloconverters*, Pittsburg, PA: John Wiley & Sons, 1971.
- [2] Burak Ozpineci and Leon. M. Tolbert, "Cycloconverters," Dept. of Elect. and Comput. Eng., University of Tennessee-Knoxville.
- [3] Yazhou Liu, Gerald Thomas Heydt, and Ron F. Chu, "The Power Quality Impact of Cycloconverter Control Strategies," *IEEE Trans. Power Del.*, vol. 20, no. 2, pp. 1711-1718, Apr. 2003.
- [4] Timpe Wolfgang, "Cycloconverter Drives for Rolling Mills," *IEEE Trans. Ind. Appl.*, vol. IA-18, no. 4, pp. 400-404, July 1982.
- [5] Harry H. Weatherford, "Real Time Diagnostic Systems For Motors and Drives," Ph.D. dissertation, Dept. Elect. Eng., Univ. of South Carolina, Columbia, SC, 2011.
- [6] Victor Guerrero, Jorge Pontt, Juan Dixon, and Jaime Rebolledo, "A Novel Noninvasive Failure-Detection System for High-Power Converters Based on SCRs," *IEEE Trans. Ind. Electron.*, vol. 60, no. 2, pp. 450 - 458, Feb. 2013.
- [7] J. Pontt, J. Rodríguez, E. Cáceres, I. Illanes, and C. Silva, "Cycloconverter Drive System for Fault Diagnosis Study: Real Time Model, Simulation and Construction," in *Power Electronics Specialists Conf. (PESC)*, Jeju, 2006, pp. 1-6.
- [8] J. Pontt, J. Rodríguez, E. Cáceres, I. Illanes, and J. Rebolledo, "Cycloconverter Behavior for a Grinding Mill Drive Under Firing Pulses Fault Conditions," in *Industry Applications Conf.*, Hong Kong, 2005, pp. 645-649.
- [9] Marcelo Vásquez, Jorge Pontt, and Victor Arredondo, "Cycloconverter Interharmonics Current Analysis Under Unbalanced Load Based on a Real-Time Simulation," in *2015 IEEE Int. Conf. on Ind. Technology (ICIT)*, Seville, 2015, pp. 683-689.
- [10] J. Pontt et al., "Current Issues on High-Power Cycloconverter-Fed Gearless Motor Drives for Grinding Mills," in *2003 IEEE Int. Symposium on Industrial Electronics*, Rio de Janeiro, 2003, pp. 369-374.
- [11] Jorge O. Pontt, José P. Rodríguez, Jaime C. Rebolledo, Kurt Tischler, and Norbert Becker, "Operation of High-Power Cycloconverter-Fed Gearless Drives Under Abnormal Conditions," *IEEE Trans. Ind. Electron.*, vol. 43, no. 3, pp. 814-820, May/June 2007.
- [12] Ronnie F. Chu and John J. Burns, "Impact of Cycloconverter Harmonics," *IEEE Trans. Ind. Appl.*, vol. 25, no. 3, pp. 427-435, May/June 1989.

- [13] Gunther, E. W. and Electrotek Concepts Inc., "Interharmonics in Power Systems," in *2001 Power Engineering Society Summer Meeting*, Vancouver, 2001.
- [14] J. Arrillaga and N.R. Watson, *Power System Harmonics*, 2nd ed.: John Wiley & Sons, 2003.
- [15] Zhuofu Liu, "A Novel Time-Frequency Analysis Method for Mechanical Failure Detection," in *Int. Conf. on Hybrid Information Technology (ICHIT)*, Jeju, 2006.
- [16] Birsen Yazıcı and Gerald B. Kliman, "An Adaptive Statistical Time-Frequency Method for Detection of Broken Bars and Bearing Faults in Motors Using Stator Current," *IEEE Trans. Ind. Appl.*, vol. 35, no. 2, pp. 442-452, Mar./Apr. 1999.
- [17] J. Rosero, J. Cusidó, A. Garcia Espinosa, J. A. Ortega, and L. Romeral, "Broken Bearings Fault Detection for a Permanent Magnet Synchronous Motor under non-constant working conditions by means of a Joint Time Frequency Analysis," in *2007 IEEE Int. Symposium on Industrial Electronics*, Vigo, 2007, pp. 3415-3419.
- [18] Nobuyuki Yamawaki, Christopher Wilke, Zhongming Liu, and Bin He, "An Enhanced Time-Frequency-Spatial Approach for Motor Imagery Classification," *IEEE Trans. Neural Syst. Rehabil. Eng.*, vol. 14, no. 2, pp. 250-254, June 2006.
- [19] Desheng Liu, Yu Zhao, Beibei Yang, and Jinping Sun, "A New Motor Fault Detection Method Using Multiple Window S-Method Time-Frequency Analysis," in *2012 Int. Conf. on Systems and Informatics (ICSAI 2012)*, Yantai, 2012, pp. 2563-2566.
- [20] Martin Blödt, Marie Chabert, Jérémie Regnier, and Jean Faucher, "Mechanical Load Fault Detection in Induction Motors by Stator Current Time-Frequency Analysis," *IEEE Trans. Ind. Appl.*, vol. 42, no. 6, pp. 1454-1463, Nov./Dec 2006.
- [21] Satish Rajagopalan, José A. Restrepo, José M. Aller, Thomas G. Habetler, and Harley G. Ronald, "Nonstationary Motor Fault Detection Using Recent Quadratic Time-Frequency Representations," *IEEE Trans. Ind. Appl.*, vol. 44, no. 3, pp. 735-744, May/June 2008.
- [22] M. Riera-Guasp et al., "Diagnosis of Induction Motor Faults via GaborAnalysis of the Current in Transient Regime," *IEEE Trans. Instrum. Meas.*, vol. 61, no. 6, pp. 1583-1596, June 2012.
- [23] Jianguo Liu, Pragasen Pillay, and Hugh Douglas, "Wavelet Modeling of Motor Drives Applied to the Calculation of Motor Terminal Overvoltages," *IEEE Trans. Ind. Electron.*, vol. 51, no. 1, pp. 61-66, February 2004.
- [24] Eduardo Cabal-Yepez, Armando G. Garcia-Ramirez, René J. Romero-Troncoso, Arturo García-Perez, and Roque A. Osornio-Rios, "Reconfigurable Monitoring System for Time-Frequency Analysis on Industrial Equipment Through STFT and DWT," *IEEE Trans. Ind. Informat.*, vol. 9, no. 2, pp. 760-771, May 2013.
- [25] J. T. Black and Ronald A. Kohser, *DeGarmo's Materials and Processes in Manufacturing*, 10th ed. Hoboken, NJ: John Wiley & Sons, 2008.

- [26] K. J. Åström, R. M. Murray, and Lars Cremean, Feedback Systems [Image], Caltech Division of Eng. & Applied Sci., Pasadena, CA, Sept. 2002.
- [27] S. Hrynkiewicz and E. Langham, "Cycloconverters and Methods of Operating Them," European Patent EP0030468 A1, Dec 5, 1980.
- [28] Christopher P. Mercer, "The Analysis, Simulation and Control of Cycloconverter Drives for Ship Propulsion," Ph.D. dissertation, Dept. Elect. and Comput. Eng., Naval Postgraduate School, Monterey, CA, 1996.
- [29] *IEEE Recommended Practices and Requirements for Harmonic Control in Electrical Power Systems*, IEEE Standard 519-1992, 1993.
- [30] Bimal K. Bose, *Modern Power Electronics and AC Drives*, Upper Saddle River, NJ: Prentice Hall, 2002.
- [31] Leon Cohen, *Time-Frequency Analysis*, Upper Saddle River, NJ: Prentice Hall, 1995.
- [32] Zhenyu Guo, Louis-Gilles Durand, and Howard C. Lee, "The Time-Frequency Distributions of Nonstationary Signals Based on a Bessel Kernel," *IEEE Trans. Signal Process.*, vol. 42, no. 7, pp. 1700-1707, Jul 1994.
- [33] Bimal Bose, *Power Electronics and Motor Drives: Advances and Trends*, Burlington, MA: Elsevier, 2006.
- [34] Carsten Fräger, "Influence of Voltage Harmonics and Cogging Torque on Speed Deviations of Servo Drives with Permanent Magnet Synchronous Motors," in *Proc. of ETG/GMM-Symposium Innovative small Drives and Micro-Motor Systems*, Cologne, Germany, September 2015.